Objective: The aim of this book is to numerically determine flow around the ship hull - DTMB 5415. Further analyses have been made on the different combinations of appendages attached to the ship's hull. As a result, influence of the appendages on the wake structure located in the propeller disk as well as the representation of the forces acting on appendages have been derived. Content and methods: • The free surface flow around a model surface ship (DTMB 5415) advancing in calm water under steady conditions is numerically simulated. The geometry of the DTMB 5415 ship hull was provided in igs file format. The combatant has been recommended by the 1996 International Towing Tank Conference as a benchmark case for CFD computations of ship resistance and propulsion. • The SHIPFLOW code was employed to evaluate the flow field structure around the ship hull, the forces acting on bare hull and appendages. The solver computed the incompressible RANS equations on structured overlapping grids by using a finite volume technique. Turbulence modelling was achieved through the k-ε and k-ω SST or EASM models. • The propeller was approximated as an active disk.

Current work: MARINO CONSULTING.Ltd – VARNA, BULGARIA as hull outfitter and structure modeller | Department of Marine Engineering from 3 years. Designer of ships and yachts in Rhinoceros, Ship Constructor 2005 and preparing workshop documentation drawings in AutoCAD. Education: European Master in Integrated Advanced Ship Design. EMSHIP

978-3-8433-6282-5

Current trends in CFD for ship design

Neykov

Svetlozar Neykov

Numerical investigation of flow around an appended ship hull DTMB 5415

Using hybrid viscous solution with potential flow free surface utilizing SHIPFLOW software for CFD problem

LAP LAMBERT Academic Publishing

Svetlozar Neykov

Numerical investigation of flow around an appended ship hull DTMB 5415

Svetlozar Neykov

Numerical investigation of flow around an appended ship hull DTMB 5415

Using hybrid viscous solution with potential flow free surface utilizing SHIPFLOW software for CFD problem

LAP LAMBERT Academic Publishing

Impressum / Imprint
Bibliografische Information der Deutschen Nationalbibliothek: Die Deutsche Nationalbibliothek verzeichnet diese Publikation in der Deutschen Nationalbibliografie; detaillierte bibliografische Daten sind im Internet über http://dnb.d-nb.de abrufbar.
Alle in diesem Buch genannten Marken und Produktnamen unterliegen warenzeichen-, marken- oder patentrechtlichem Schutz bzw. sind Warenzeichen oder eingetragene Warenzeichen der jeweiligen Inhaber. Die Wiedergabe von Marken, Produktnamen, Gebrauchsnamen, Handelsnamen, Warenbezeichnungen u.s.w. in diesem Werk berechtigt auch ohne besondere Kennzeichnung nicht zu der Annahme, dass solche Namen im Sinne der Warenzeichen- und Markenschutzgesetzgebung als frei zu betrachten wären und daher von jedermann benutzt werden dürften.

Bibliographic information published by the Deutsche Nationalbibliothek: The Deutsche Nationalbibliothek lists this publication in the Deutsche Nationalbibliografie; detailed bibliographic data are available in the Internet at http://dnb.d-nb.de.
Any brand names and product names mentioned in this book are subject to trademark, brand or patent protection and are trademarks or registered trademarks of their respective holders. The use of brand names, product names, common names, trade names, product descriptions etc. even without a particular marking in this work is in no way to be construed to mean that such names may be regarded as unrestricted in respect of trademark and brand protection legislation and could thus be used by anyone.

Coverbild / Cover image: www.ingimage.com

Verlag / Publisher:
LAP LAMBERT Academic Publishing
ist ein Imprint der / is a trademark of
OmniScriptum GmbH & Co. KG
Bahnhofstraße 28, 66111 Saarbrücken, Deutschland / Germany
Email: info@lap-publishing.com

Herstellung: siehe letzte Seite /
Printed at: see last page
ISBN: 978-3-8433-6282-5

Copyright © 2016 OmniScriptum GmbH & Co. KG
Alle Rechte vorbehalten. / All rights reserved. Saarbrücken 2016

CONTENTS

CONTENTS 1

NOMENCLATURE 10

1. INTRODUCTION 11

2. DESCRIPTION OF USED SOFTWARE 18

2.1. Ship Flow Overview 18

2.1.1. Ship Resistance 19

2.1.2. Propulsion 19

2.1.3. Maneuvering 19

2.2. Software Structure 20

2.2.1. Pre-processing / Input Data Modules: 20

2.2.2. Processing Data Modules: 20

2.2.3. Post-processing data modules: 23

2.3. SHIPFLOW application 24

2.3.1. Geometry preparation 24

3. POTENTIAL FLOW METHOD 28

3.1. Description of the method 28

3.2. Mathematical model of Potential flow theory 29

3.2.1. Hypothesis. Governing Equations 29

3.2.2. Boundary Conditions for Potential Flow Method 31

3.2.3. Boundary layer theory 34

4. FREE SURFACE FLOW SIMULATION AROUND COMBATANT SHIP 35

4.1.1. Description of this Chapter 35

4.1.2. Panelization 35

4.2. Results and Discussion for Potential Flow Free Surface Solution 40

4.2.1. Free-surface elevation and body pressure distribution 47

4.2.2. Skin friction coefficient 50

4.3. Conclusions of Potential Flow Computation 51

5. VISCOUS FLOW METHOD 52

5.1. Mathematical Model 52

5.1.1. Governing Equations 53

5.1.2. Turbulence Modeling 56

5.1.3. Boundary conditions 57

5.1.4. Numerical Scheme 59

5.1.5. Advantages and Disadvantages of Viscous Flow Method. 59

6. RESULTS AND DISCUSSION FOR VISCOUS FLOW SOLUTION AROUND COMBATANT SHIP 60

6.1.1. Description of the chapter 60

6.1.2. Grid generation 60

6.1.3. Discussion on computed results 70

6.1.4. Initial results for Fn = 0.401 taken from experimental results with rudder case..... 71

6.1.5. Pressure results for Fn = 0.28 bare hull no refined and refined - compared 78

6.1.6. Results for Fn = 0.28 and Fn = 0.41 bare hull - compared 79

6.1.7. Results for Fn = 0.28 with rudder and rudder bracket and shaft 83

6.1.8. Additional Results for Fn = 0.41 bare hull 84

6.1.9. Propeller model 86

6.1.10. Results for Fn =0.28 no propeller and propeller and Fn = 0.41 compared 87

6.1.11. Results for Fn = 0.28 and Fn = 0.41 hull with appendages and propeller compared 90

6.1.12. Additional results at Fn = 0.28 no propeller, propeller and Fn=0.41 propeller..... 92

6.2. Conclusions of Viscous Flow Computation 98

7. CONCLUSIONS AND PRESPECTIVE 99

8. REVIEWER COMMENTS 103

9. ACKNOWLEDGEMENTS 109

10. REFERENCES 110

Appendix A1: Resistance theory describing physics of the problem 114

TABLE OF FIGURES

Fig. 1:Combatant ship David Taylor Model Basin (DTMB) model 5415 9
Fig. 2 Computer visualization combatant ship David Taylor Model Basin (DTMB) model 5415 with appendages 16
Fig. 3 Former XVISC simulation of the viscous flow 22
Fig. 4 Transforming coordinate systems from offset file to SHIPFLOW 25
Fig. 5 Geometry of DTMB 5415 26
Fig. 6 Offset file of DTMB 5415 26
Fig. 7 Groups used for DTMB 5415 26
Fig. 8 Transversal cross section - station of ship geometry used in offset file of SHIPFLOW 27
Fig. 9 Structure of offset file 27
Fig. 10 Potential flow with free surface 32
Fig. 11 Boundary conditions for the free surface 32
Fig. 12 Domain relationship with number of panels 36
Fig. 13 Transom and body relationship with number of panels 36
Fig. 14 Side view of the hull panelization 37
Fig. 15 Forward part of the ship - (Side view) 37
Fig. 16 Aft part of the ship - (Side view) 37
Fig. 17 Sonar panelization (Bottom view) 37
Fig. 18 Free surface no transom case 39
Fig. 19 Free surface with transom case 39
Fig. 20 Total Resistance [Rt] in function of Froude number [Fn] 43
Fig. 21 Coefficient of wave making resistance [Cw] in function of Froude number [Fn] 43
Fig. 22 Skin friction coefficient [Cf] vs Froude number [Fn] 45
Fig. 23 % Difference with experimental data vs Foude Number [Fn] 46
Fig. 24 Representation of free surface elevation using DTMB 5415, perspective and top view 47
Fig. 25 Free surface elevation on the water and pressure distribution on the hull 49
Fig. 26 Skin friction coefficient for no transom, no trim fn= [0.24] 50
Fig. 27 Solution domain 58
Fig. 28 Domain regions for DTMB 5415 63
Fig. 29 No grid refinement in the forward part of the ship, sonar region 64
Fig. 30 Grid refinement in the forward part of the ship, sonar region 64
Fig. 31 Grid in transom part of the ship hull 64
Fig. 32 Overall view of the grid 65
Fig. 33 Free surface grid from potential flow solution 66
Fig. 34 Mesh on viscous flow solution 66
Fig. 35 Fitting of the free surface grid from potential flow solution as a boundary over viscous flow solution 66

Fig. 36 Fitting of the free surface grid from potential flow solution as a boundary over viscous flow solution symmetry plane..... 66
Fig. 37 Zoom in the aft region of whole viscous domain with free surface from potential flow - hybrid method..... 67
Fig. 38 Zoom in bow region of whole viscous domain with free surface from potential flow - hybrid method..... 67
Fig. 39 Hybrid method - Perspective view of whole viscous domain 67
Fig. 40 Overlapping grid of shaft - green, rudder – orange, ruder bracket – blue 68
Fig. 41 Used rudder grid for computation analysis..... 69
Fig. 42 Grid around the rudder and background grid of the domain overlapping. 69
Fig. 43 Grid around stern part of the ship without appendages 70
Fig. 44 Grid of the rudder bracket and hull of DTMB 5415..... 70
Fig. 45 Grid around stern part of the ship with appendages 70
Fig. 46 Overall pressure distribution on the hull at, Fn = 0.401, rudder 71
Fig. 47 Pressure distribution on sonar dome and forward part of the ship at, Fn = 0.401, rudder..... 72
Fig. 48 Pressure distribution on aft part of the ship 72
Fig. 49 Axial velocity on forward part of the ship in the sonar region at, Fn = 0.401 rudder..... 73
Fig. 50 Axial velocity in the aft part of the ship at, Fn = 0.401 74
Fig. 51 Axial velocity around the hull at, Fn = 0.401, rudder - perspective view 75
Fig. 52 Axial velocity around the mid and sonar part of the hull at, Fn = 0.401, rudder - perspective view 75
Fig. 53 Free surface wave elevation - velocity Z taken from potential solution, in perspective view at Fn = 0.401, rudder 76
Fig. 54 Pressure distribution on the rudder surface plus bracket at, Fn = 0.401 77
Fig. 55 Pressure results at sonar region for Fn = 0.28 bare hull no refined 78
Fig. 56 Pressure results at sonar region for Fn = 0.28 bare hull refined 78
Fig. 57 Pressure results at sonar region for Fn = 0.28 bare hull 79
Fig. 58 Pressure results at sonar region for Fn = 0.41 bare hull 79
Fig. 59 Pressure results at ship aft region for Fn = 0.28 bare hull 80
Fig. 60 Pressure results at ship aft region for Fn = 0.41 bare hull 80
Fig. 61 Axial velocity results at ship sonar region for Fn = 0.28 bare hull 81
Fig. 62 Axial velocity results at ship sonar region for Fn = 0.41 bare hull 81
Fig. 63 Axial velocity results at ship stern region of the hull for Fn = 0.28 bare hull..... 82
Fig. 64 Axial velocity results at ship stern region for Fn = 0.41 bare hull 82
Fig. 65 Pressure results at ship stern with rudder, rudder bracket and shaft at Fn = 0.28..... 83

Fig. 66 Axial velocity results at midplane slice in XZ direction in ship stern region for hull at Fn = 0.28 with rudder and rudder bracket..... 83
Fig. 67 Axial velocity results at ship stern zoom out region for Fn = 0.41 bare hull..... 84
Fig. 68 Axial velocity contours at different slices of the hull Fn = 0.41 bare hull 85
Fig. 69 Axial velocity contours at different slices of the hull Fn = 0.41 bare hull 85
Fig. 70 Pressure acting on the hull and appendages at Fn = 0.28 no propeller - slice on rudder 87
Fig. 71 Pressure acting on the hull and appendages at Fn =0. 28 propeller - slice on rudder..... 87
Fig. 72 Pressure acting on the hull and appendages at Fn = 0.41 propeller - slice on rudder..... 87
Fig. 73 Axial velocity acting around hull and appendages at Fn =0.28 no propeller - slice on rudder 88
Fig. 74 Axial velocity acting around hull and appendages at Fn = 0.28 propeller - slice on rudder..... 88
Fig. 75 Axial velocity acting around hull and appendages at Fn = 0.41 propeller - slice on rudder..... 88
Fig. 76 Axial velocity around hull and appendages at Fn = 0.28 no propeller - slice on midplane..... 89
Fig. 77 Axial velocity around hull and appendages at Fn = 0.28 propeller - slice on midplane 89
Fig. 78 Axial velocity around hull and appendages at Fn = 0.41 propeller - slice on midplane 89
Fig. 79 Pressure distribution around the hull at Fn = 0.28 with appendages and propeller..... 90
Fig. 80 Pressure distribution around the hull at Fn = 0.41 with appendages and propeller..... 91
Fig. 81 Pressure distribution on the aft part of the hull at Fn = 0.28 for appendages and no propeller 92
Fig. 82 Axial velocity distribution transversal slices on the aft part of the hull at Fn = 0.28 with appendages and no propeller 93
Fig. 83 Axial velocity distribution on the aft part of the hull at Fn = 0.28 with appendages and no propeller - longitudinal slice at propeller plane - Less contours 94
Fig. 84 Axial velocity distribution on the aft part of the hull at Fn = 0.28 with appendages and no propeller - longitudinal slice at propeller plane - More contours 95
Fig. 85 Axial velocity at the propeller slice x=0.947814 at Fn=0.28 – bare hull96
Fig. 86 Axial velocity at the propeller slice x=0.947814 at Fn=0.28 - hull with appendages 96

Fig. 87 Axial velocity at the propeller slice x=0.947814 Fn=0.28 - hull with appendages and propeller 97
Fig. 88 Transom region views of Potential flow mesh 105
Fig. 89 SHIPFLOW User Manual example 106
Fig. 90 With transom and no transom functions for XMESH module 108
Fig. 91: Ship resistance representation..... 114
Fig. 92: Buoyancy of immersed body 116
Fig. 93: Buoyancy of fully submerged body..... 117
Fig. 94: Dynamic Pressure on fully submerged body 118
Fig. 95: Dynamic pressure on fully submerged symmetrical body with viscosity 119
Fig. 96: Combined non-viscous and viscous theories..... 122
Fig. 97: Symmetrical blunt submerged body 123
Fig. 98: Pressure acting on the free surface 125
Fig. 99: Free surface waves..... 126
Fig. 100: Wave parameters..... 127
Fig. 101: Two cases of position of waves crests generated on the stern depending on geometry of the stern without viscosity. 128
Fig. 102: Reduces of the wave crest in viscosity case 129
Fig. 103: Wave breaking on blunt hull types 130
Fig. 104: Wave slope on blunt body 131
Fig. 105: Total resistance components..... 132
Fig. 106: Total resistance alternative 133
Fig. 107: Total resistance diagram - final 134
Fig. 108: Reynolds experiment 147
Fig. 109 Reynolds experiment zoom in 147
Fig. 110: Cf as function of Reynolds number 150
Fig. 111: Total resistance coefficient in function of Reynolds number..... 153
Fig. 112: Total resistance coefficient in function of Reynolds number 2..... 154
Fig. 113: Total resistance coefficient in function of Reynolds number 3..... 155
Fig. 114: Worst case of summation of surface frictional and winemaking pressure resistance in submarines 157
Fig. 115: Moving High pressure point forward in fluid..... 158
Fig. 116: Free surface waves on conventional merchant ship 159
Fig. 117: Free surface waves on conventional merchant ship 2 160
Fig. 118: Pressure resistance on point on symmetry. Wigley hull..... 162
Fig. 119: Wigley free surface wave distribution..... 163
Fig. 120: Difference between Wigley hull and conventional merchant ship.... 164
Fig. 121: Resultant wave visualization in side view..... 164
Fig. 122: Wave interference with the hull..... 166
Fig. 123: Transversal wave velocity 167
Fig. 124: Velocity of transversal and divergent wave systems..... 167
Fig. 125:Rt vs Fn 168

Fig. 126: Ct vs Fn 169
Fig. 127: Source and sink 170
Fig. 128: Source plus sink dipole represent discontinuity in uniform flow 170
Fig. 129: Angle of entrance importance in ship wave making resistance 171
Fig. 130: Interference of waves in front part of the ship with and without bulbous profile 172
Fig. 131: Cross section view of normal ship and ship with bulbous form 173
Fig. 132: Waterline of flat plate and curved plate, with same Reynolds number 174
Fig. 133: Boundary layer on the moving ship 175
Fig. 134: Prolonged imaginary body due to effect of boundary layer 175
Fig. 135: Velocity distribution around the boundary layer 176
Fig. 136: Extreme blunt case in forward end 177
Fig. 137: Ct vs Rn 178
Fig. 138: Wind blowing at the angle through the ship 180
Fig. 139: Transversal projected area to the wind. Front view 180
Fig. 140: Velocity of air changes in height above the water 181

ABSTRACT

Objective:

The aim of this book is to numerically determine flow around the ship hull - DTMB 5415. Further analyses have been made on the different combinations of appendages attached to the ship's hull. As a result, influence of the appendages on the wake structure located in the propeller disk as well as the representation of the forces acting on appendages have been derived.

Content and methods:

- The free surface flow around a model surface ship (DTMB 5415) advancing in calm water under steady conditions is numerically simulated. The geometry of the DTMB 5415 ship hull was provided in igs file format. The combatant has been recommended by the 1996 International Towing Tank Conference as a benchmark case for CFD computations of ship resistance and propulsion.
- The SHIPFLOW code was employed to evaluate the flow field structure around the ship hull, the forces acting on bare hull and appendages. The solver computed the incompressible RANS equations on structured overlapping grids by using a finite volume technique. Turbulence modelling was achieved through the k-ε and k-ω SST or EASM models.
- The propeller was approximated as an active disk for which the solution has been given by a simplified hydrodynamic model. For practical reasons, XCHAP module has coupled a body forces method and a RANS-based finite volume solver to take into account the interactions between the hull and the appendages mounted on it: propellers, rudders, shaft lines, bossings, and brackets.
- Various configurations are investigated to establish the influence induced by the appendages on the flow filed.
- The numerical solutions obtained are compared with available experimental and other numerical data.

Expected results:

First step towards getting good experimental results is the potential flow calculation using mesh convergence study. After choosing good mesh, a preliminary potential flow resistance computation for five different speeds is being made. Then using the free surface results gained from the potential flow computation, new viscous flow resistance computations of bare hull DTMB 5415 are being made. The latter are compared with specific speeds for which experimental data already exists.

Final viscous flow calculations are done for the same hull but with different appendages using experimental speeds. Results show time averaged velocity, pressure, and turbulent quantities. They together will reveal not only the influences exerted by different configurations of the appendages on the wake structure in the propeller disk but also the forces acting on appendages.

Fig. 1:Combatant ship David Taylor Model Basin (DTMB) model 5415

Keywords: Free surface Flow, Overlapping Grids, Finite Volume Technique, Active Disk, Body Force Method

NOMENCLATURE

k – Turbulent kinetic energy

P – Instantaneous pressure

p – Time average pressure

p''_i – Fluctuating pressure

R_i – Volume force

Re – Reynolds number

S_{ij} – Strain-rate

U_i – Mean velocity components (i=1, 2, 3)

u_i – Time average velocity components

ui''_i – Fluctuating velocity components

W_{ij} – Rotation - rate

x_i – Cartesian coordinates

ϕ - General variable

ρ - Fluid density

σ_{ij} – Total stress tensor

μ - Dynamic viscosity

μ_T – Turbulent dynamic viscosity

υ - Kinematic viscosity ($=\mu/\rho$)

υ_T – Turbulent kinematic viscosity ($=\mu_T/\rho$)

δij – Kronecker delta

ω - Specific dissipation of turbulent kinetic energy

1. INTRODUCTION

The availability of the robust commercial computational fluid dynamics (CFD hereafter) software and high speed computing lead to increasing use of the CFD techniques for solving difficult problem regarding flow around complex geometry and different physical phenomena, such free surface and turbulence. The ships traveling at sea are with full appendages, and not only with bare hull. This influences the flow around the ship hull. Appendages part of the ship resistance is particular for each ship depending of the placement and geometry shapes. Differences in configurations of propeller, shaft line, struts, brackets, rudder, bilge keels, bow or stern thrusters, can greatly influence the resistance. Analysis of the flow around appended hull is beneficial for its practical use in the design process. Deeper knowledge of the physics about distribution of forces acting on the hull and interactions between them is needed. Enhanced understanding of the flow around appended hull will give option for further optimization of the hull shape and change the design in direction of increasing its performance and decreasing its economic cost. Another practical contribution with ship resistance investigation is determining hydrodynamic forces acting locally on the appendages. This data later on can be used for structural optimization.

In this context, **main objective** of this book is numerical investigation the flow around fully appended ship in order to determine the ship resistance and influences of appendages on ship propulsion.

The flow around appended ship hull can be investigated in four main manners:

a. Using data derived from published tests of series similar geometry ship models and interpolated by statistical approaches for particular warship dimensions.
b. Using towing tank tests from scaled model
c. Using computer simulation based on numerical methods on potential, boundary element and viscous theories
d. Using data from see trial test of constructed full (real) scale ship

Option a) does not have use for extensive investigation of the flow around ship hull. Option d) is unfeasible due to lack of tests from real build ship. In the book options, of towing tank simulations of different Froude numbers have been conducted. The numerical computations can help computer to solve such complicating problem like ship resistance. However, verification and validation from real world is still needed, that is the reason why towing tank tests are still extensively used. Towing tanks are expensive and complicated to do, which makes computer preferable choice if simulated results are good and they are topic for future research. Using traditional design techniques, many model tests in towing tank are required, the disadvantage is that they are expensive and need time. An alternative is needed and engineers start investigating in numerical simulations. Combination of Experimental Fluid Dynamics (hereafter EFD) such as towing tank tests and CFD techniques provide good investigation of local flow characteristics. With the help of this information, naval architect can improve the design.

Possibilities for reducing appendages drag from the total resistance can be done using study of each design configuration with appendages separately by CFD methods and model experiments. Realization of many experiments in testing facilities like towing tank on similar hull and appendages shapes with minor changes is impossible intended for industrial practices for costly and time-consuming reasons. Better alternative is using CFD software, which can make virtual towing tank. This way many different designs for optimization purposes can be investigated. With the optimized hull and appendage geometry or placement, an improved design of the ship will be achieved giving performance and economic benefits.

Wake is the region of recirculating flow immediately behind a moving ship, caused by the flow of surrounding fluid around the ship. Correct estimation of the effective wake can be used to make good propeller design. This wake is resulting from interaction of propeller's wake (when the propeller is working) and hull wake considering added effects from appendages. Overall shape of the wake becomes complex and can be further investigated only numerically with CFD or with experimental tests.

The SHIPFLOW 4.6 code is employed in the present study to evaluate the flow field around the appended ship hull, the forces acting on ship hull and appendages. The software consists of different modules: potential flow theory (XPAN), boundary layer theory (XBOUND), RANS and theory of actuator disk (XCHAP). Combination of the potential flow based on Rankine source method and boundary layer method for viscous effects is used for a set of preliminary computations in order to investigate the flow around bear hull.

Viscous free surface flow calculations investigate critical flow regions, allowing the naval architect to improve the hull forms and make homogeneous velocity distribution. Viscous methods are used for studying the hydrodynamic interactions between various appendages and arrangements; and to investigate regions with possible flow separations. Therefore, an understanding of the flow around the stern part of ship is of great practical interest. Viscous flow theory used in the thesis, describes the solution using Reynolds Averaged Navier Stokes equations solver (RANS hereafter). The solver computes the incompressible RANS equations on structured overlapping grids using finite volume method formulation, involving EASM and k-ω SST turbulence model. The RANS computations include the propeller model, which calculates the body-forces based on the effective wake field. This means that the implemented propeller solver in RANS code is running interactively with the RANS solver.

The book helps to reach the goal for investigation the flow around fully appended hull. Warship DTMB 5415 is ship, which has complicated hull shape, various appendages that has proven and it is used for testing in towing tanks. The combatant has been recommended by the 1996 International Towing Tank Conference as a benchmark case for CFD computations of ship resistance and propulsion as well as it has many results from towing tank tests. Taking into consideration the goal of the thesis for numerically investigating the flow around fully appended ship, hull form DTMB 5415 been chosen as a suitable test case.

Research is made of free surface flow and resistance at fixed trim around a hull in model scale of a naval ship DTMB 5415 advancing with constant speed and in calm (still) water under steady conditions. Initial free surface is undisturbed and considered flat. Combatant has been recommended by the 1996 International Towing Tank Conference (ITTC 1996) [12] as a benchmark case for CFD computations of ship resistance and propulsion computations. There is a large EFD database for Model 5415 due to a current international collaborative study on EFD/CFD and uncertainty assessment between Iowa Institute of Hydraulic Research (IIHR), Istituto Nazionale per Studi ed Esperienze di Architettura Navale (INSEAN), and the Naval Surface Warfare Center, Carderock Division (NSWC, formerly DTMB). Hull forms presented in ITTC 1996 can be used to verify computational codes with data measured from experimental tests. Validation data includes boundary layer and wake, longitudinal wave cuts, bow and transom wave fields, and wave breaking.

Model 5415 of David Taylor Model Basin were conceived as a preliminary design for a Navy surface combatant in 1980. The hull geometry includes both a sonar dome and transom stern further complicating the flow around the hull. Propulsion is provided through twin open-water propellers driven by shafts, supported by struts. Bare-hull surface geometry has been provided in universal standard IGES file format. Model with appendages but with different scale can be found in websites [24] and [25].

Table 1 Main particulars of DTMB

Designation	Prototype	Scaled Model
Scale ratio	1	1:24.82517
Length(m)	142.0	5.720
Breadth (m)	19.06	0.768
Depth (m)	11.00	0.443
Draft (m)	6.15	0.248
Displacement (m^3)	8424.4	0.552
Wetted surface (m^2)	2972.6	4.861
Block coefficient (C_B)	0.507	0.507

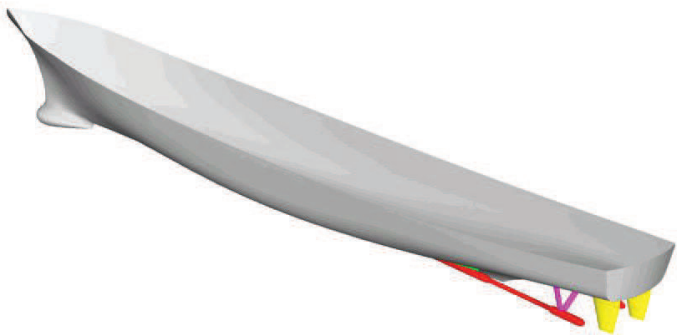

Fig. 2 Computer visualization combatant ship David Taylor Model Basin (DTMB) model 5415 with appendages

This section describes the structure of the report:

Chapter two short description of SHIPFLOW software.

Chapter three includes brief explanation of the governing equations, used hypothesis, boundary conditions, advantages, and disadvantages of the potential flow method and boundary element theory. As final the results from preliminary computation using potential flow method are being provided.

Chapter four consists of theoretical methods used in viscous computation, description of hypothesis, mathematical model, numerical scheme, boundary conditions used for running the viscous flow computation in SHIPFLOW, advantages and disadvantages of the method. As final the results from viscous flow computation are made for different Froude numbers as well

as compared with experimental data for the Froude numbers 0.28 with Reynolds number Rn=8.31e+06 and Froude numbers Fn = 0.41 with Reynolds number Rn=1.24E+07. Calculations with free surface used from potential flow solution are made for bare hull, bare hull plus rudder for 6000 iterations of the viscous solver.

Chapter four presents a conclusion and future perspective of the work for investigating the flow around fully appended ship hull.

Definition of offset file (prepared for discretization of the hull) based on geometry of the ship given in IGES file format.

Solutions of the flow using potential model for various Froude and Reynolds numbers, used later for compare wave resistance, lift and as input for boundary layer method to predict the transition and characteristics of boundary layer in the forward half of the ship.

Solutions of the flow, using viscous RANS code with free surface boundary conditions defined by potential flow results. The free surface is obtained as potential-flow solution and it is kept fixed for the solution of the RANS equations.

Two main solutions will be made with experimental results for Froude numbers: 0.28 and 0.41: bare hull, bare hull with rudder.

2. DESCRIPTION OF USED SOFTWARE

2.1. Ship Flow Overview

Used software for the simulating performances of DTMB 5415 is FLOTECH SHIPFLOW version 4.6.00-x86_64. This CFD code has following computation capabilities: resistance, propulsion, and manoeuvring.

XCHAP is a module of SHIPFLOW, which solves Reynolds Averaged Navier-Stokes equations using one of several available turbulence models (EASM, k-ω BSL, k-ω SST). With XCHAP it is possible to use overlapping grids and the module can be used for both zonal and global approaches. XCHAP uses the grid generated by XGRID but it is also possible to import grids created by other software. By using this solver, it is possible to get the time averaged velocity, pressure, and turbulent quantities.

Methods for simulating ship resistance problems are incorporating different theories like potential flow theory, boundary layer theory and RANS viscous theory. The main difficulty is to determine the fluid forces acting on the hull (including propeller and rudder) due to ship motion. The free surface and viscous effects also should be considered.

2.1.1. Ship Resistance

In SHIPFLOW resistance problem is computed in still water with simplified form of Navier Stokes equations of motion. There are two ways for calculating the resistance using:

a. Potential flow theory utilizing Laplace equation combined with boundary layer theory
b. Viscous flow theory utilizing RANS (Reynolds Averaged Navier Stokes equations).

2.1.2. Propulsion

SHIPFLOW has two options for computation of propulsion: propeller open water test and self-propulsion test. First, one determines the performance of the propeller in uniform flow, and second determines performance of the propeller in the wake of the ship. In self-propulsion test, the hull creates non-uniformity of the flow, which propagates to the propeller and changes the magnitude and distribution of the forces. SHIPFLOW incorporates hybrid method based on RANS equations, lifting line, and actuator disk theories.

2.1.3. Maneuvering

In SHIPFLOW manoeuvring is based on RANS method, and if propeller is simulated there is incorporation of lifting line method. SHIPFLOW cannot compute the flow around ship with rotating propeller. Two type of test can be simulated:

a. Computation of oblique flow with different drift angles and different angle of attack of the rudder
b. Rotating arm test

2.2. Software Structure

SHIPFLOW has several modules. The software operating process has been divided on three main parts: pre-processing, processing and post processing.

2.2.1. Pre-processing / Input Data Modules:

Pre-processing part contains of two files, which need to be provided to SHIPFLOW to start simulation:

a. OFFSET FILE, which contain information about hull shape;
b. COMMAND FILE, which contains the configuration for the solution.

These two files are read and processed by next modules.

Offset file is used for review and edit the ship coordinates at different sections. It can be generated from external software like Tribon M3 or Rhinoceros - from iges or dxf/blines file formats. Visual verification and edit of different sections can be made with software SHIPFLOW DESIGN.

Command file gives instructions and configures SHIPFLOW solver. It is edited by Notepad++ and trough plug-in attachment SHIPFLOW program is started using command file.

2.2.2. Processing Data Modules:

a. Modules for potential flow solver are:

- XMESH is a panel generator of the ship hull and free surface for the potential flow. Reads offset file then discretizes the ship and free surface.

- XPAN is the flow solver for the potential flow around three-dimensional bodies based on a surface singularity panel method. It reads command file.

- XBOUND is a module used for turbulent boundary layer computations. The momentum integral equations for boundary layers are solved along streamlines traced from a potential-flow computation. XBOUND is also capable of computing the laminar boundary layer and the transition to the turbulent boundary layer for simpler cases with a well-defined stagnation point or line. The computations can be carried out for a smooth surface or for a specified surface roughness. It also reads command file.

b. Modules for viscous flow solver are:

- XGRID is a panel generator of the ship and the volume around it for the viscous flow. It makes a grid with one boundary surface fitted to the free surface computed by XPAN. Reads offset file and discretizes the ship and whole water domain it is used for the viscous computations in XVISC and XCHAP. XGRID cannot handle appendages. It computes boundary points, makes interpolation to 3D grid, then with Poisson solver computes control functions by iteration makes coarse grid and refines it using interpolation. A special restriction applies for XGRID about constant x-frames and frames in the abgr must be continued in the ogrp. Two ways of defining grid exists with half ship length (zonal approach) and with full ship length.

- XVISC is former viscous module based on a finite difference schemes code that solves the Reynolds Averaged Navier Stokes equations on stern part of the ship. It uses a standard two-equation turbulence model (k-epsilon). Boundary conditions are generated from results provided by XPAN and XBOUND (the zonal approach). For rest the flow XVISC can use information derived from solved potential flow and boundary layer theory solution. Limitations include twin skeg, appendages, deep submerged transom, pronounced tunnel stern, restricted water (shallow water, canal), and free surface effects.

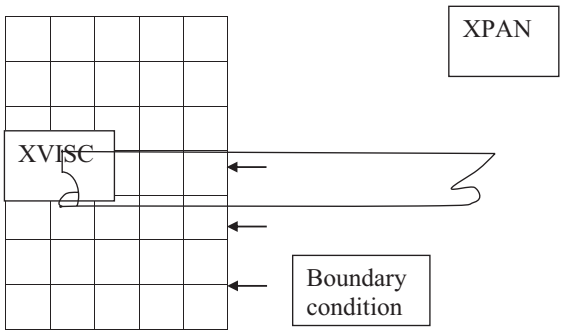

Fig. 3 Former XVISC simulation of the viscous flow

- XCHAP is a finite volume code that solves full viscous flow using the Reynolds averaged Navier-Stokes equations. It uses several turbulence models (EASM, k-ω BSL, k-ω SST). The solver can be used in a zonal or a global approach it can handle overlapping grids. Grids can also be imported from external grid generators. There are also two actuator disk models available, a simple force model, and a lifting line model. The flow on free surface can be computed with a double model or with a prescribed free surface from XPAN. XCHAP can use the grid provided by XGRID. Inflow boundary conditions are generated from results provided by XPAN and XBOUND when zonal approach is used. XCHAP can also use block-structured grids generated in an external grid generator. These grids can be either the entire hull so that no XGRID grid is needed or appendage grids that are added to XGRID grid. XCHAP has limitations in working at restricted waters.

2.2.3. Post-processing data modules:

- SPOST is module controlling visualization of the output data but it is not user-friendly.

Additional output files in SHIPFLOW gives different output files as data or visualization like:

- id_cgns, file which can be used with visualization software like TECPLOT to visualize the solution.

- id_OUTPUT give summary of results like Cw, Cf – wave and friction coefficients, hydrostatics, grid information.

- id_CONV Gives norms of residuals from last run of XCHAP.

- id_FORCELOG gives history of integrated forces in viscous flow from the last run.

- id_OPTRES gives results for ship computed resistance, displacement, LCB and wetted surface area.

- id_SUMMARY makes of SHIPFLOW calculations for resistance, sinkage and trim.

Task & Case Study: Simulate and compare free surface flow around a model surface ship DTMB 5415 advancing in calm water under steady conditions with experimental results. Combatant has been recommended by the 1996 International Towing Tank Conference as a benchmark case for CFD computations of ship resistance and propulsion.

2.3. SHIPFLOW application

2.3.1. Geometry preparation

The geometry must be already defined in design software. For this reason, the hull is modelled in TRIBON M3 system where the mesh is exported in ".dxf" file format and imported into Rhinoceros. Using command: Generate sections (stations) --> Generate the points on each station, Rhinoceros allows making points with coordinates, which lie on the surface. There the points on the each needed transversal stations are generated. Stations are many around 200 for one offset file, and can be more, where there is more curvature or need for more accurate results. The coordinates file is exported as ".txt" format and imported in offset file. This offset file needs to be transferred, and transformed so SHIPFLOW software can understand it.

When transitioning from offset file to SHIPFLOW, there is a change in the coordinate system. In the offset file, the coordinate system is on the bottom of the rudderpost. It is transferred to intersection between free surface and ship hull in the fore part of the ship for the calculation needs of the solver. This transformation of the coordinate system is done in configuration file utilizing function "offsetfile", in which xori = length between perpendiculars of the ship and zori = draft of the ship. If offset file is done in the as in DTMB 5145 first the bulb group and then the hull group no need of longitudinal transformation of coordinate system is needed and xori = zero.

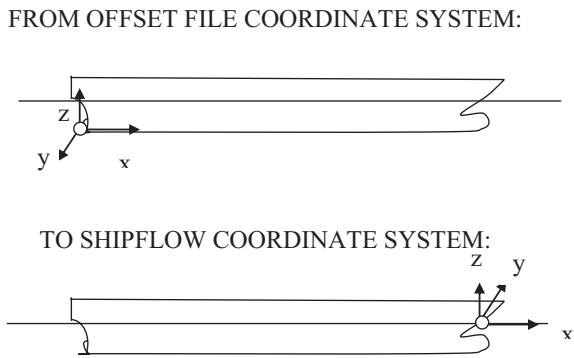

Fig. 4 Transforming coordinate systems from offset file to SHIPFLOW

For input data SHIPFLOW software is using offset file, introducing x, y, z coordinates of points in different stations of the hull. With the help of different panelization modules like XMESH or XGRID, SHIPFLOW generates discretized surface on the body, which is then used for the calculations. The discretization depends on the configuration of the modules, and it interpolates the already given geometry points from the offset file. In this way, one geometry file can have different grids and meshes for potential and viscous flow computations to satisfy requirements for each solution.

a. Offset file structure

Offset file is divided on offset groups. Each group contains number of transversal stations. Different points on station have the same x coordinate and dissimilar coordinates in y and z direction. Stations are differentiated beginning from bow to stern, points are ordered starting from keel to deck. Usually on the standard ship hulls, they are 4 main groups: 1 H1GR - hull, 2 OGRP – stern overhand, 3 FBGR – fore bulb, 4 ABGR – aft bulb. However, for investigated hull shape DTMB 5415 there are only two groups named 1 H1GR = hull and 3 FBGR = fore bulb - sonar.

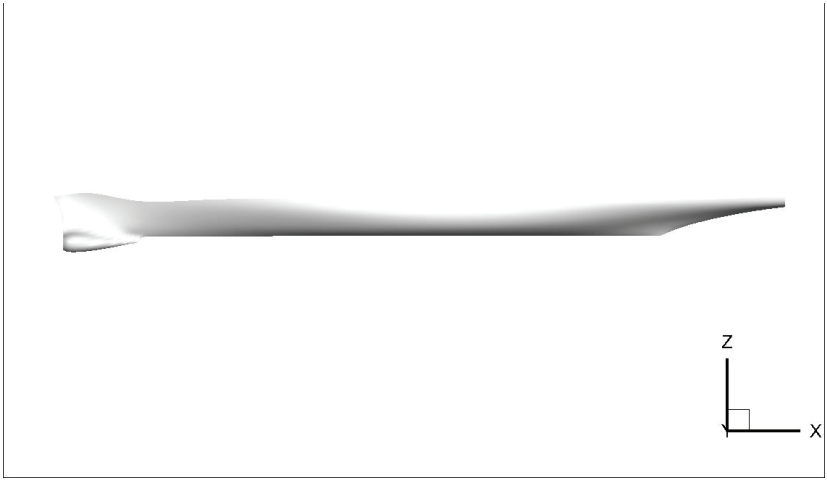

Fig. 5 Geometry of DTMB 5415

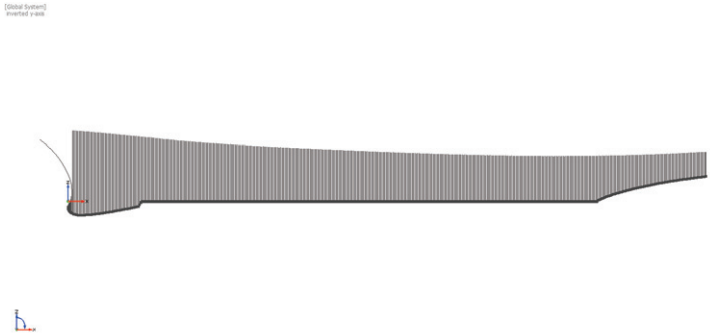

Fig. 6 Offset file of DTMB 5415

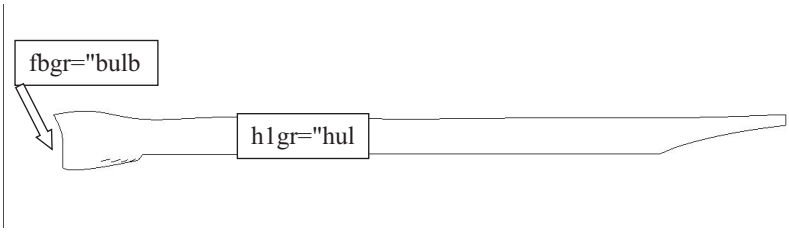

Fig. 7 Groups used for DTMB 5415

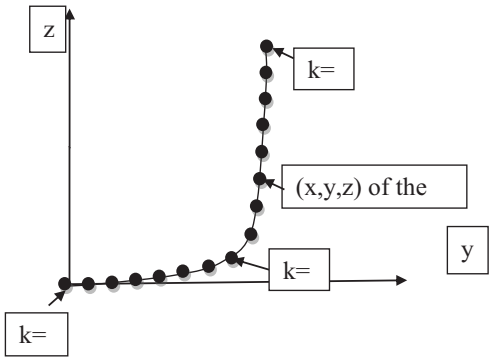

Fig. 8 Transversal cross section - station of ship geometry used in offset file of SHIPFLOW

Each offset file consists of following structure. First, there is the name of the group and then four columns of data about the point coordinates in the different stations. After the first group is over then the next group is starting again with name and four columns of data and this process is repeated until the "end" command when the whole ship is defined. First column shows x value, second shows y value and third shows z value of the coordinates for each point part of that group and station. There is fourth column called the "k". It can take three values with three different meanings for the function of the point: 1 – starting point of group, 0 - inside point of group, 9 - last point from group.

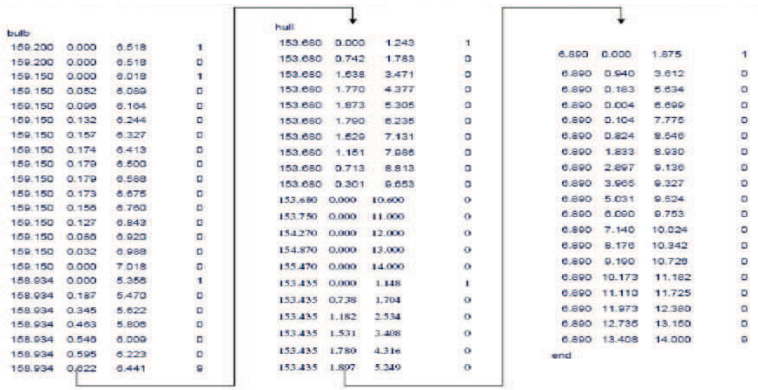

```
bulb
159.200  0.000  6.518  1
159.200  0.000  6.518  0
159.150  0.000  6.018  1
159.150  0.052  6.089  0
159.150  0.098  6.164  0
159.150  0.132  6.244  0
159.150  0.157  6.327  0
159.150  0.174  6.413  0
159.150  0.179  6.500  0
159.150  0.179  6.588  0
159.150  0.173  6.675  0
159.150  0.158  6.760  0
159.150  0.127  6.843  0
159.150  0.086  6.923  0
159.150  0.032  6.988  0
159.150  0.000  7.018  0
158.934  0.000  5.356  1
158.934  0.187  5.470  0
158.934  0.345  5.622  0
158.934  0.463  5.806  0
158.934  0.546  6.009  0
158.934  0.595  6.223  0
158.934  0.622  6.441  9
hull
153.680  0.000  1.243  1
153.680  0.742  1.783  0
153.680  1.638  3.471  0
153.680  1.770  4.377  0
153.680  1.873  5.305  0
153.680  1.790  6.235  0
153.680  1.629  7.131  0
153.680  1.151  7.986  0
153.680  0.713  8.813  0
153.680  0.301  9.653  0
153.680  0.000  10.600  0
153.750  0.000  11.000  0
154.270  0.000  12.000  0
154.870  0.000  13.000  0
155.470  0.000  14.000  0
153.435  0.000  1.148  1
153.435  0.738  1.704  0
153.435  1.182  2.534  0
153.435  1.531  3.408  0
153.435  1.780  4.316  0
153.435  1.897  5.249  0
6.890  0.000  1.875  1
6.890  0.940  3.612  0
6.890  0.183  5.634  0
6.890  0.004  6.699  0
6.890  0.104  7.775  0
6.890  0.824  8.846  0
6.890  1.833  9.930  0
6.890  2.897  9.136  0
6.890  3.965  9.327  0
6.890  5.031  9.524  0
6.890  6.090  9.753  0
6.890  7.140  10.024  0
6.890  8.176  10.342  0
6.890  9.190  10.729  0
6.890  10.173  11.182  0
6.890  11.110  11.725  0
6.890  11.973  12.380  0
6.890  12.735  13.150  0
6.890  13.408  14.000  9
end
```

Fig. 9 Structure of offset file

3. POTENTIAL FLOW METHOD

3.1. Description of the method

First step in CFD investigation of the flow around hull without appendages is making resistance calculations using potential flow method and boundary layer theory.

Two main reason of making this simulation exists:

- First reason behind doing potential flow computation accompaniment with boundary layer theory is to determine preliminary view of the flow.

- Second reason is to determine the free surface. It is needed for starting the viscous flow computation, which will to fit the viscous mesh of the solution with respect free surface grid. This method is hybrid between potential flow solution for free surface and viscous flow solution.

In the thesis is performed potential flow computation, to have first view of free surface and flow around the ship hull. This determines the free surface elevation, which is needed for importing in viscous computation. The free surface computation has good results in potential flow, and the free surface can be imported in viscous flow solution.

3.2. Mathematical model of Potential flow theory

3.2.1. Hypothesis. Governing Equations

Assumption is made that the ship hull advances in the undisturbed water with a constant velocity U_∞. The potential flow assumption of inviscid and irrotational flow is made for the steady flow around the hull. Equation field and boundary conditions are expressed in terms of velocity potential. The problem is numerically solved making use of distribution of Rankine sources on the boundary surface. Potential flow theory determines wave resistance component of the total resistance and it is based on integration of the pressure acting on the ship hull when it is moving through the water. It works on basis of Rankine source panels with options of calculating transom, lift, sinkage and trim. The ship is specified in a coordinate system having its x-axis parallel to the longitudinal direction, the y-axis to the direction of starboard and the z-axis pointing upwards. The coordinate system has the same speed as the ship but does not follow the ship movements such trim and sink.

Considering that the flow is inviscid, which means that the fluid is frictionless and it is irrotational, so the particles in the fluid cannot rotate, the governing equation of the flow is continuity equation. The general expression of conservation of mass equation is:

$$\frac{\partial \rho}{\partial t} + \frac{\partial(\rho u)}{\partial x} + \frac{\partial(\rho v)}{\partial y} + \frac{\partial(\rho w)}{\partial z} = 0 \tag{1}$$

The incompressibility of the fluid is generally assumed in all physical modelling of phenomena in which fluid is water. Moreover, when the flow is steady the pressure does not depend on time and it is constant so its derivative with respect to time is removed. The continuity equation becomes:

$$\frac{\partial u}{\partial x} + \frac{\partial v}{\partial y} + \frac{\partial w}{\partial z} = 0 \tag{2}$$

From mathematical point of view, if the flow is inviscid, irrotational, and incompressible, a scalar function named the velocity potential ϕ can be defined. Thus, velocity vector can be expressed as a gradient of velocity potential:

$$u = \frac{\partial \phi}{\partial x} v = \frac{\partial \phi}{\partial y} w = \frac{\partial \phi}{\partial z} \text{ or } \mathbf{V} = \nabla \phi \tag{3}$$

In the end, by introducing the velocity (3) into the continuity equation (2) the Laplace equation is obtained:

$$\frac{\partial^2 \phi}{\partial x^2} + \frac{\partial^2 \phi}{\partial y^2} + \frac{\partial^2 \phi}{\partial z^2} = 0 \text{ or } \nabla^2 \phi = 0 \tag{4}$$

Using finite elements, volumes, or difference schemes the equations for boundary conditions and Laplace can be solved. Laplace equation is linear and solutions can be superimposed. The Panel Method described in [33] is used for finding solutions to the Laplace equation. This method is implemented in the SHIPFLOW software, was used in this investigation. The 3D problem is solved using surface descriptions with common elementary solutions like: free stream flow, point source/sink, and point doublet.

Bernoulli equation shows that pressure, kinetic energy and, potential energy must be constant along streamline.

$$\rho + \frac{\rho u^2}{2} + \rho g h = C \tag{5}$$

Linearity of Laplace equation offers the possibility to combine elementary solutions (sources, sinks, doublets) to arbitrarily complicated solutions. Thus, one can consider the total velocity potential as a sum of double model velocity potential and the perturbation velocity potential due to presence of free surface:

$$\phi = \phi_0 + \phi_w \tag{6}$$

3.2.2. Boundary Conditions for Potential Flow Method

Douglas method is used for solving potential flow without lift and without free surface for 3D surfaces. It uses flat panels with constant source strength with two boundary conditions. The method computes velocity and pressure solving linear system of equations by Gaussian elimination with an iterative solver. With free surface option, disturbances are generated on the hull and on the waves, which need to be captured. The potential is subject to the several conditions on the hull and free-surface boundaries.

a. Boundary conditions of potential flow without free surface

First boundary condition imposed on the hull surface requires that the velocity potential normal to the hull surface should be equal to zero:

$$\frac{\partial \phi}{\partial n} = 0 \tag{7}$$

Limit of the potential as it goes away from hull surface is equal to U speed.

$$\lim_{r \to \infty} \nabla \phi = U \tag{8}$$

b. Boundary conditions of potential flow with free surface

Potential flow solution with free surface further complicates boundary conditions; they are described below in figures (Fig.10, Fig.11) as well as formulated as follows.

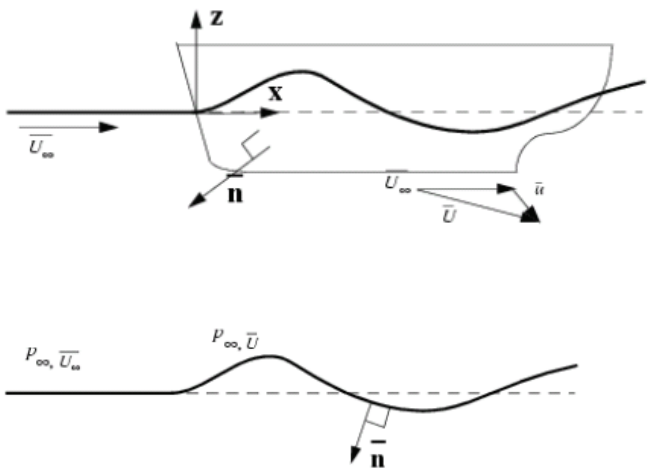

Fig. 11 Boundary conditions for the free surface

Kinematic boundary condition – the flow in normal direction of the free surface is equal to 0. The flow potential in the normal direction of the free surface is zero. The mathematical expression of kinematic free surface boundary condition is:

$$\frac{\partial \phi}{\partial x}\frac{\partial h}{\partial x}+\frac{\partial \phi}{\partial y}\frac{\partial h}{\partial y}-\frac{\partial \phi}{\partial z}=0 \tag{9}$$

The other condition to be satisfied on the free surface comes from the fact that the pressure on the free surface must be equal to the atmospheric pressure, which we assume that is constant. This condition is derived from Bernoulli equation

$$h+0.5(\left(\frac{\partial\phi}{\partial x}\right)^2+\left(\frac{\partial\phi}{\partial y}\right)^2+\left(\frac{\partial\phi}{\partial z}\right)^2-U_\infty{}^2=0 \tag{10}$$

Upstream disturbance by a moving ship vanishes at infinity:

$$\lim_{r\to\infty}|\nabla\phi|=0 \tag{11}$$

Finally, the radiation condition must be imposed (enforced) to avoid upstream waves. The radiation condition cannot be described by an exact mathematical expression. It has to be enforced by exact mathematical expressions. It has to be enforced by numerical schemes.

The free-surface problem described above it is difficult to solve since the free surface boundary conditions are non-linear and must be satisfied on the initially unknown wavy surface. The solution for this problem is to linearize the free surface boundary conditions around a known solution and solve the problem in an iterative manner. In the first iteration, the problem is linearized around the double model solution and then around the solution obtained from previous iteration.

Moreover, a boundary condition for transom stern can be imposed:

$$\frac{\partial\phi}{\partial x}+\sqrt{U^2-gz_T}=0 \tag{12}$$

In the end, forces and moments, including wave resistance are computed by integrating pressure over the ship hull.

$$Rw=-\iint_S \rho n_x dS \qquad T=\iint_S \rho n_z dS \qquad MT=\iint_S \rho n_z(x-x_0)dS \tag{13}$$

Potential flow future supports free surface calculations with linear or nonlinear boundary conditions. Limitations are in wave breaking, forming sprays as well as viscous interaction on wave making. The method works in only for some ranges of speeds.

All theoretical mathematic derivations have been referenced from [29] to [36].

3.2.3. Boundary layer theory

Boundary layer theory is used to assist potential flow with computing friction coefficient, used compute the total resistance. It has capabilities as simulating streamlines (potential-flow streamlines show the flow direction at the outer edge of the boundary layer) as well as limiting streamlines (show the flow direction at the hull surface) and calculation with free surface. Streamlines are series of curves running tangent to the means of velocity vectors taken for short time exposure. Method is accurate over main part of the hull and captures transition from laminar to turbulent flow. The theory usually fails to compute complicated flows such as regions around stern of the ship. In the aft part, usually there are violent turbulent phenomena, which cannot be captured by this methodology.

Theory of boundary layer has limitations for working only with very thin boundary layers. Reason behind is very limiting assumption of using the input data from potential flow calculation in which the velocity is varying in only one direction of the flow. Pressure resistance and separated flow also cannot be computed. Potential flow theory combined with boundary layer theory is the first and fast option for calculating ship resistance via SHIPFLOW and they both support high-speed vessels such as warships. It can visualize streamlines of the flow, boundary layer thickness, and skin friction coefficient on the hull. Results include local skin friction coefficient, boundary layer thickness, displacement thickness, momentum thickness, wall cross flow angle. Advantages are that the method is very fast and accurate over the main part of the hull. It calculates also the transition between laminar and turbulent phenomenon. Disadvantages are it is unusable for big boundary layers, vortexes, and separation, this means regions like stern or complicated hull shapes like sonar part of the DTMB 5415.

More theoretical methodology about boundary layer theory can be found [36].

4. FREE SURFACE FLOW SIMULATION AROUND COMBATANT SHIP

4.1.1. Description of this Chapter

This chapter presents penalization, for different cases with transom and without transom, number of required panels for each examined Froude number. Results for four different cases at six Froude numbers: no transom, no trim; No transom, trim; transom, no trim; transom, trim are given. Graphs of total resistance coefficient, wave coefficient, and skin friction coefficient as well as percentage difference from experimental data are shown. Free surface elevation and pressure distribution are presented for transom, no trim case. Conclusions are made below each graph.

4.1.2. Panelization

A good panelization is one of the most important elements of getting a good solution and a reasonable balance between computing time and accuracy. As long as Panel Method is boundary value method, only hull and free surface should be discretized.

Few lines about dimensions of the domain (The calculation are done for surface domain of range 0.3-0.57 ship length upstream, 0.73 – 1.46 ship length downstream, the width of the free surface is 0.53-1.54 ship length.) For infinite depth, the angle of the dihedron of Kelvin is constant and does not depend on the shape of the floating body stays at 19,28^{o}. That is the reason to choose greater width of the domain capturing the dihedron.

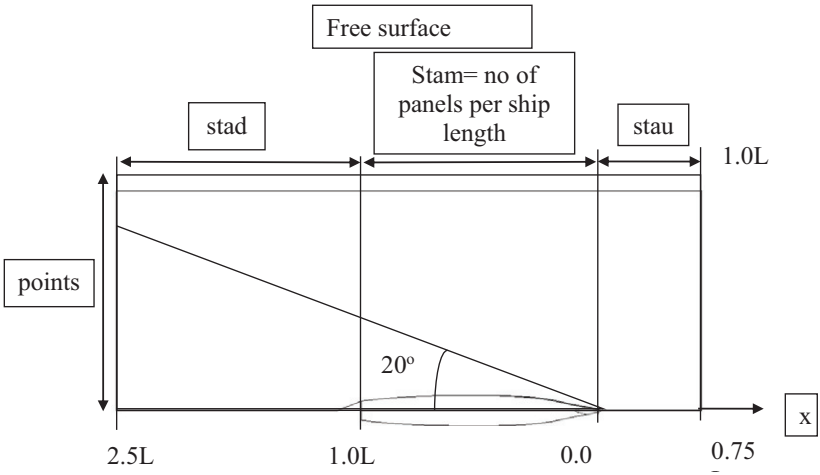

Fig. 12 Domain relationship with number of panels

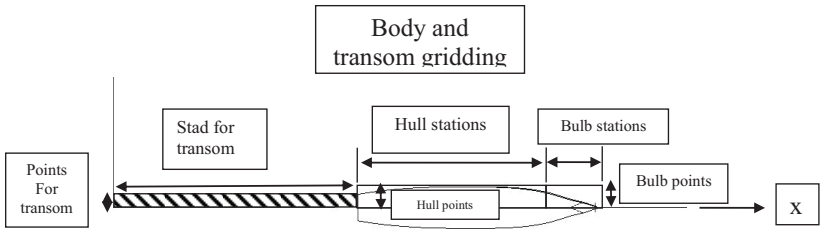

Fig. 13 Transom and body relationship with number of panels

The number of hull panels depends on the curvature of hull surface. If there is higher curvature, more panels need to be used. All panels must be clustered towards the bow and stern on the hull. The reason is of the larger flow gradients and complex curvature of the geometry in these parts. The hull is discretizing in range 6359 - 10650 panels as it is depicted in Figure 14. Detailed views of the fore and aft panelization are represented Figures 15 - 16.

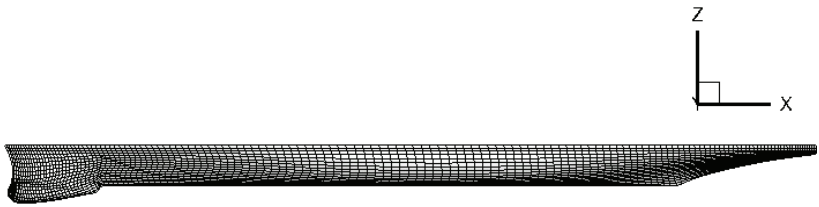

Fig. 14 Side view of the hull panelization

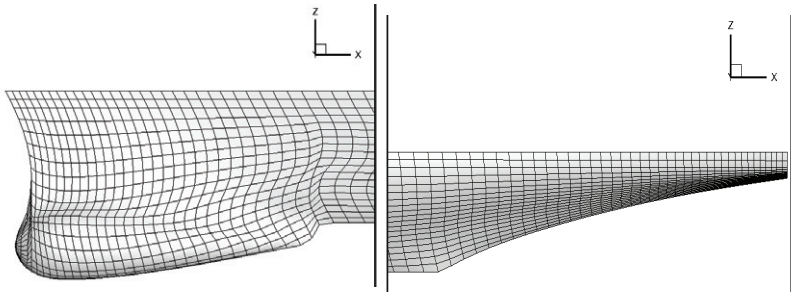

Fig. 15 Forward part of the ship - (Side view)

Fig. 16 Aft part of the ship - (Side view)

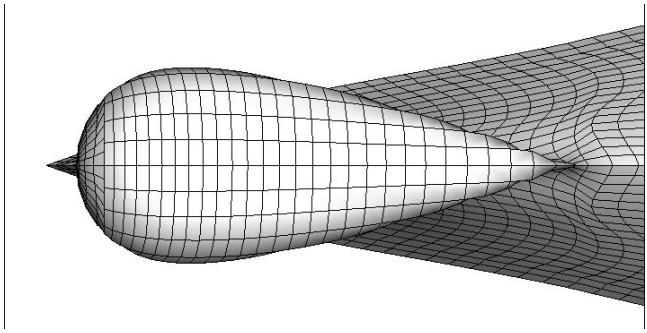

Fig. 17 Sonar panelization (Bottom view)

In order to obtain accurate results, the free surface should be discretized on longitudinal direction by minimum 25-30 panels by wavelength. Moreover, stretching functions must be also used for cluster the panels towards the regions where it is expected to develop wave crests. The numbers of panels on the free

surface are determined by the Froude number and depend on the domain dimensions. The wavelength (λ) of the wave generated by the ship depends on the Froude number and can be calculated by formula:

$$\lambda = 2\pi LFn^2 \tag{14}$$

Considering the computational time and the accuracy of the solution, thirty panels were chosen for transversal directions.

Transom option of potential flow module XMESH makes discretization of the free surface downstream the transom stern. This option it is used for high speed vessels, sailing yachts, tunnel sterns and for flat overhang sterns and it usually works with Froude numbers bigger than 0,22. This is because the speed of flow is fast enough to detach in the aft part of the ship. If velocity is smaller, there will be so-called dead water and viscous effects, which cannot be captured with potential flow Figures 18, 19 depicts panelization of the free surface in no transom case (left) and transom case (right). Dense mesh is also made around the waterline of the hull on the free surface.

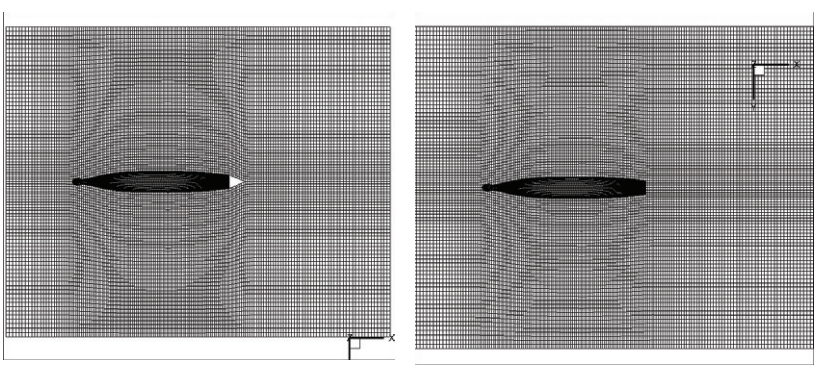

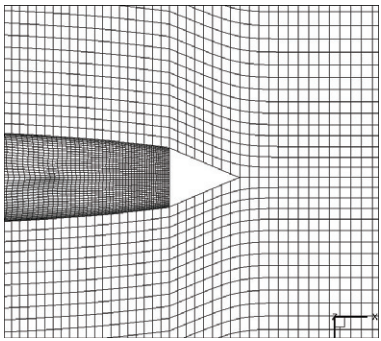

Fig. 18 Free surface no transom case

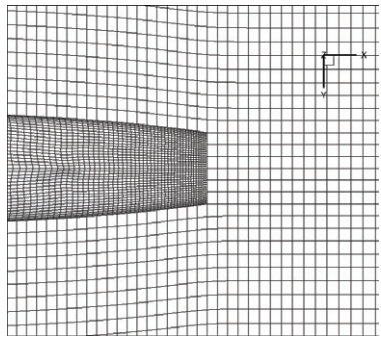

Fig. 19 Free surface with transom case

For no transom case total number of panels is in range 6045 – 10247 and for transom case is in rage 6523 – 10894.

Table 2: Minimum Number of panels for different Froude Numbers

Minimum required number of pannels	Wavelenght - λ	Speed =Fn.sqrt(gL)	Froude Number
[m]	[m]	[m/s]	-
60	1.99	1.76	0.24
82	2.74	2.07	0.28
100	3.35	2.29	0.31
129	4.29	2.59	0.35
172	5.74	2.99	0.40
209	6.96	3.30	0.44

Minimum number of panels to capture the wavelength resolutions is 30 recommended by SHIPFLOW manual, computed numbers of panels are with good correspondence with the requirement.

Table 3: Used grid properties for no transom case and transom case

	Free surface				Hull		Bulb		No Transom		Transom			
Froude	points	stau	stam	stad	station	point	station	points	Total number of panels	Total number of nodes	points	stad	Total number of panels	Total number of nodes
0.24	45	25	84	61	150	18	5	18	10247	10650	4	61	10427	10894
0.28	43	21	63	54	150	18	5	18	8569	8938	4	54	8728	9154
0.31	43	20	53	50	150	18	5	18	7939	8293	4	50	8086	8493
0.35	42	18	43	47	150	18	5	18	7204	7542	4	47	7342	7730
0.40	43	17	33	43	150	18	5	18	6381	6703	4	43	6507	6875
0.44	43	16	28	41	150	18	5	18	6045	6359	4	41	6165	6523

The user grids used for different Froude numbers are with good agreement with experimental free surface, and can be used for viscous flow computation.

4.2. Results and Discussion for Potential Flow Free Surface Solution

Results given from experimental data are for Froude numbers between FN=0.1 to 0.45. From CFD simulation limitations it was decided that the investigated Froude numbers will be in the range from 0.2 to 0.45. Potential flow simulation use XPAN and XBOUND modules. Total resistance (Rt) obtained from the computations is based on the fallowing expression:

$$Rt = 0{,}5.\rho U^2.WSA.Lpp^2(Cw + Cftot) \qquad (15)$$

Where ρ=1000 kg/m^3, U is ship speed, WSA – wetted surface area, Lpp – length between perpendiculars, Cw – wave resistance coefficient, and Cftot is the friction resistance computed in XBOUND. All results are non-dimensionalized with Lpp or ship speed. For resistance Rt is given in Newtons.

In the EFD it is not specified if the measurements are performed with or without trim. That is the reason for taking different cases mentioned below.

Taking into consideration the wide range of Froude numbers, four sets of numerical simulation were performed in order to accurate determine the total resistance and free surface elevation:

1. No transom, no trim;
2. No transom, trim;
3. Transom, no trim;
4. Transom, trim;

Percentage differences between experimental and calculated results are given in Table 9.

The colour specification in the tables of results is as follows: in red are shown results with greater values, which it is not good from resistance point of view. In green are shown good values from resistance point of view. In blue, yellow, and grey background are shown problem solutions and their modification.

In Froude **0.35** they are no computed results for Cf so corresponding value for Rt from modified grid case is used. Taken value is with grey background.

In Froude **0.24,** Cf is used from simulated values in case TRANSOM with NO TRIM, and Rt is recalculated using following formula from SHIPFLOW manual to receive estimation of final results for problematic Froude numbers. This is done for two cases in first Froude number of NO TRANSOM and NO TRIM, and TRANSOM with TRIM. Recalculated values are with blue background.

There is a problem of Cf coefficient in Froude number **0.40**, and it is being linearly interpolated from near values for all the cases it is marked with yellow background.

Table 4: 5 FROUDE NUMBERS, NO TRANSOM and NO TRIM

Froude	Rt	Cw	Cf
0.24	31.2	1.07E-04	4.05E-03
0.28	43.4	1.90E-04	4.00E-03
0.31	56.3	4.52E-04	4.00E-03
0.35	73.6	5.37E-04	4.00E-03
0.40	127.8	1.88E-03	4.01E-03
0.44	184.5	3.00E-03	4.01E-03

Table 5: 1 FROUDE NUMBERS, Modified grid, NO TRANSOM and NO TRIM

Froude	Rt	Cw	Cf
0.35	73.55	5.30E-04	4.00E-03

Table 6: 5 FROUDE NUMBERS, NO TRANSOM and TRIM

Froude	Rt	Cw	Cf
0.24	33.29	0.00038	0.00404
0.28	45.45	0.00035	0.00403
0.31	57.37	0.00054	0.00400
0.35	75.59	0.00062	0.00404
0.40	129.09	0.00198	0.00397
0.44	184.04	0.00307	0.00392

Table 7: 5 FROUDE NUMBERS, TRANSOM and NO TRIM

Froude	Rt	Cw	Cf
0.24	35.05	0.00062	0.00405
0.28	49.26	0.00074	0.00401
0.31	63.27	0.00099	0.00402
0.35	82.40	0.00106	0.00402
0.40	139.38	0.00244	0.00398
0.44	196.65	0.00352	0.00395

Table 8: 5 FROUDE NUMBERS, TRANSOM and TRIM

Froude	Rt	Cw	Cf
0.236	38.377	0.001	0.004
0.277	52.985	0.001	0.004
0.306	66.231	0.001	0.004
0.346	85.739	0.001	0.004
0.400	143.827	0.003	0.004
0.441	200.907	0.004	0.004

Table 9: SUMMARY OF RESULTS FROM POTENTIAL FLOW CASES

General Table of the resistance under potantial flow										
			Case 1		Case 2		Case 3		Case 4	
		Experimental	No transom, No trim		No transom, Trim		Transom, No Trim		Transom, Trim	
Speed =Fn.sqrt(gL)	Froude	results [N]	Value	% difference from Experimental data	Value	% difference from Experimental data	Value	% difference from Experimental data	Value	% difference from Experimental data
1.76	0.24	30.6	31.2	0.02	33.3	0.09	35.0	0.15	38.4	0.25
2.07	0.28	44.3	43.4	-0.02	45.5	0.03	49.3	0.11	53.0	0.19
2.29	0.31	57.9	56.3	-0.03	57.4	-0.01	63.3	0.09	66.2	0.14
2.59	0.35	78.1	73.6	-0.06	75.6	-0.03	82.4	0.06	85.7	0.10
2.99	0.40	135.3	127.8	-0.06	129.1	-0.05	139.4	0.03	143.8	0.06
3.30	0.44	196.7	184.5	-0.06	184.0	-0.06	196.6	0.00	200.9	0.02

Results show good correlation between simulation and experiment in No transom, no trim case for low Froude numbers and good results for Transom, no trim case for high Froude numbers, and penalization of free surface can be used for further investigation with viscous computation.

Figure 20 depicts the comparison between ship resistance curves calculated for each case and measured. Rt from different cases has same trend as

the experimental results, this means that the physics are captured well. The slope for curves of Cw for different cases changes at the same speed.

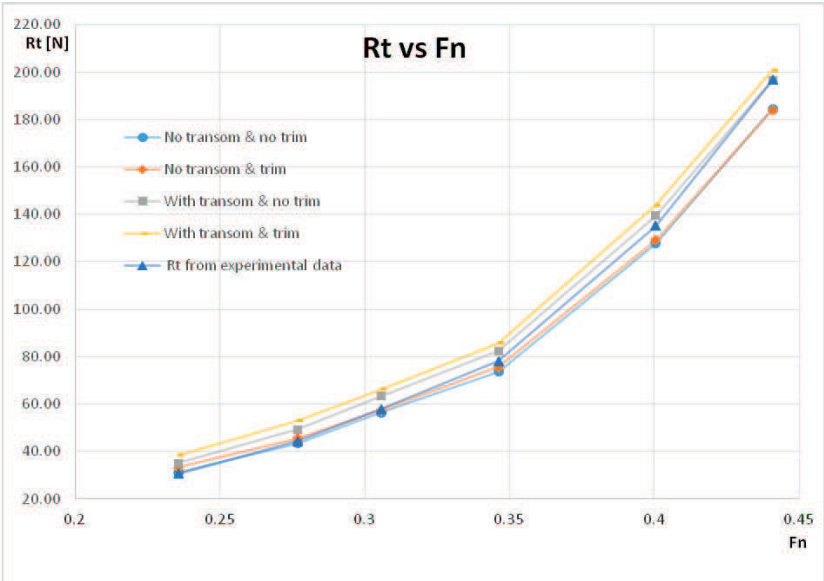

Fig. 20 Total Resistance [Rt] in function of Froude number [Fn]

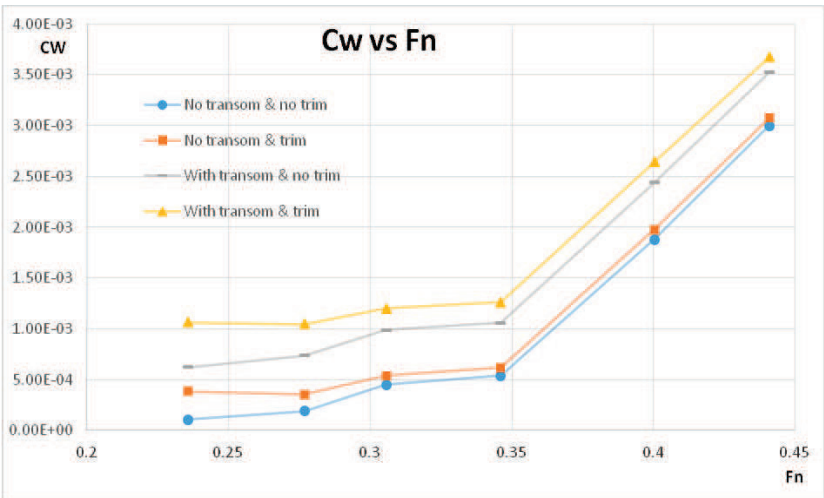

Fig. 21 Coefficient of wave making resistance [Cw] in function of Froude number [Fn]

Wave resistance coefficient Cw behaves as predicted from the theory, rising with increase of Froude number. It has two local lowering of the values around Froude numbers 0.28 and 0.35. This is explained from the four oscillating terms added to the pressure resistance depending on the waves created from the bow part, bow shoulder part, stern part, and stern shoulder part that are superimposing each other making total wave making resistance. The terms change because the waves oscillate, thus changes the Cw locally. If there is, a crest on the bow wave and crest on the stern wave matching there will be bigger support motion. If there is crest and trough from bow and stern end, which coincide, the supporting force at the stern will reduce, from reduced stern wave, therefore Cw increases. This interaction depends on the ships speed. In critical Froude speeds the ship length coincides with wavelength of transvers waves $Lw=2\pi.V^2/g$ which are moving as the same speed with the ship, or with divergent waves where $Lw=2\pi.V^2/g\cos$ of the angle between the diverging wave and the ship longitudinal axis, moving axially with the ship speed. When this is happening the ships interference with the waves. This interference is calculated and is found that there are Froude numbers around, which ship interferes with minimums or maximums reaction with the wave. For local minimums Froude numbers are 0.187, 0.231, 0.345, and for local maximums 0.173, 0.205, 0.269, 0.476.

$Cw=V^4$[const+4 oscillating terms coming from the four prominent wave interference] (16)

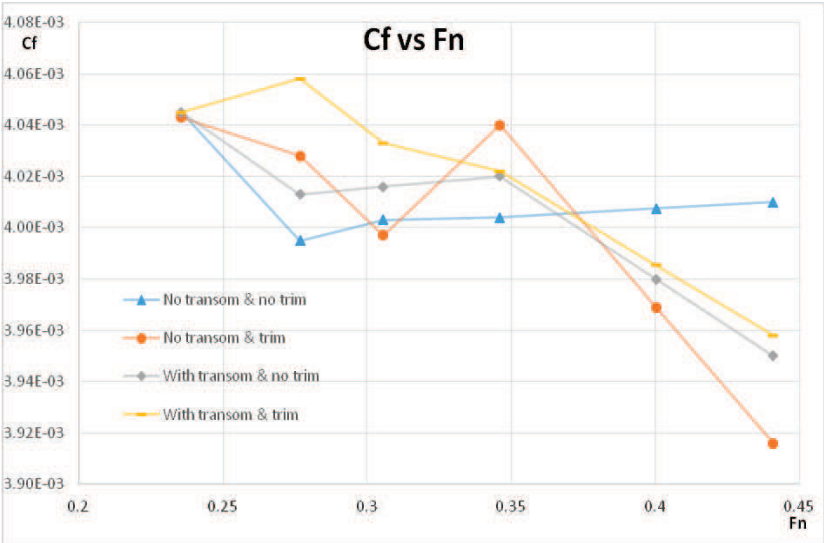

Fig. 22 Skin friction coefficient [Cf] vs Froude number [Fn]

Skin friction coefficient Cf is reducing with increase of Reynolds number. In the performed computation Reynolds number increases with increase of Froude taken from experimental data. Xbound did not put form factor in the computations for Cf as well as computing eddies and separation and sonar dome makes turbulent flow, from the forward part of the ship, which can lead to these effects. The boundary layer theory works only on thin boundary layer in module Xbound. That is the reason for detailed viscous flow computation, which can resolve bigger turbulence effects.

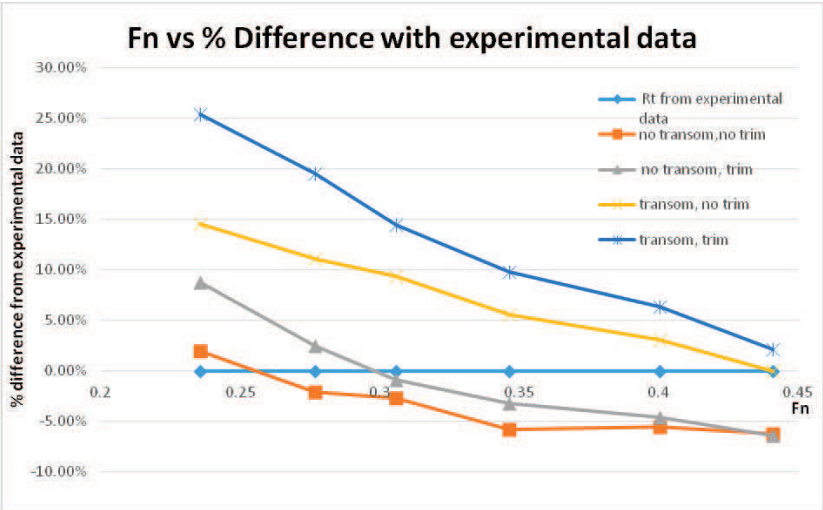

Fig. 23 % Difference with experimental data vs Foude Number [Fn]

At low Froude numbers cases with no transom and no trim perform up to 3% difference except for Froude 0.35 in which the difference is 6%. For higher Froude numbers 0.40 and 0.45 cases with transom and o trim are preferred, which give less than 3% difference. This difference below 3% is good enough for using for industrial practices.

4.2.1. Free-surface elevation and body pressure distribution

All the results for free-surface wave elevation are given nondimentional form of Lpp. Therefore, each value must be multiplied by Lpp of the ship 5.7 m to receive wave height in meters for specific spot.

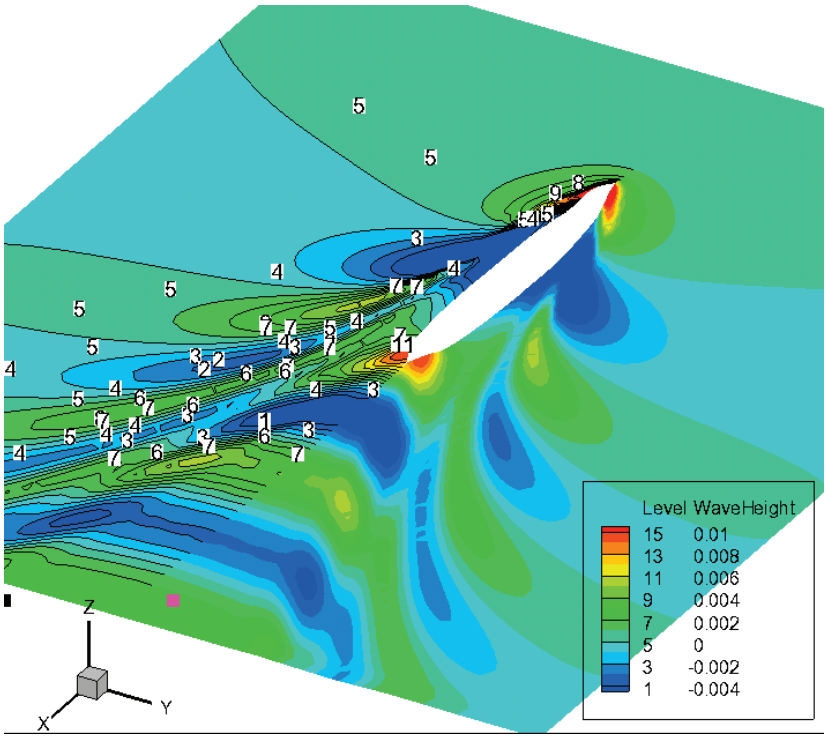

Fig. 24 Representation of free surface elevation using DTMB 5415, perspective and top view

Next figures show free surface computation and pressure distribution for range of Froude numbers of case transom, no trim.

Fn = [0.24]

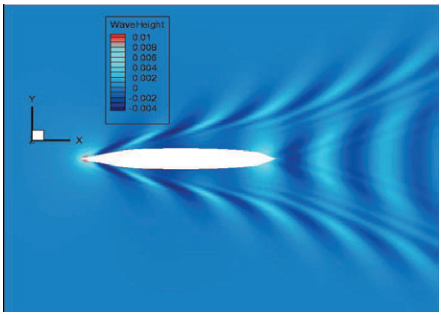

Free surface computation

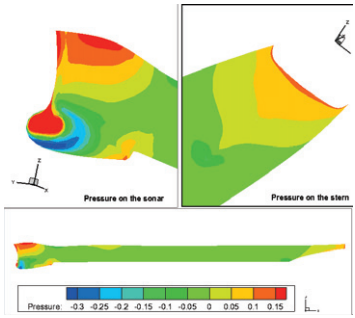

Pressure distribution

Fn = [0.28]

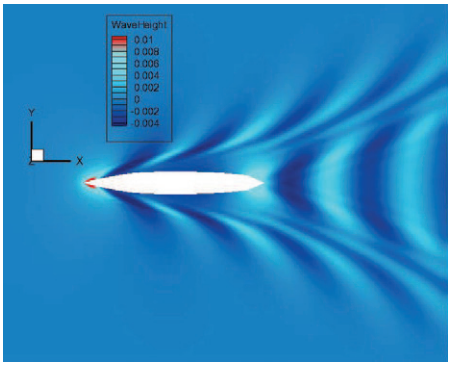

Free surface computation

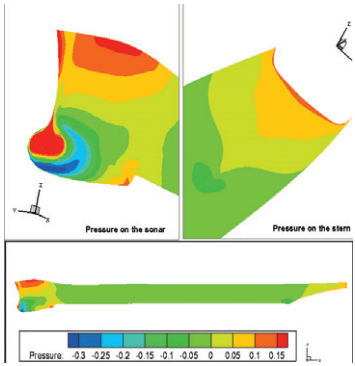

Pressure distribution

Fn = [0.31]

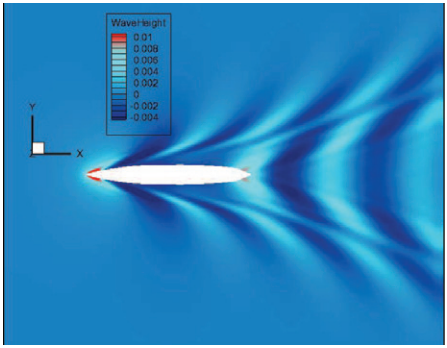

Free surface computation

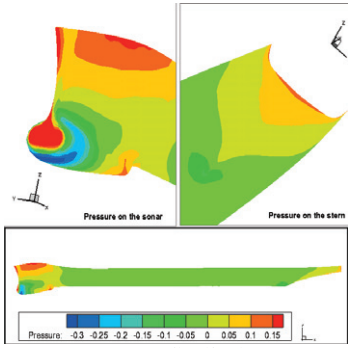

Pressure distribution

Fn = [0.35]

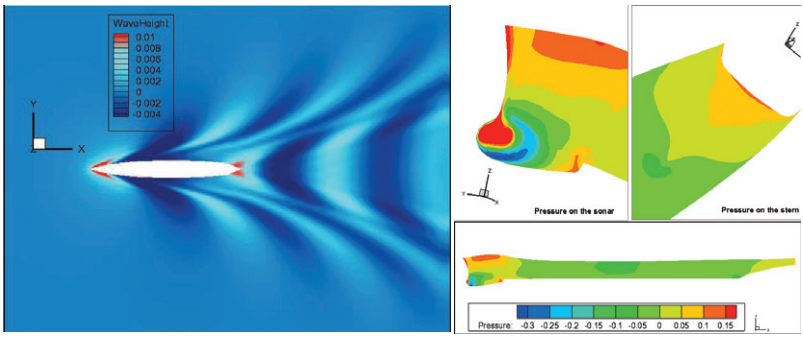

Free surface computation Pressure distribution

Fn = [0.40]

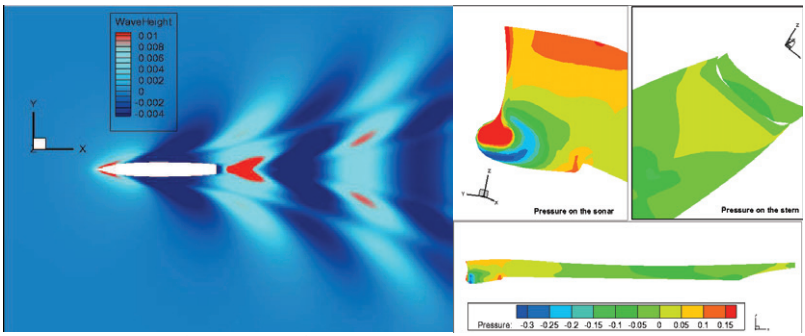

Free surface computation Pressure distribution

Fn = [0.44]

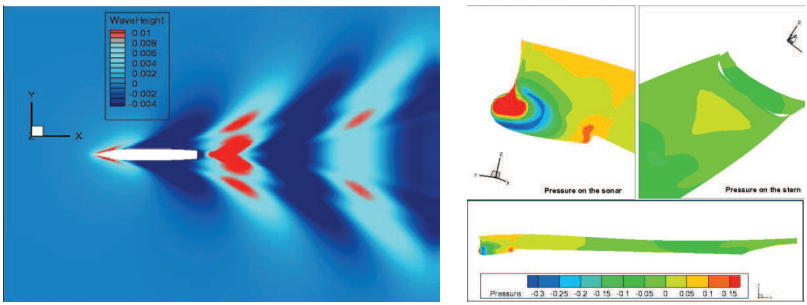

Free surface computation Pressure distribution

Fig. 25 Free surface elevation on the water and pressure distribution on the hull

There is formation of two regions in the bow area and stern with developing big divergent gravity waves and increasing the wave field pattern tremendously. This is visible more in higher speeds. Typically, in war ship forms with Fn > 30, Cw resistance coefficient on the front part of ship is 50% of the total resistance.

Biggest pressure is found on the tip front part of sonar, where the flow meats the hull and it starts slowing down the velocity drops. Then there is an acceleration region of the flow in the middle part of sonar, until the end part of it, where again higher pressure is found which slows the flow, the velocity of the water particles becomes smaller. At stern region, there is a sharp curvature change, which again leads to high pressure part but not as prominent as the sonar in the front part of the ship.

4.2.2. Skin friction coefficient

Largest skin friction coefficient is located at the bow, and smallest at the stern. At the stern part boundary layer becomes thicker, this reduces skin friction coefficient. Because of the sonar part in the front of the ship hull there is a region with higher turbulent fluctuations and a need of thicker boundary layer to investigate them in the stern part, Velocity gradient becomes smaller in the aft part near the hull and thus it lowers the skin friction at the stern.

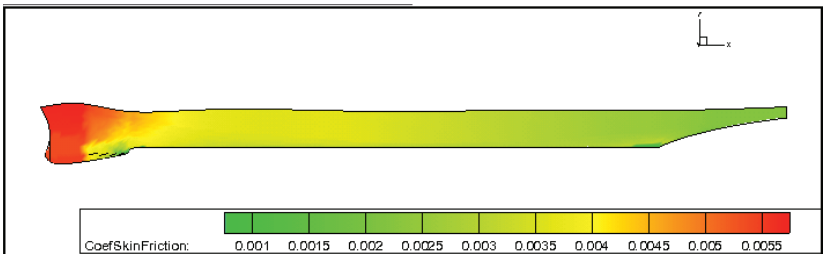

Fig. 26 Skin friction coefficient for no transom, no trim fn= [0.24]

4.3. Conclusions of Potential Flow Computation

Potential flow theory determined the free surface elevation successfully, which give good quality and accuracy as a starting point for further investigation with viscous flow theory.

It is recommended to use for free surface elevation computation the cases without transom for smaller Froude numbers, and cases with transom for bigger Froude numbers.

Four cases have been investigated in order to find good correlation with experimental data. Possible reasons for deviations with experimental results is not good meshing for the free surface or too much turbulence flow with eddies created by sonar part in front of the ship, which cannot be captured with boundary layer method as well as form factor definition, which is not defined in resistance computation of potential flow.

Boundary layer theory does not capture well the turbulence effects around the appendages, for investigation of the local flow viscous flow computation is needed done in the next chapter.

5. VISCOUS FLOW METHOD

5.1. Mathematical Model

Viscous flow theory is second alternative of investigation ship resistance in the software SHIPFLOW. Viscous free-surface flow calculations provide a detailed insight into the critical flow regions, allowing the naval architect to improve the hull forms for achieving a homogeneous velocity distribution, for determining the optimum inclination angle for shaft brackets, for studying the hydrodynamic interactions between various appendages and arrangements, and to investigate regions with possible flow separations. Therefore, an understanding of the flow around fully appended hull is of great practical interest. Using RANS (Reynolds-Averaged Navier-Stokes) equations larger boundary layers can be handled and turbulent flows in the wake region around stern part of the hull can be captured.

Two important aspects of the flow associated with ship hull, which influence the hydrodynamic performances are (a) - the separated flow around appendages governed by the viscous effects, and (b) - the waves generated at the free surface governed by the gravity forces. Computing the RANS solutions on powerful computers by employing robust numerical algorithms, nowadays one may get a grasp of complete understanding on all features of the flow around the appended ship hull. Accuracy requires careful attention to the physical modelling, particularly to the effects of turbulence, and to the numerical discretization. In the present study, the turbulence closure is attained through the EASM [1] model.

5.1.1. Governing Equations

CFD as an alternative to experimental measurements can be used to predict the fluid velocity distribution by solving the fundamental equations of motion using numerical methods. These equations called Navier-Stokes equations are fundamental for the fluid flow. They describe the conservation of fluid mass and momentum in equations of continuity. Even with the fastest supercomputers and with largest memory available it is impossible to solve for practical cases. That is why engineers use averaged versions of the equations over a period to ease the computational difficulties of modern machines. The equations changes introducing new variables known as Reynolds stresses. To close the set of equations, for example to have as many equations as unknowns, turbulence models are used for expressing this Reynolds stresses.

The Navier-Stokes equations can be solved numerically by resolving all scales for turbulent flows, which requires extremely dense grids to resolve the smallest turbulent length scales. This is unfeasible for industrial purposes in the near future. Used SHIPFLOW 4.6 relies on Reynolds decomposition model, in which the continuity equation states that mass is conserved:

$$\frac{1}{\rho} \cdot \frac{\partial \rho}{\partial t} + \frac{\partial U_i}{\partial x_i} = 0 \tag{17}$$

Only incompressible flow is considered in the present study. That means that the changes in density are negligible. Then the continuity equation can be written:

$$\frac{\partial U_i}{\partial x_i} = 0 \tag{18}$$

The Navier-Stokes equations of motion can be written in the following form:

$$\rho \frac{\partial U_i}{\partial t} + \rho \frac{\partial (U_j U_i)}{\partial x_j} = \rho R_i + \frac{\partial \sigma_{ij}}{\partial x_j} \tag{19}$$

where σ_{ij} is the total stress and for a Newtonian fluid can be written as:

$$\sigma_{ij} = -P\delta_{ij} + 2\mu\left(S_{ij} - \frac{1}{3}S_{kk}\delta_{ij}\right) \tag{20}$$

and S_{ij} is the strain-rate defined as:

$$S_{ij} = \frac{1}{2}\left(\frac{\partial U_i}{\partial x_j} + \frac{\partial U_j}{\partial x_i}\right) \tag{21}$$

S_{kk} in (20) is zero for incompressible flow

$$S_{kk} = \frac{1}{2}\left(\frac{\partial U_k}{\partial x_k} + \frac{\partial U_k}{\partial x_k}\right) = \frac{\partial U_k}{\partial x_k} = 0 \tag{22}$$

There are different methods to solve the equations.

Using Reynolds decomposition of so-called Reynolds Averaged Navier Stokes equations (RANS hereafter), which takes average value and fluctuating part is the method being used currently.

The RANS equations can be derived from Navier-Stokes equations (19) by splitting the instant velocity components U_i in time mean velocity u_i, and time fluctuating velocity u_i'',

$$U_i = \overline{U_i} + u_i'' \equiv u_i + u_i'' \tag{23}$$

instant pressure, *P*, mean pressure in time, *p*, and time fluctuating pressure, p'',

$$P = \overline{P} + p'' \equiv p + p'' \tag{24}$$

The time mean of a variable is defined as:

$$\overline{\phi} = \lim_{T\to\infty}\frac{1}{2T}\int_{-T}^{T}\phi \cdot dt \tag{25}$$

The following rules of averaging apply for any two turbulent quantities ϕ_1 and ϕ_2:

$$\phi_1 = \overline{\phi_1} + \phi_1'' ; \qquad \overline{\phi_1''} = 0; \qquad \overline{\overline{\phi_1}} = \overline{\phi_1}; \qquad \overline{\overline{\phi_1}\phi_2} = \overline{\phi_1}\overline{\phi_2};$$
$$\overline{\phi_1''\overline{\phi_2}} = 0; \qquad \overline{\frac{\partial \phi_1}{\partial s}} = \frac{\partial \overline{\phi_1}}{\partial s}; \qquad \overline{\phi_1 + \phi_2} = \overline{\phi_1} + \overline{\phi_2}; \qquad \overline{\phi_1\phi_2} = \overline{\phi_1}\overline{\phi_2} + \overline{\phi_1''\phi_2''} \tag{26}$$

Taking the time average of continuity equation gives:

$$\overline{\frac{\partial U_i}{\partial x_i}} = \frac{\partial \overline{U}_i}{\partial x_i} = \frac{\partial u_i}{\partial x_i} = 0 \tag{27}$$

Subtracting (27) from (18) gives that also the time fluctuating velocity fulfils the incompressible continuity equation:

$$\frac{\partial u_i''}{\partial x_i} = 0 \tag{28}$$

Then taking the time average of N-S equations (first moving all the terms to the left hand side):

$$\rho\frac{\partial U_i}{\partial t} + \rho\frac{\partial (U_j U_i)}{\partial x_j} - \rho R_i + \frac{\partial P}{\partial x_i} - \frac{\partial}{\partial x_j}\left(\mu\left(\frac{\partial U_i}{\partial x_j} + \frac{\partial U_j}{\partial x_i}\right)\right) =$$
$$\rho\frac{\partial \overline{U}_i}{\partial t} + \rho\frac{\partial (\overline{U_j U_i})}{\partial t} - \rho\overline{R}_i + \frac{\partial \overline{P}}{\partial x_i} - \frac{\partial}{\partial x_j}\left(\mu\left(\frac{\partial \overline{U_i}}{\partial x_j} + \frac{\partial \overline{U_j}}{\partial x_i}\right)\right) = \tag{29}$$
$$\rho\frac{\partial U_i}{\partial t} + \rho\frac{\partial (u_j u_i + \overline{u_j'' u_i''})}{\partial x_j} - \rho\overline{R}_i + \frac{\partial p}{\partial x_i} - \frac{\partial}{\partial x_j}\left(\mu\left(\frac{\partial u_i}{\partial x_j} + \frac{\partial u_j}{\partial x_i}\right)\right)$$

Hence, the time averaged continuity equation and N-S equation for incompressible flow can be written as follows:

$$\frac{\partial u_i}{\partial x_i} = 0 \tag{30}$$

$$\frac{\partial u_i}{\partial t} + \frac{\partial (u_j u_i + \overline{u_j'' u_i''})}{\partial x_j} = \overline{R}_i - \frac{1}{\rho}\frac{\partial p}{\partial x_i} + \frac{\partial}{\partial x_j}\left(\upsilon\left(\frac{\partial u_i}{\partial x_j} + \frac{\partial u_j}{\partial x_i}\right)\right) \tag{31}$$

where:

$\upsilon = \dfrac{\mu}{\rho}$ kinematic viscosity of the fluid in this case water (m^2/s) x 10^{-6}.

5.1.2. Turbulence Modeling

In an EASM model, the Reynolds stress components are explicitly determined from the tensor functions of the velocity gradients, turbulent kinetic energy, and turbulent length scale. These models have the advantage explicit solution of the Reynolds stresses at each computational iteration. Starting from a Reynolds stress closure model, Gatski and Speziale [9] developed the algebraic EASM model by using a three-term tensor basis and the Galerkin method to determine the coefficients of the model. The resulting model is relatively complex and assumes that convective effects are negligible. In this approach, the EASM model approximates the predictions of a full Reynolds stress closure model, which is an approximation in itself.

The Boussinesq assumption

$$\rho\overline{u_i''u_j''} = \mu_T\left(\frac{\partial u_i}{\partial x_j} + \frac{\partial u_j}{\partial x_i}\right) + \frac{2}{3}\rho k\delta_{ij} \tag{32}$$

is a linear eddy viscosity model. Since it is a linear model, it sometimes fails to give satisfactory results and to improve this, nonlinear terms can be added. The Explicit Algebraic Stress Model (EASM) is such a model that includes nonlinear terms. The Reynolds stress tensor is then given by

$$\rho\overline{u_i''u_j''} = \frac{2}{3}\rho k\delta_{ij} - \mu_T\left(S_{ij} + a_2a_4\left(S_{ik}W_{kj} - W_{ik}S_{kj}\right)\right) - a_3a_4\left(S_{ik}S_{kj} - \frac{1}{3}S_{mn}S_{mn}\delta_{ij}\right) \tag{33}$$

and the turbulent viscosity by

$$\nu_T = \max\left(-k\alpha_1, \frac{0.0005k}{\beta^*\omega}\right) \tag{34}$$

α_1 is obtain from the following formula

$$\left(\frac{\alpha_1}{\tau}\right)^3 - \frac{\gamma_1}{\eta^2\tau^2\gamma_0}\left(\frac{\alpha_1}{\tau}\right)^2 + \frac{\gamma_1^2 - 2\eta^2\tau^2\gamma_0 a_1 - \frac{2}{3}\eta^2\tau^2 a_3^2 + 2R\eta^2\tau^2 a_2^2}{\left(2\eta^2\tau^2\gamma_0\right)^2}\left(\frac{\alpha_1}{\tau}\right) = \frac{\gamma_1 a_1}{\left(2\eta^2\tau^2\gamma_0\right)^2} \quad (35)$$

Where

$$W_{ij} = \frac{1}{2}\left(\frac{\partial U_i}{\partial x_j} - \frac{\partial U_j}{\partial x_i}\right) \qquad \eta^2 = S_{ij}S_{ij} \qquad R^2 = \frac{W_{ij}W_{ij}}{\eta^2}$$

$$a_1 = \frac{1}{2}\left(\frac{4}{3} - C_2\right) \qquad a_2 = \frac{1}{2}\left(2 - C_4\right) \qquad a_3 = \frac{1}{2}\left(2 - C_3\right)$$

$$a_4 = \frac{\tau}{\gamma_1 - 2\gamma_0(\alpha_1/\tau)\eta^2\tau^2} \qquad \gamma_0 = \frac{C_1^1}{2} \qquad \gamma_1 = \frac{C_1^0}{2} - \frac{C_{\varepsilon 2} - C_{\varepsilon 1}}{C_{\varepsilon 2} - 1} \quad (36)$$

$$C_{\varepsilon 1} = 1.44 \qquad C_{\varepsilon 2} = 1.83 \qquad C_1^0 = 3.4 \qquad C_1^1 = 1.8$$

5.1.3. Boundary conditions

A **boundary fitted coordinate system** is employed to allow a more accurate formulation of the boundary conditions, which requires the **no-slip condition** for the velocity the hull surface, a **Neumann-type condition** for the pressure, while for k and ω, **Dirichlet conditions** are used. The **zero-gradient Neumann** conditions are imposed for all the variables in the symmetry plane. At the upstream, the oncoming flow velocity is supposed to be constant, as k and ω are, whereas the pressure is extrapolated with zero-gradient. At the downstream, the velocity, k and ω are extrapolated with zero-gradient, while the dynamic pressure has the zero value.

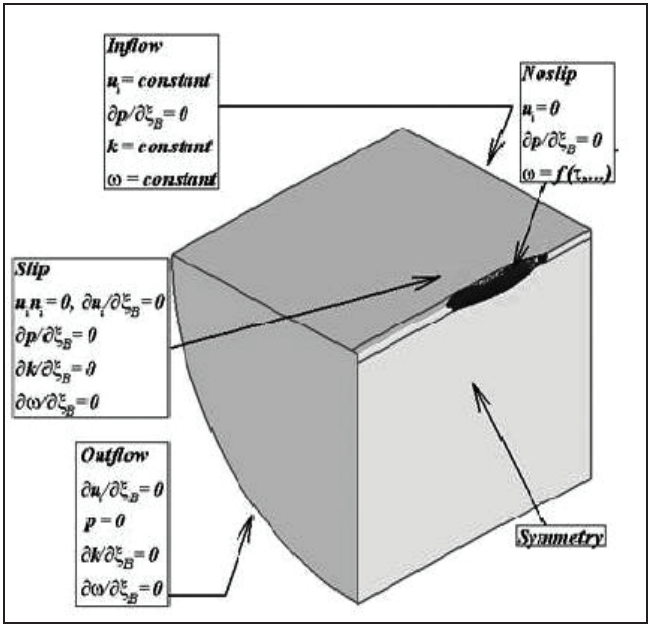

Fig. 27 Solution domain

Boundary conditions used to describe the problem are given in Table 10

Table 10 Boundary condition s for the domain

	No slip	Slip	Inflow	Outflow
u	$u_i = 0$	$u_i n_i = 0, \frac{\partial u_i}{\partial \xi_B} = 0$	$u = \text{Constant}$	$\frac{\partial u_i}{\partial \xi_B} = 0$
p	$\frac{\partial p}{\partial \xi_B} = 0$	$\frac{\partial p}{\partial \xi_B} = 0$	$\frac{\partial p}{\partial \xi_B} = 0$	$p = 0$
k	$k = 0$	$\frac{\partial k}{\partial \xi_B} = 0$	$k = \text{Constant}$	$\frac{\partial k}{\partial \xi_B} = 0$
ω	$\omega = f(u_T, ...)$	$\frac{\partial \omega}{\partial \xi_B} = 0$	$\omega = \text{Constant}$	$\frac{\partial \omega}{\partial \xi_B} = 0$

5.1.4. Numerical Scheme

The CHAPMAN solver based on the finite volume method is employed to solve the RANS equations. The convective terms are discretized using the approximate **Riemann solver of Roe** and a second order explicit defect correction is used to achieve the second order of accuracy. The rest of terms are discretized by **central differences**. A local artificial **time-step** is added to the equations and the discrete coupled equations are solved using the ADI technique. The chosen method provides the time averaged pressure and velocity components. Since the time fluctuating components are generally much smaller in amplitude, knowing the average is usually enough for most of the applications.

The tri-diagonal system of the ADI scheme contains the first-order Roe convective terms and the second order diffusive terms, while the second order flux corrections are used as an explicit defect correction. Each element in the tri-diagonal matrix is a 6x6-element matrix. For each sweep, a local artificial time-step is calculated based on the CFL and von Neumann numbers in all directions except the implicit one.

All theoretical mathematic derivations have been referenced from [29] to [36].

5.1.5. Advantages and Disadvantages of Viscous Flow Method.

RANS equations are solved based on finite volume methods, which discretize whole volume of fluid domain, not only free surface and ship surface. Limitation is that RANS method in SHIPFLOW does not capture free surface behaviour. There is possibility to import into RANS solution results from free surface computation in potential flow and so SHIPFLOW can fit both grids together to compute the flow around wavy surface.

6. RESULTS AND DISCUSSION FOR VISCOUS FLOW SOLUTION AROUND COMBATANT SHIP

6.1.1. Description of the chapter

Grid computation has been presented for the cases with or without refinement. Using Chimera technique, the rudder and bracket grids are overlapped each other to make denser grid in the required places of appendages with sharp or higher curvature.

Results for Froude Fn = 0.401 are given to get general overview on the accuracy on the solution. A case for bare hull with no refinement and with refinement on the sonar mesh has been performed. The rest of the results are being provided with refinement on the sonar dome. Later in the chapter investigated Froude Numbers Fn = 0.28 with Rn = 8.31e+06 and Fn = 0.41 with Rn = 1.24E+07 are calculated with 6000 iterations for two cases: bare hull case, and full appended case and full appended with propeller. The free surface from potential flow solution is taken on consideration for the computation of the viscous flow. Results show free surface elevation, pressure, axial velocity for two different Froude Numbers 0.28 and 0.41.

6.1.2. Grid generation

The **SHIPFLOW** code is employed to evaluate the flow field structure around the ship hull, the forces acting on bare hull and appendages. The solver computes the incompressible RANS equations on **structured overlapping grids** by using a finite volume technique.

RANS solution results are taken from free surface computation in potential flow and so SHIPFLOW can fit both grids of potential flow free surface grid and of viscous flow domain mesh together to compute the flow around wavy surface.

For complex geometries such as a fully appended ship hull, the grid generation is a very complicated and time-consuming task to accomplish. Two are the main approaches to deal with such complex geometries: composite structured grid schemes and unstructured grid schemes. Unstructured grid is generally considered to be more versatile and easier to adapt to complex geometry, while composite structured methods seems to use more numerically efficient algorithms and require less computational effort.

The **Chimera** technique was preferred since grids can be fitted together as patches, which overlap on the boundaries. In overset schemes, intermediate boundary curves can be placed arbitrarily and the solutions can be imported from one grid to another. This is a powerful technique for efficiently solving problems in complex, possibly moving, geometry. An overlapping grid consists of a set of structured grids that overlap and cover the computational domain. By allowing the grids to overlap, grids for complex geometries can be more easily constructed. Overset grids can easily be repositioned everywhere in the domain, thus variable geometry can be tested without regridding the entire mesh. A detailed description of the Chimera technique is given by Steger et al. [16], [17].

The Chimera technique was preferred since grids can be fitted together as patches, which overlap on the boundaries. In overset schemes, intermediate boundary curves can be placed arbitrarily and the solutions can be imported from one grid to another. Overset grids can easily be positioned everywhere in the domain, thus variable geometry can be tested without re-gridding the entire mesh. Muscari et al., identified the following issues whenever the overlapping grids are employed [3]: (a) - detection of the non-fluid cells (cells are discarded since they are placed outside of the domain); (b) - the detection of the interpolation cells (where variables must be interpolated from the other sub-grids); (c) - the interpolation scheme (the information is transmitted from one grid to another inside the mutual overlapping regions through the interpolation of the field variables).

The computational domain must be large enough to assume that influence of the external boundaries is negligible. XGRID uses information about the longitudinal size of the domain and the clustering done on it. The size of the domain is defined with commands: Xstart and Xend in Xdistribution option.

For clustering are used:

NU – number of panels in longitudinal (ξ) direction between coordinates XSTART and XFPU

XFPU – The x-coordinate of the change in stretching of the bow region upstream of forward perpendicular on the ship

NF- number of panels in the longitudinal direction between coordinates XFPU and XFPD

XFPD – The x-coordinate of the change in stretching of the bow region downstream on the forward perpendicular of the ship

NM – number of panels in longitudinal direction between coordinates XFPD and XAPU

XAPU – The x-coordinate of the change in stretching of the stern region upstream of the aft perpendicular on the ship

NA – number of panels in longitudinal direction between coordinates XAPU and XAPD

XAPD – The x-coordinate of the change in stretching of the stern region downstream of the aft perpendicular on the ship.

NW – number of panels in longitudinal direction between coordinates XAPD and XEND

XEND – The coordinate of the end of the grid.

The domain regions are presented in Figure 28

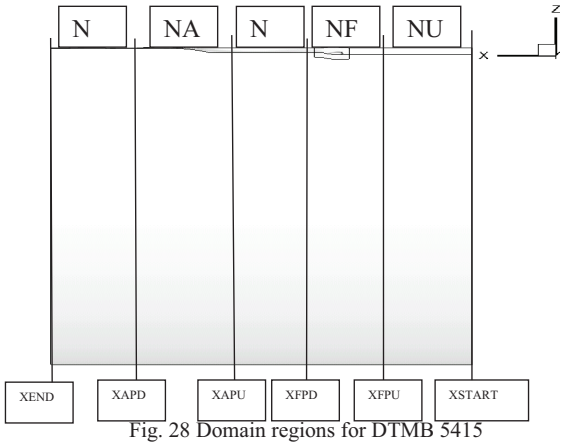

Fig. 28 Domain regions for DTMB 5415

For most applications it is advisable to utilize clustering to represent the hull shape better in the high curvature regions, and to resolve the flow better. This saves number of cells and decreasing the computational time.

The number of panels of clusters is specified with:

KSIMAX – number of panels (of clusters) in the longitudinal direction – ξ

ETAMAX – Number of panels in the circumferential direction - η

ZETAMAX – Number of panels in radial direction - ζ.

From the figure can be seen that ξ = NW+NA+NM+NF+NU

In this particular case of a fully appended twin screw combatant hull, a mono-block structured grid has been generated to cover the entire computational domain along the bare hull. On the Figure 29 and Figure 30 are shown the grid of the forward part of the ship hull DTMB 5415 with and without refinement. Grid refinement in sonar dome region is needed for better capturing the turbulence structure developed in the sonar zone. In the Figure 32 is seen that the number of cells is increasing. This is needed for places with higher curvature such as sonar dome in the combatant. Figure 31 shows that transom part of the grid, which is denser to capture any fluctuations on the hull pressure at the stern region.

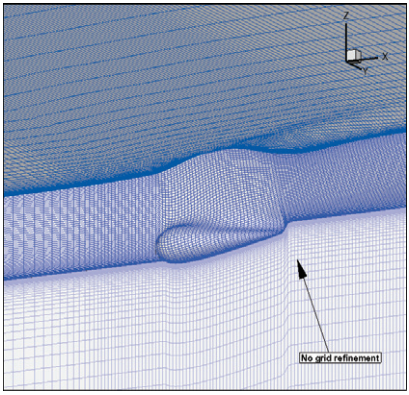

Fig. 29 No grid refinement in the forward part of the ship, sonar region

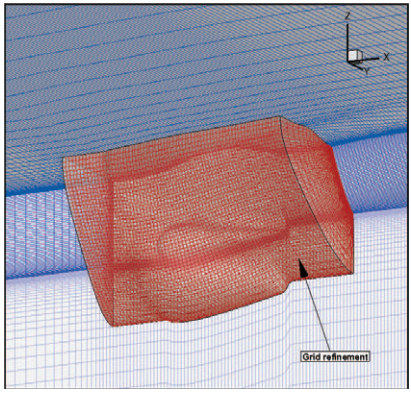

Fig. 30 Grid refinement in the forward part of the ship, sonar region

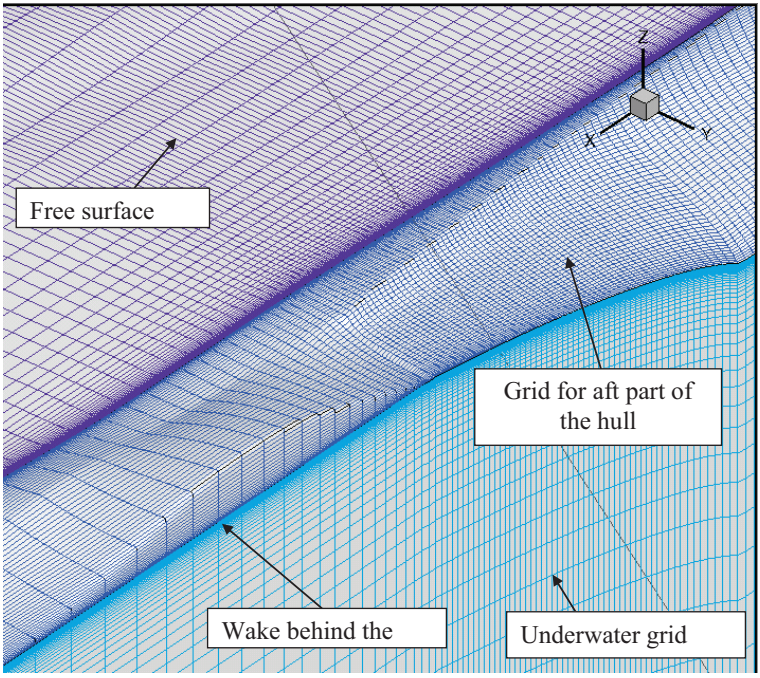

Fig. 31 Grid in transom part of the ship hull

On the Figure 32 there are shown refined regions in the stern part and in the bow part as well as special volume shape refinement made for the sonar part

marked with red. This is needed for capturing certain specific details of the flow more reasonably.

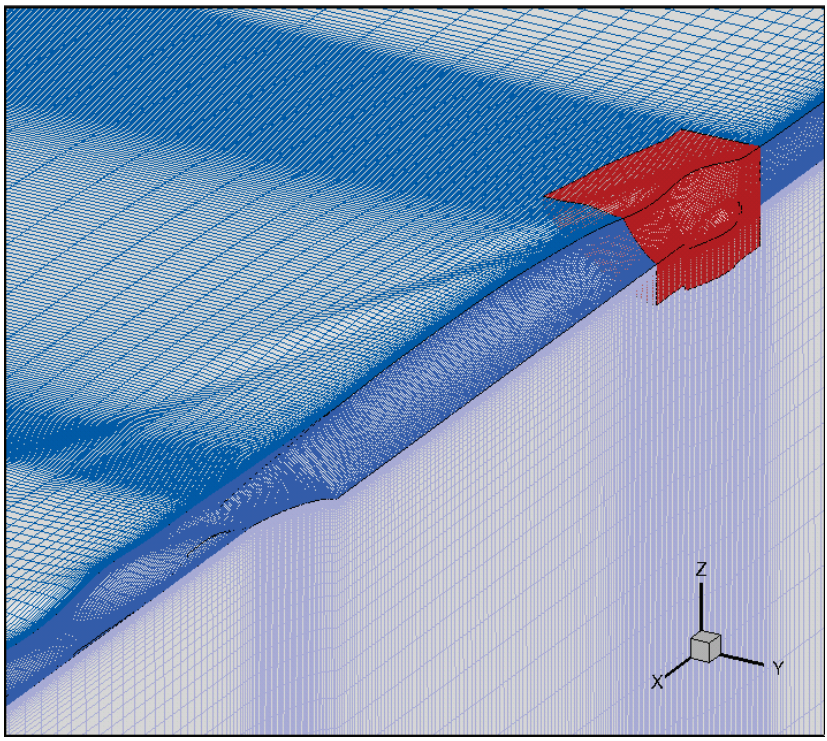

Fig. 32 Overall view of the grid

The free surface is normally treated as a slip plane but can be fitted to the free surface computed by free-surface potential flow solver based on **Rankine sources method**. Hybrid panalization is combining free surface from potential flow and viscous grid for viscous computation with free surface.

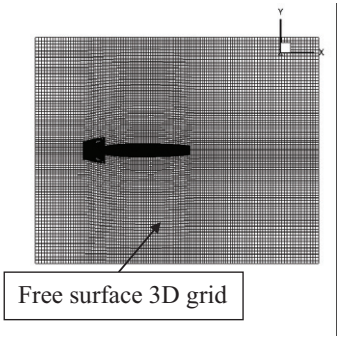

Fig. 33 Free surface grid from potential flow solution

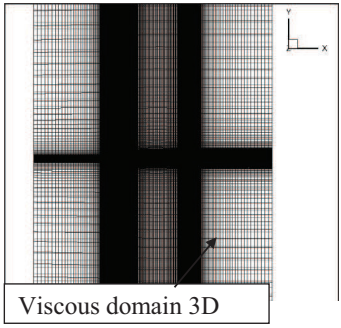

Fig. 34 Mesh on viscous flow solution

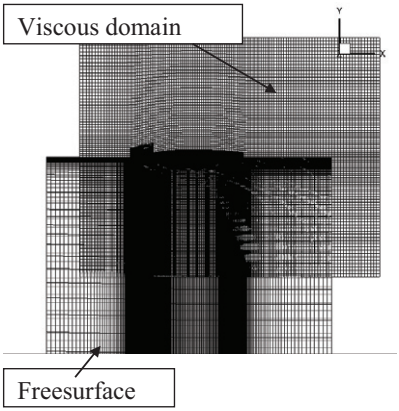

Fig. 35 Fitting of the free surface grid from potential flow solution as a boundary over viscous flow solution

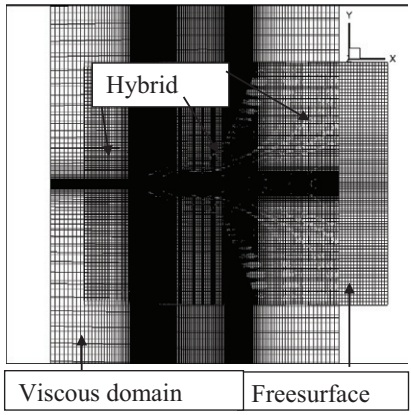

Fig. 36 Fitting of the free surface grid from potential flow solution as a boundary over viscous flow solution symmetry plane.

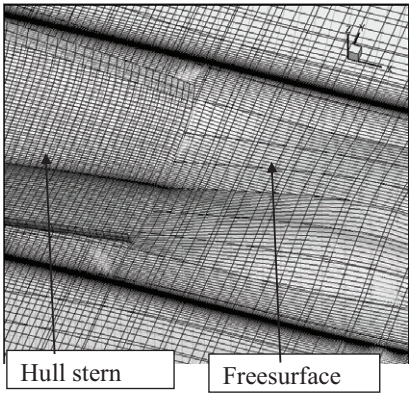

Fig. 37 Zoom in the aft region of whole viscous domain with free surface from potential flow - hybrid method

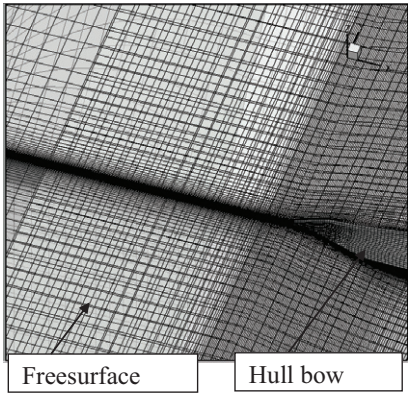

Fig. 38 Zoom in bow region of whole viscous domain with free surface from potential flow - hybrid method

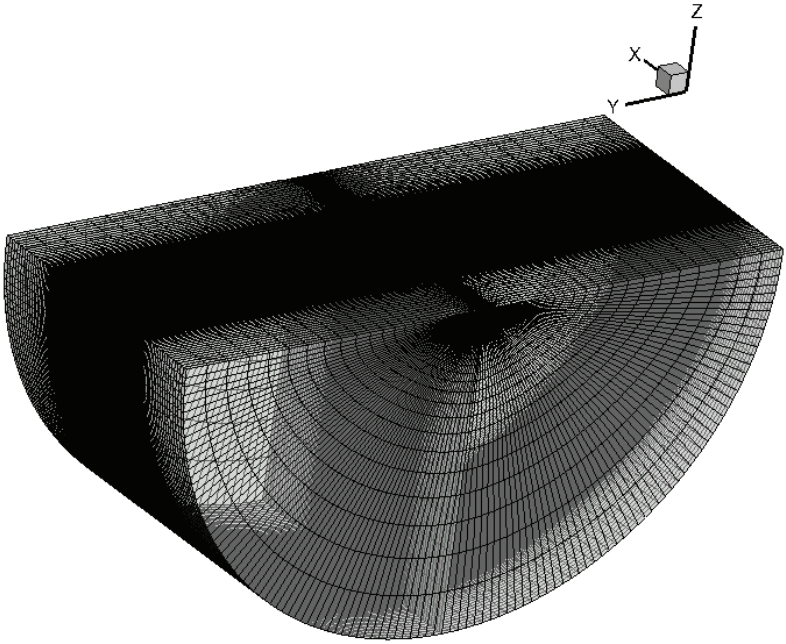

Fig. 39 Hybrid method - Perspective view of whole viscous domain

For fully appended hull forms, such those equipped with shafts and struts, generating good structured grids is not only an important in getting accurate numerical solutions, but also extremely difficult because of the geometric complexity of the domain. **Chimera-type schemes**, which allow grid blocks to overlap in arbitrary manner and unstructured grid schemes, can be used for flow computations over such complicated domains. Unstructured grid is generally considered to be more versatile and easier to adapt to complex geometry, while composite structured methods seems to use more numerically efficient algorithms and to require less computational effort.

Utilizing structured overlapping grids on DTMB 5415, they are needed for the complex geometry of the appendages. Description on the rudder grid can be seen on Figure 41, which is used in the computations. The solver described above can handle overlapping grids. Several parametric models of appendages such as rudders, shafts, and so on, are available in the computational code, but grid can also be imported from other grid generators.

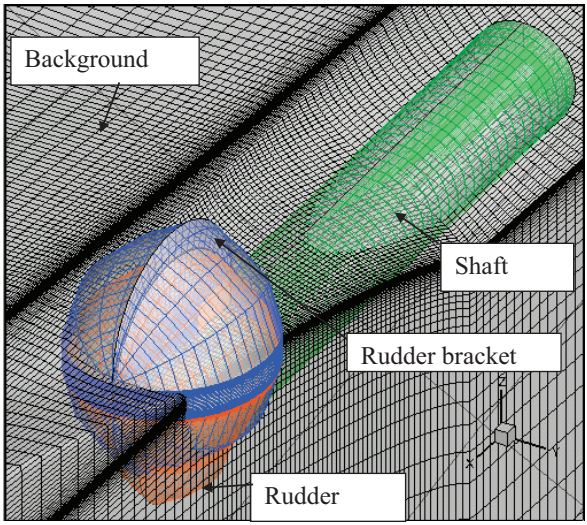

Fig. 40 Overlapping grid of shaft - green, rudder – orange, ruder bracket – blue

Total number of cells of the mesh for bare hull case with no refinement is 1 742 262, with refinement is 2 011 962. For the case of rudder 2 543 484 is the total number of cells being used. For a case of hull with appendages and propeller the maximum number of overlapped grids are 8 with maximum number of cells 3 222 290. Used rudder grid for the computation has 2448 number of cells shown in Figure 41 and around zone shown in the Figure 42 has 149328 number of cells.

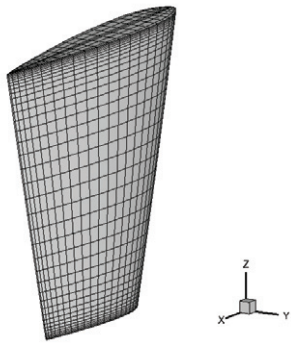

Fig. 41 Used rudder grid for computation analysis

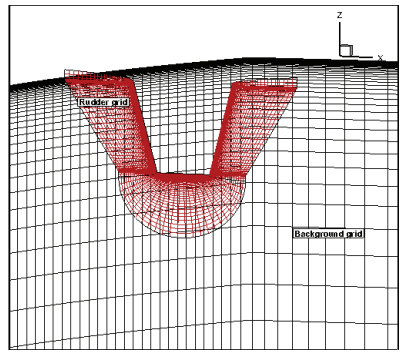

Fig. 42 Grid around the rudder and background grid of the domain overlapping.

Grid without appendages and with using parametric appendages shown in the flowing Figures 43, 44 and 45.

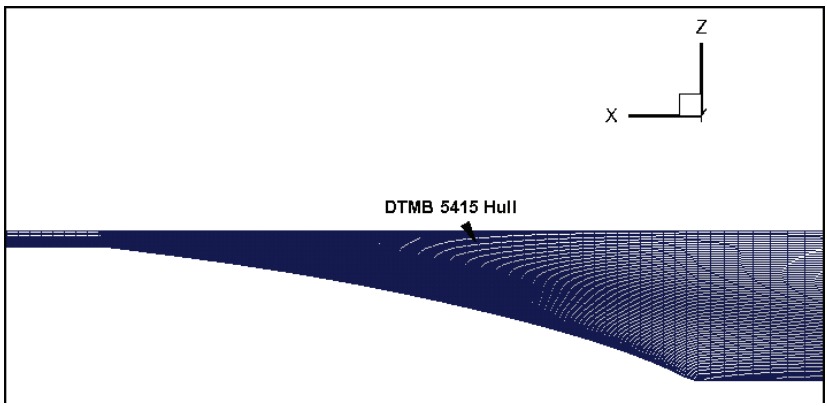

Fig. 43 Grid around stern part of the ship without appendages

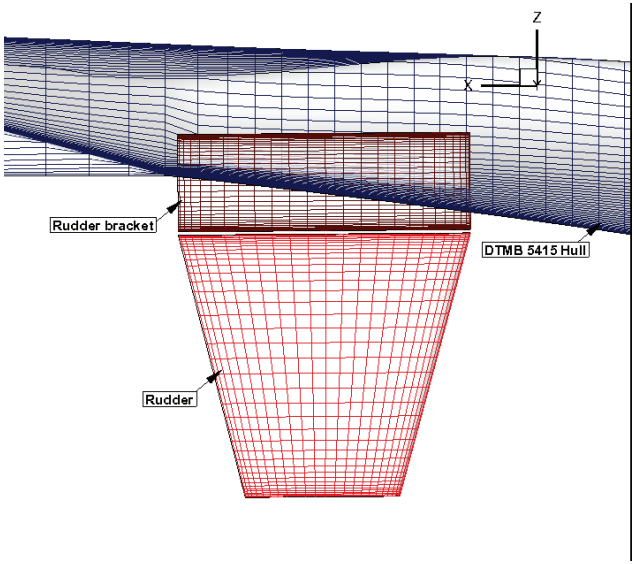

Fig. 44 Grid of the rudder bracket and hull of DTMB 5415.

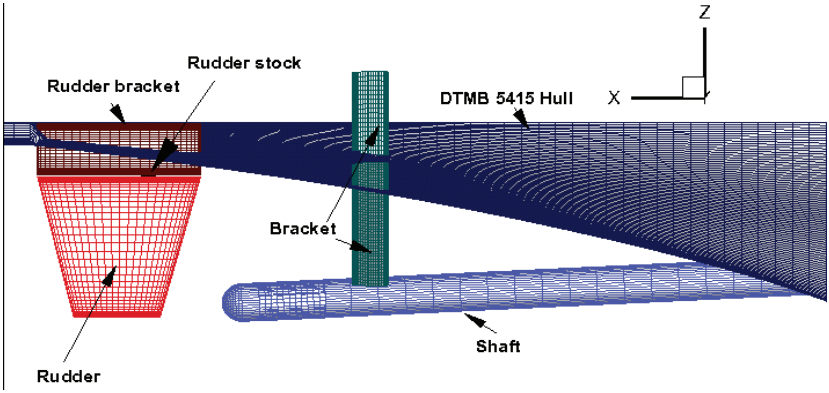

Fig. 45 Grid around stern part of the ship with appendages

6.1.3. Discussion on computed results

For viscous solution the solver from XCHAP module is used with 4 parallel threads on 10 computers with Core I5 processor. Computations are done

for 2-4 days for the viscous per run and few hours for potential flow. Example file of viscous computation can be seen in the appendix.

All results of pressure are represented with solid lines positive pressure regions and with dashed lines negative pressure regions

6.1.4. Initial results for Fn = 0.401 taken from experimental results with rudder case.

As seen in the Figure 46 there are three main high pressure zones two in the front and one in the aft part of the ship. Main low-pressure zone is developed throughout the mid part of the hull.

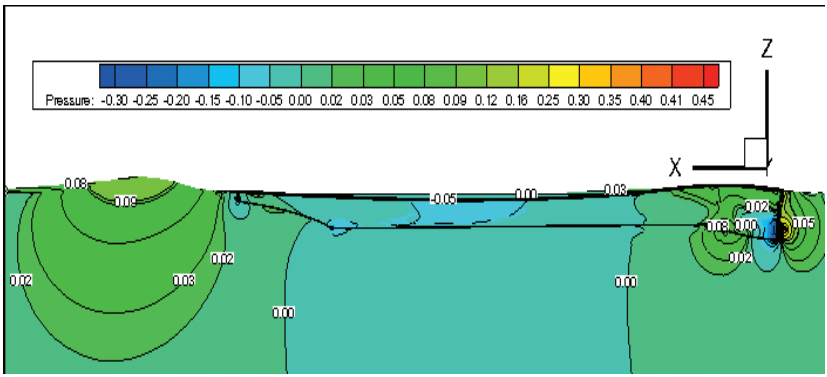

Fig. 46 Overall pressure distribution on the hull at, Fn = 0.401, rudder

In the sonar dome region shown in Figure 47 there are two high-pressure regions, in the tip of the dome which meats the water first and in the back part of the dome due to closure of curvature. There is a big low-pressure zone forming ring with high velocity water just behind the forward tip with high-pressure zone

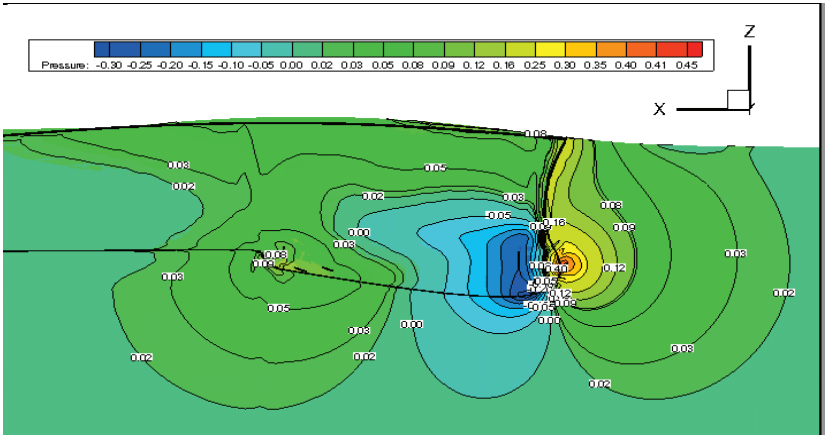

Fig. 47 Pressure distribution on sonar dome and forward part of the ship at, Fn = 0.401, rudder

There are two low-pressure regions, one is located on the bottom part of the transom stern, and the other is positioned at the junction between the hull bottom and the beginning of the slope of the stern part. Between them on the slope of the curvature there is a high-pressure region seen in Figure 48. This happens because of the higher changing of the curvature on the ship.

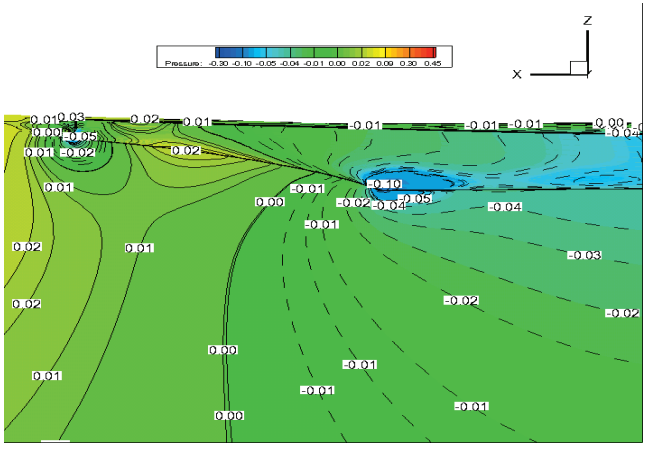

Fig. 48 Pressure distribution on aft part of the ship

Axial velocity figure describes increase of speed in the region behind the tip of the sonar, which gives good confirmation with the pressure results. In Figure 49 axial velocity behind sonar dome is changed from the formation of turbulence in the forward part of the ship. There is a possibility to receive circulation regions and separations in higher speeds.

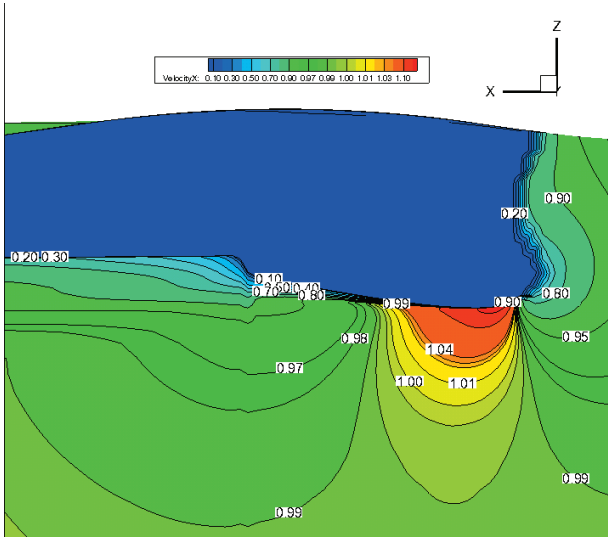

Fig. 49 Axial velocity on forward part of the ship in the sonar region at, Fn = 0.401 rudder

In Figure 50 Axial velocity on the stern part is high just before where the bottom part starts curving with constant slope leading to formation of the transom. The rest of the region are with relatively low axial velocity near the hull.

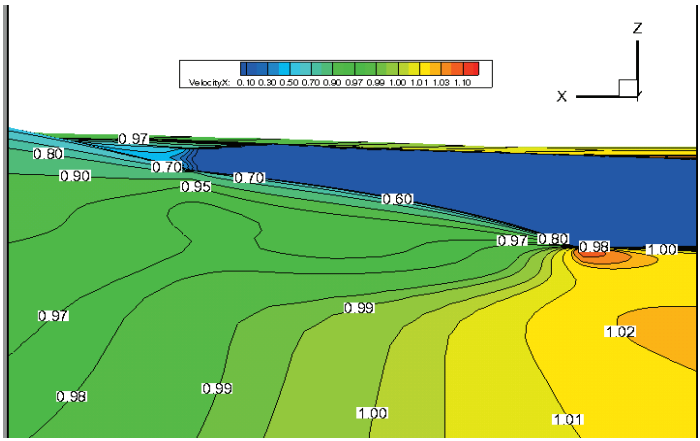

Fig. 50 Axial velocity in the aft part of the ship at, Fn = 0.401

As seen in the Figure 51 there is a low velocity region developing downstream the hull. Formation of boundary layer is the reason water to be less accelerated along the ship hull, and if going away transversely from the hull, the axial velocity increases rapidly until it reaches the horizontal velocity of the water when it leaves the boundary layer. Downstream there is a developing of a wake on the hull, where the water velocities increase slowly and inconsistently and the turbulent effects there develop as a result from the friction between the roughness of the hull plus appendages and the water flow. Sonar part develops turbulent flow structures, which also affects the boundary layer.

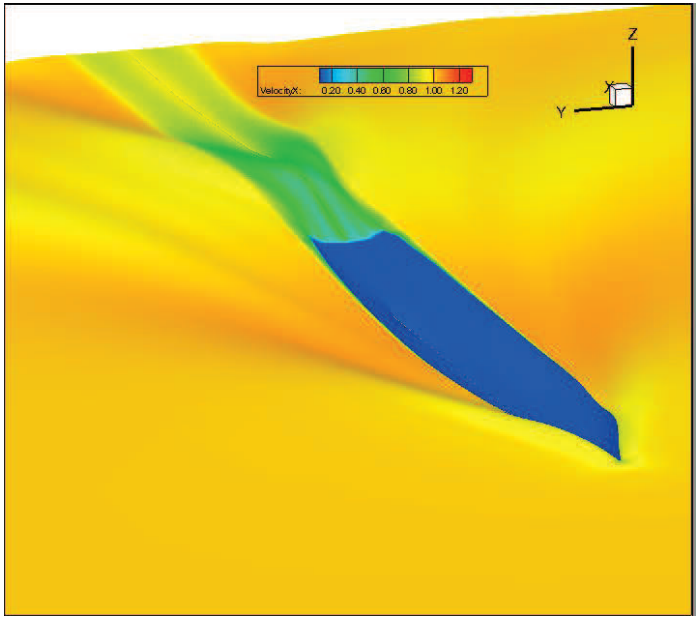

Fig. 51 Axial velocity around the hull at, Fn = 0.401, rudder - perspective view

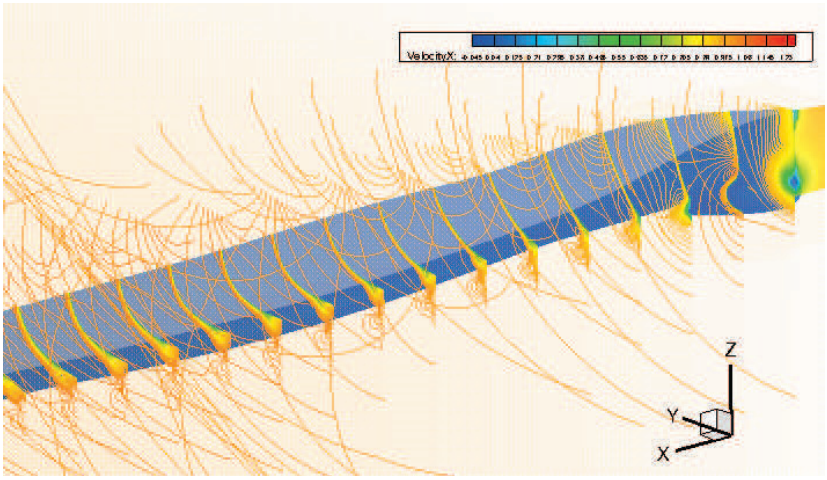

Fig. 52 Axial velocity around the mid and sonar part of the hull at, Fn = 0.401, rudder - perspective view

Free surface wave elevation as velocity Z is represented in Figure 53 in perspective view to give better overall representation of the free surface flow taken from potential solution around bare hull DTMB 5415.

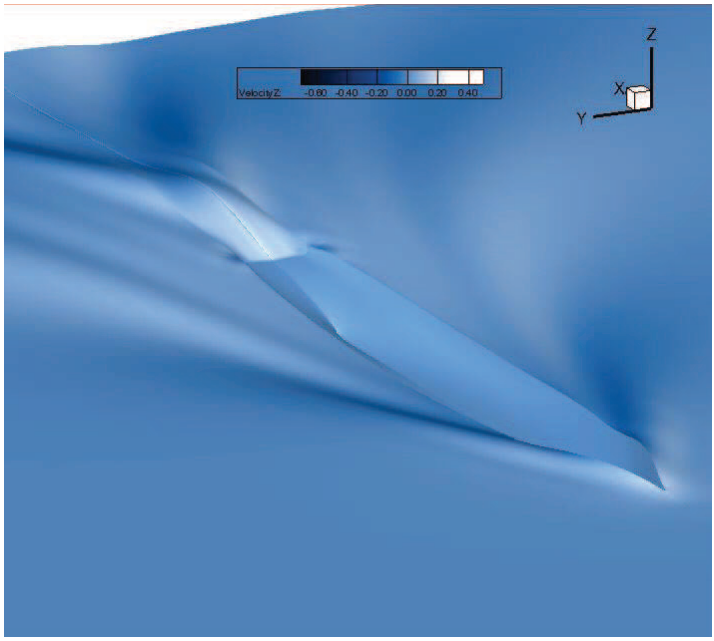

Fig. 53 Free surface wave elevation - velocity Z taken from potential solution, in perspective view at Fn = 0.401, rudder

Pressure on the rudder on Figure 54 shows as expected forming of high stagnation pressure region in forward part, which meets the flow. This region stops the water flow, and forces it to separate and pass around the body. The flow is slowing down from the friction with the surface of the rudder when it is passing through. This flow makes high-pressure region in the leading edge of the rudder. After this region, there is a pressure drop and velocity increases flowing pass the surface of the rudder until it normalises at the end of the ruder.

In the Figure 54 is seen also how is the resistance of the bracket to the flow, which adds to the frictional resistance form appendages pressure on the upper part is not affected due to the attached part to ship hull.

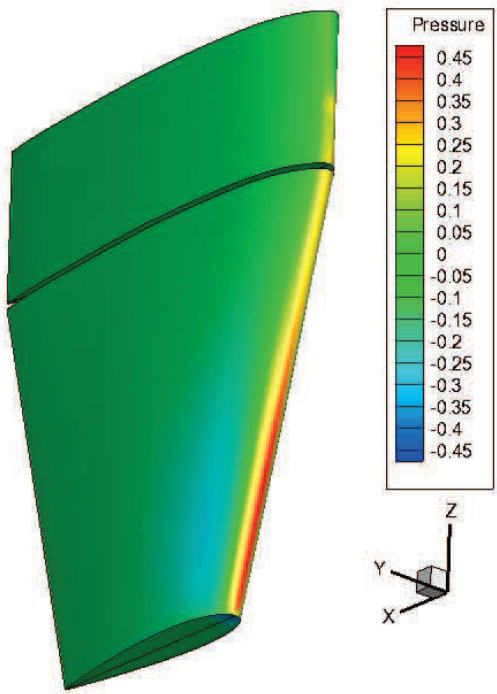

Fig. 54 Pressure distribution on the rudder surface plus bracket at, Fn = 0.401

Froude numbers which are further investigated are Fn = 0.28 and 0.41. Their results are presented in the flowing pages.

6.1.5. Pressure results for Fn = 0.28 bare hull no refined and refined - compared

Two cases are simulated for bare hull no refined and refined for 6000 iterations.

Results with refinement case were better capture the physics of the flow and the rest results are used only with refinement case. Dashed lines correspond to negative pressure in all the figures with pressure below. Solid lines correspond to positive pressure.

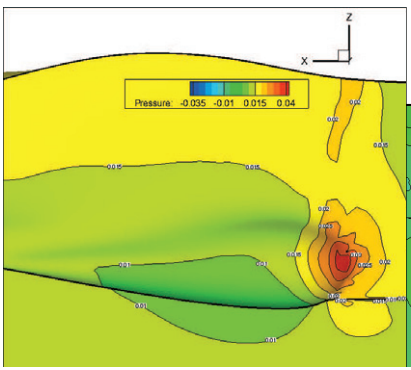

Fig. 55 Pressure results at sonar region for Fn = 0.28 bare hull no refined

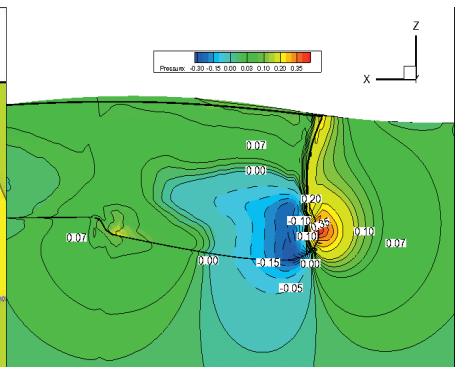

Fig. 56 Pressure results at sonar region for Fn = 0.28 bare hull refined

Pressure on the sonar region has stagnation positive point on the tip of the sonar and ring with negative pressure in its widest part just below and behind its positive stagnation point, which coincides good with this geometry shape. At the end of the sonar there is a second increase of the pressure because of the closing of the curvature by the potential theory. If there is a negative pressure region this means that there can occur cavitation leading to inconsistencies of the flow.

6.1.6. Results for Fn = 0.28 and Fn = 0.41 bare hull - compared

At Froude number 0.41 pressure gradient is more prominent with larger pressure region compared with Froude 0.28. There is a secondary higher pressure region developing on the back part of the sonar shown in the Figures 57 and 58.

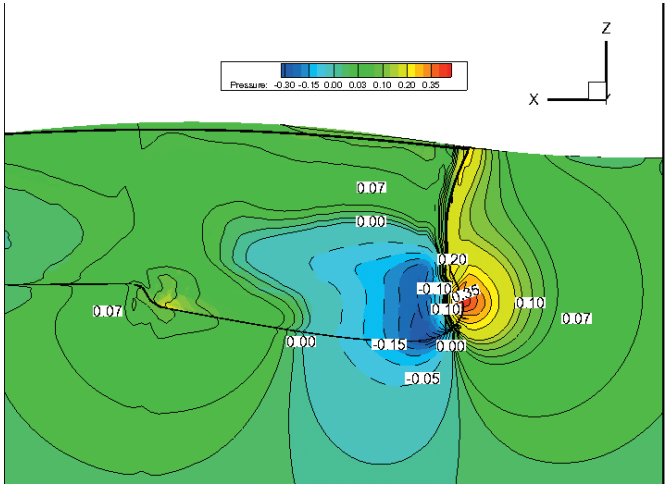

Fig. 57 Pressure results at sonar region for Fn = 0.28 bare hull

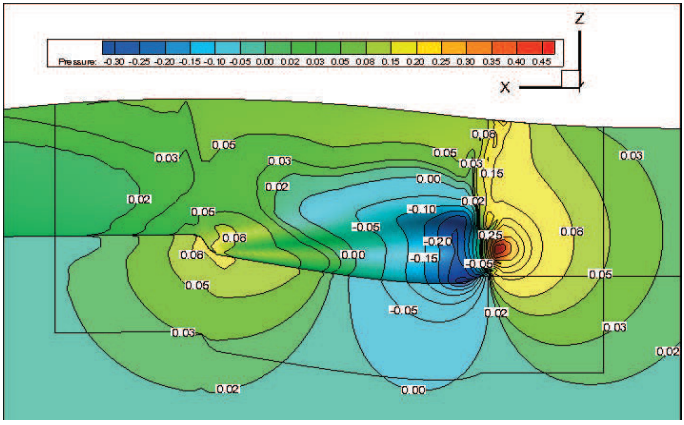

Fig. 58 Pressure results at sonar region for Fn = 0.41 bare hull

The Figure 59 shows two regions with negative pressure, which gives possibility of occurring cavitation phenomenon; there is saddle high-pressure part in the slope curvature of the stern between the low-pressure parts.

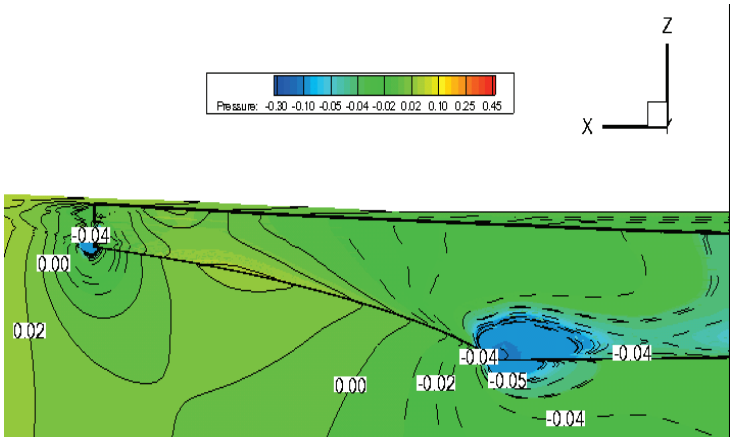

Fig. 59 Pressure results at ship aft region for Fn = 0.28 bare hull

In Figure 60 the two low pressure regions can be seen as in Froude number 0.28, with higher-pressure region develop between them

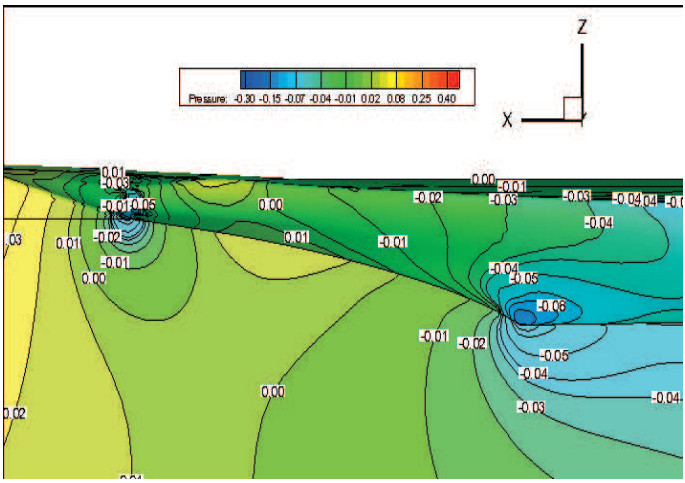

Fig. 60 Pressure results at ship aft region for Fn = 0.41 bare hull

Figure 61 shows acceleration of water around the sonar with slowing down at the beginning when the water meets the sonar and then accelerating rapidly until middle part of the curvature of the sonar when there is again slowing down of the water.

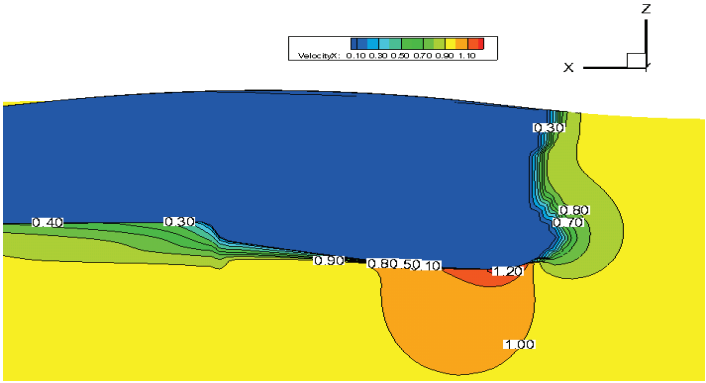

Fig. 61 Axial velocity results at ship sonar region for Fn = 0.28 bare hull

Axial velocity results on the sonar part in Figure 62 show the contours developed around the sonar part of the hull with lower velocities at the tip and back of the sonar and higher velocities just behind the tip of the sonar part.

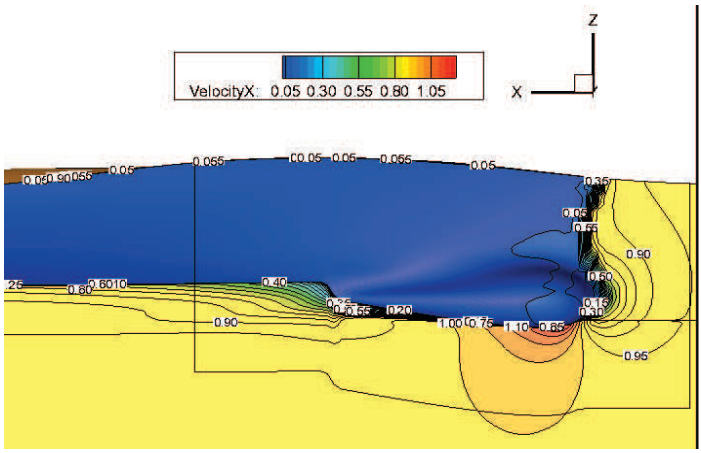

Fig. 62 Axial velocity results at ship sonar region for Fn = 0.41 bare hull

Aft region shows that there is a faster zone bellow the transom, which may come from the higher slope on the junction between the bottom part of the hull and long curved stern. Behind the transom part there is a region with low axial velocity, which leads to wake boundary layer that drags the water along the hull with lesser speed that ship speed and thus aggregating more to the frictional drag.

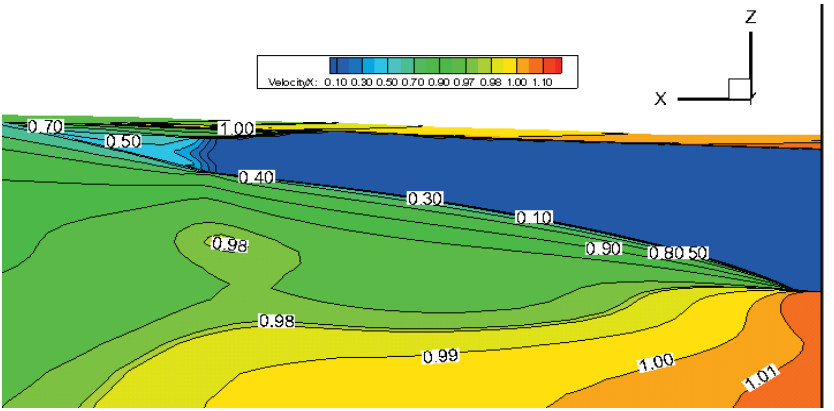

Fig. 63 Axial velocity results at ship stern region of the hull for Fn = 0.28 bare hull

The contours in Figure 64 cover the flow around the stern part smoothly, no disturbances are noticed for this case.

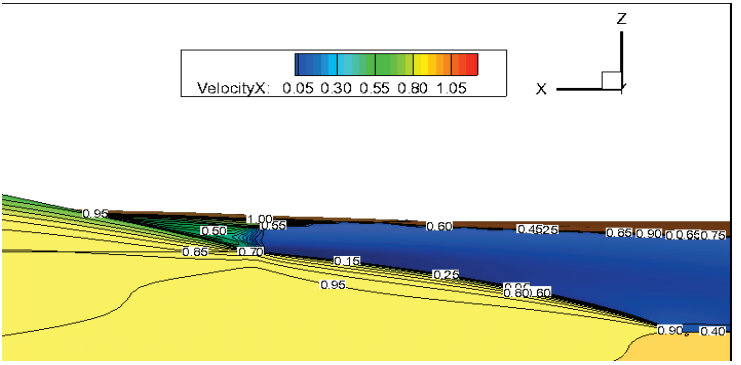

Fig. 64 Axial velocity results at ship stern region for Fn = 0.41 bare hull

6.1.7. Results for Fn = 0.28 with rudder and rudder bracket and shaft

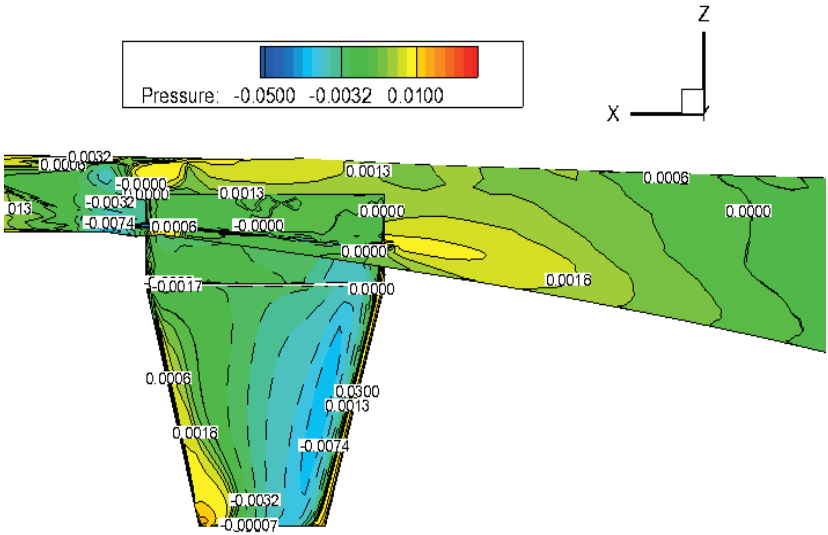

Fig. 65 Pressure results at ship stern with rudder, rudder bracket and shaft at Fn = 0.28

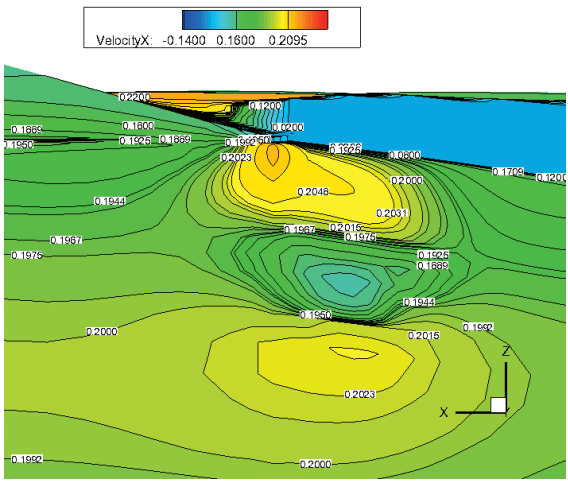

Fig. 66 Axial velocity results at midplane slice in XZ direction in ship stern region for hull at Fn = 0.28 with rudder and rudder bracket

Compared Figure 66 with Figure 63 for bare hull case, can be deducted that change in velocity contours is from the added rudder and bracket. There are two regions with high velocity and one region between them with low velocity because the rudder stops the free flowing of the flow. Axial velocity on the hull is zero because of no slip condition on the hull.

6.1.8. Additional Results for Fn = 0.41 bare hull

Axial velocity starts lowering down going from the bottom of the sea to the wave surface, because is hard for the water to rise the curvature of the wave created by the pressure gradients shown in the Figure 67

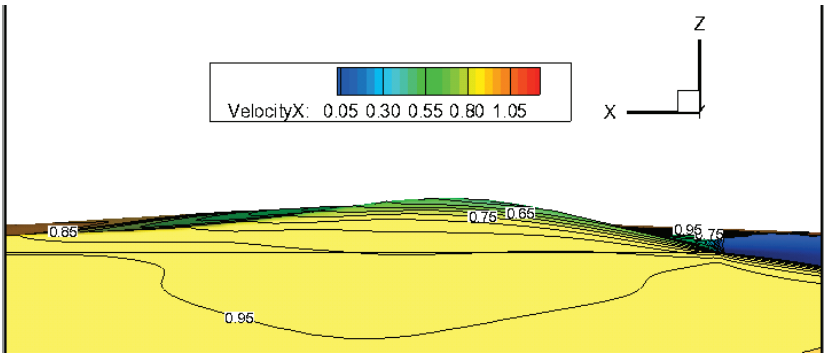

Fig. 67 Axial velocity results at ship stern zoom out region for Fn = 0.41 bare hull

Axial velocity contours show increase rapidly in the middle of the sonar region of velocity then there is sudden drop of velocity as it goes to the end of the sonar and this drop of velocity continues decreasing as going further away towards the aft part of the ship as seen in the Figure 68. The shape of the contours shows formation of circulation zones from both sides of the sonar below and towards the stern with possibility of forming eddies and separation which can create eddies drag.

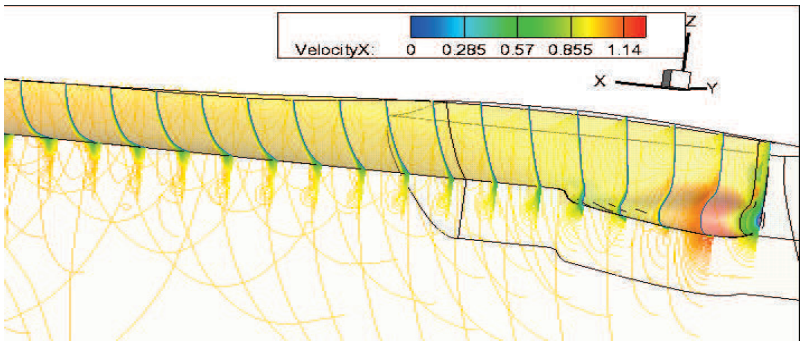

Fig. 68 Axial velocity contours at different slices of the hull Fn = 0.41 bare hull

Towards the stern part the velocity around the hull keeps the pattern gradient from low 0 near the hull to up to velocity of the flow further away presented in Figure 69.

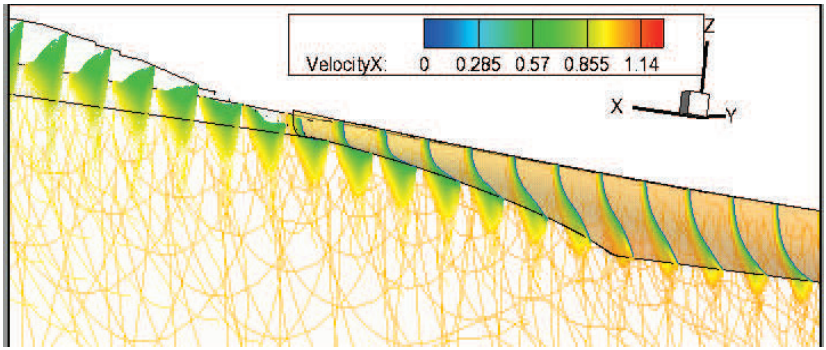

Fig. 69 Axial velocity contours at different slices of the hull Fn = 0.41 bare hull

6.1.9. Propeller model

The propeller model calculates the body-forces based on the effective wake field, which means that the propeller solver implemented in CFD code is running interactively with the RANS solver. The viscous module specifies body forces in the cells of an additional cylindrical grid that covers the location of the propeller. The body forces are distributed between the hub and the maximum propeller diameter and in the axial direction to avoid big changes in concentration of introduced forces.

Propeller is modelled as actuator disk with prescribed thrust and torque, or using the lifting line theory. The propeller position, detailed geometry, and advance ratio are specified for lifting line method, while if a force actuator disk model is used, the detailed geometry is not necessary. Along the whole hull, single structured 3D numerical grid is created with clustering cells near the bow and stern regions. There is a need of clustering using 3D overlapping grid generator close to the hull surface where the height of the cells should be very thin. Additional cylindrical grids are added to simulate operating propellers.

The grids are fitted behind the ship to compute trust and torque. Using the velocity computed in each numerical cell within the propeller disk, the lifting line program computes the circulation and thereby the axial and tangential body forces, which are returned to the flow solver in an iterative process. The propeller and hull geometries are represented by no-slip faces resolved directly in RANS approach and therefore they become part of the viscous solution. Further ships motion and resistance can be explored for optimization purposes.

6.1.10. Results for Fn =0.28 no propeller and propeller and Fn = 0.41 compared

Pressure acting on the leading side of the rudder is increased from lower to higher Froude as well as when propeller is put the interactions can be seen on Figures 70 to 72.

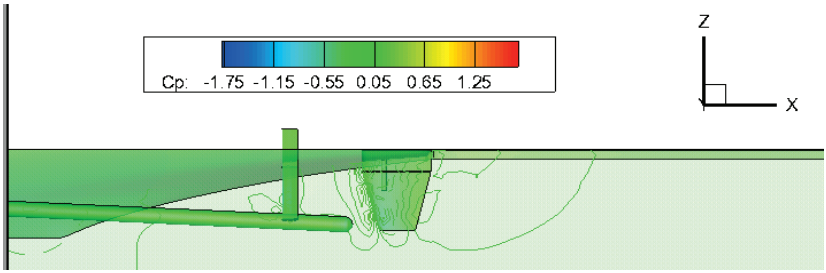

Fig. 70 Pressure acting on the hull and appendages at Fn = 0.28 no propeller - slice on rudder

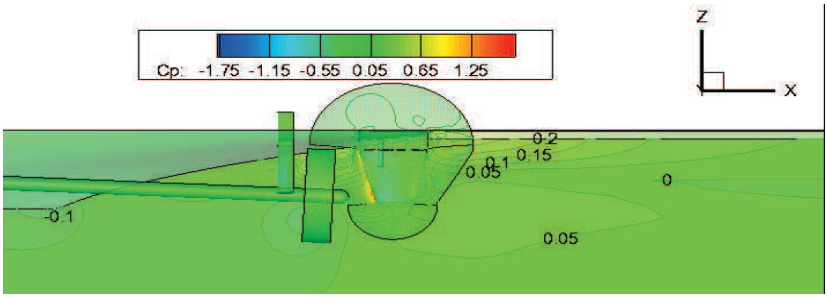

Fig. 71 Pressure acting on the hull and appendages at Fn =0. 28 propeller - slice on rudder

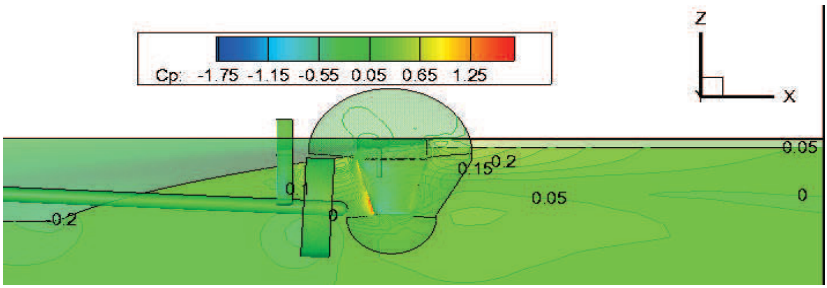

Fig. 72 Pressure acting on the hull and appendages at Fn = 0.41 propeller - slice on rudder

Axial velocity acting on the bottom part of the rudder is increased from lower to higher Froude as well as when propeller is put the interactions can be seen on Figures 73 to 75. There is a negative axial velocity region acting on the leading edge on the rudder. Longitudinal cross section at rudder can be seen on Figure 73-75 on the rudder plane with the developing high in the bottom part of the leading edge with solid lines and low axial velocity distributions with dashed lines.

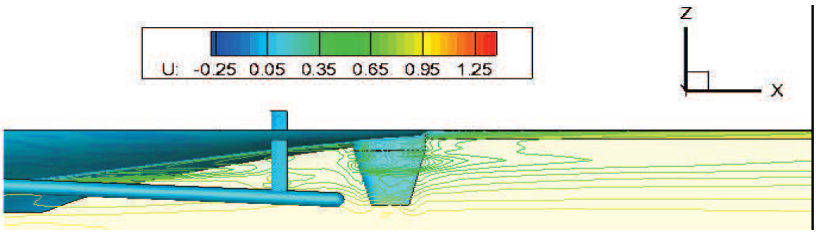

Fig. 73 Axial velocity acting around hull and appendages at Fn =0.28 no propeller - slice on rudder

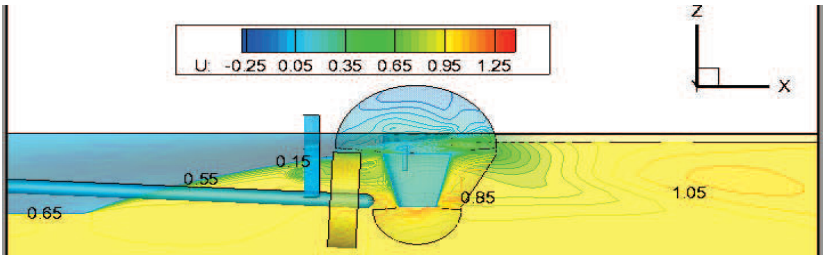

Fig. 74 Axial velocity acting around hull and appendages at Fn = 0.28 propeller - slice on rudder

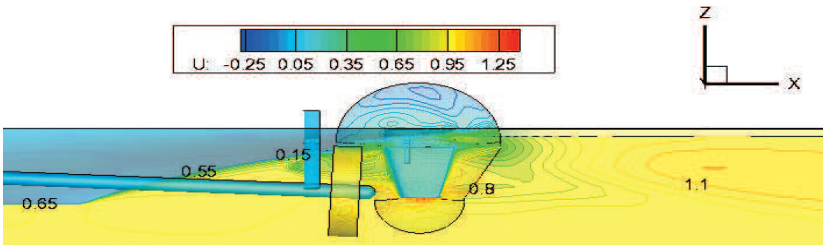

Fig. 75 Axial velocity acting around hull and appendages at Fn = 0.41 propeller - slice on rudder

Axial velocity acting after the shaft is increased from lower to higher Froude as well as when propeller is put using Actuator disc theory. The interactions can be seen on Figures 76 to 78. There is a positive axial velocity region coming from propeller and streaming bottom portion of the rudder. Longitudinal cross section at midplane can be seen on Figure 76 to 78 with the developing high in red and low axial velocities in blue.

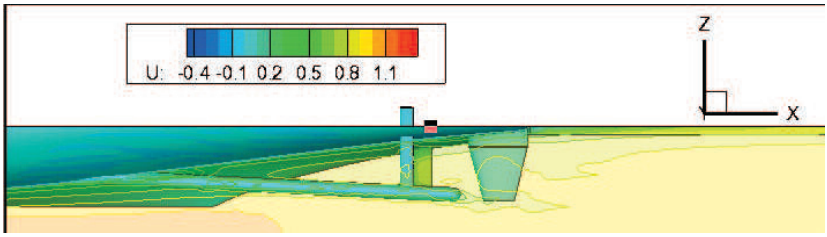

Fig. 76 Axial velocity around hull and appendages at Fn = 0.28 no propeller - slice on midplane

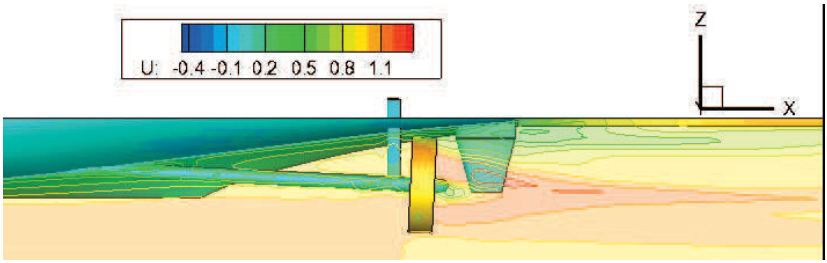

Fig. 77 Axial velocity around hull and appendages at Fn = 0.28 propeller - slice on midplane

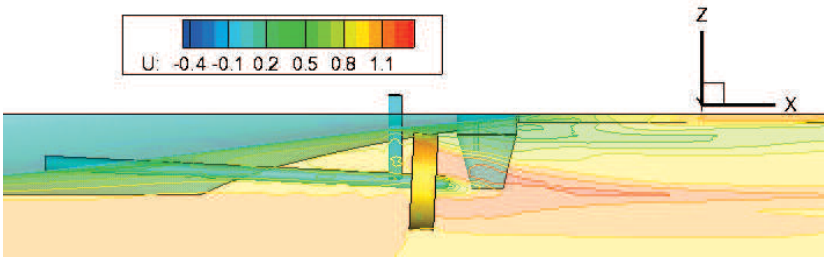

Fig. 78 Axial velocity around hull and appendages at Fn = 0.41 propeller - slice on midplane

6.1.11. Results for Fn = 0.28 and Fn = 0.41 hull with appendages and propeller compared

Better representation of the pressure without seen geometry of propellers to disturb the view can be seen on Figure 79 and Figure 80.

There is increase in the pressure acting on the hull of the connection between the rudder bracket and the hull seen in Figure 80.

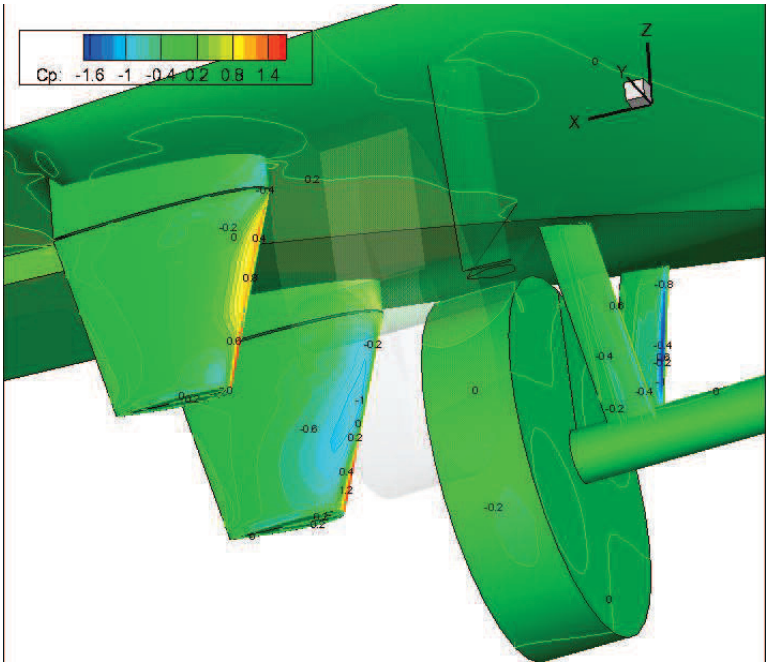

Fig. 79 Pressure distribution around the hull at Fn = 0.28 with appendages and propeller

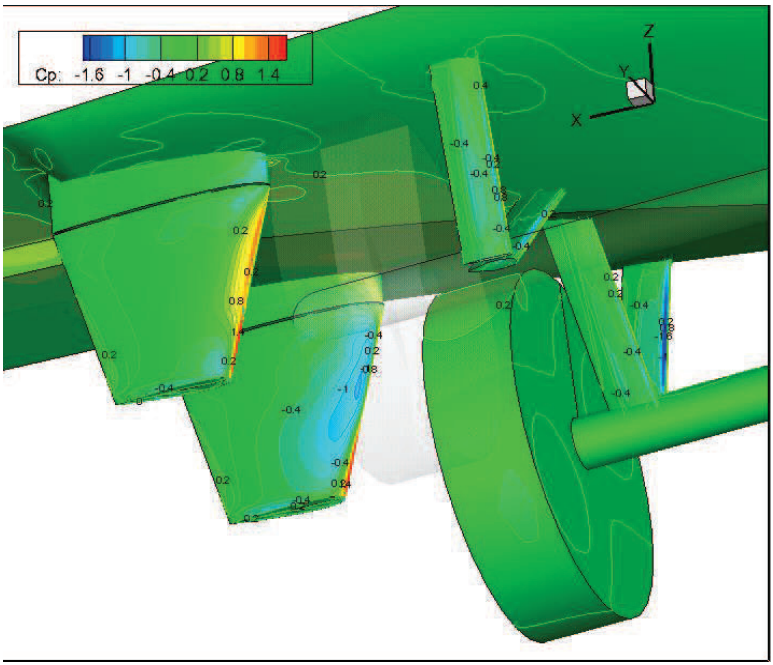

Fig. 80 Pressure distribution around the hull at Fn = 0.41 with appendages and propeller

6.1.12. Additional results at Fn = 0.28 no propeller, propeller and Fn=0.41 propeller

Overall view of the pressure acting on the frame brackets holding the shaft, to which the propeller is attached, the rudder the rudder bracket and the hull can be seen on Figure 81.

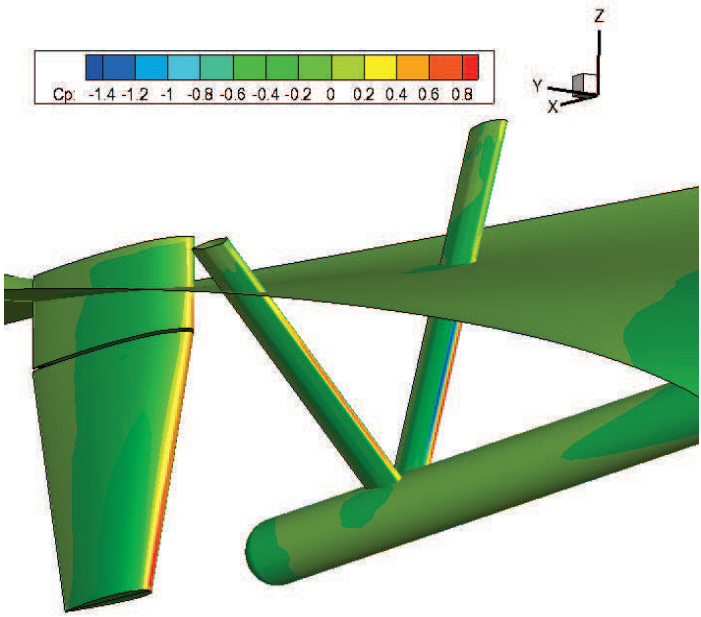

Fig. 81 Pressure distribution on the aft part of the hull at Fn = 0.28 for appendages and no propeller

Overall view of the axial velocity acting on the frame brackets holding the shaft, to which the propeller is attached, the rudder the rudder bracket and the aft part of the hull can be seen on Figure 82 with made transversal cross sections with the developing high velocities in red and low velocities in blue. It can be seen how the A frames holding the shaft create disturbances on the flow which is transmitted to the propeller and rudder consequently, as well as shaft effect in the bottom part acting on the bottom part of the rudder. If there is a region with negative velocity this means that it changes the direction, and make circulation, which can lead to separation and eddie drag.

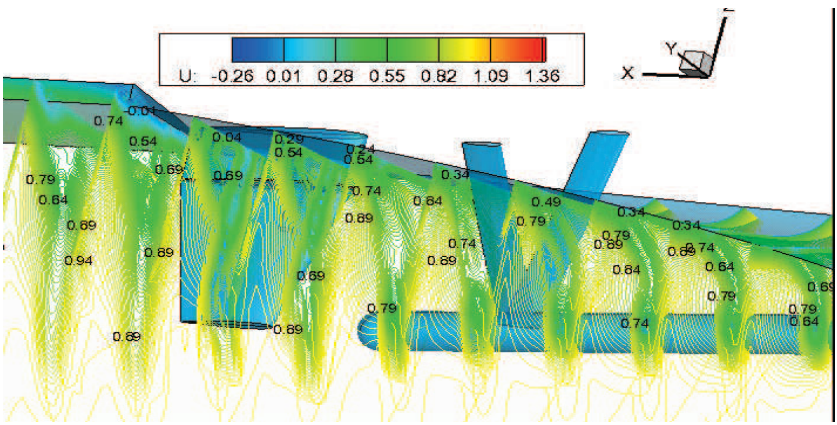

Fig. 82 Axial velocity distribution transversal slices on the aft part of the hull at Fn = 0.28 with appendages and no propeller

With less contours the most prominent regions can be found, the chosen option depends on the level of investigation, this can be seen on Figures 83 and 84 about the difference between the axial velocity distributions.

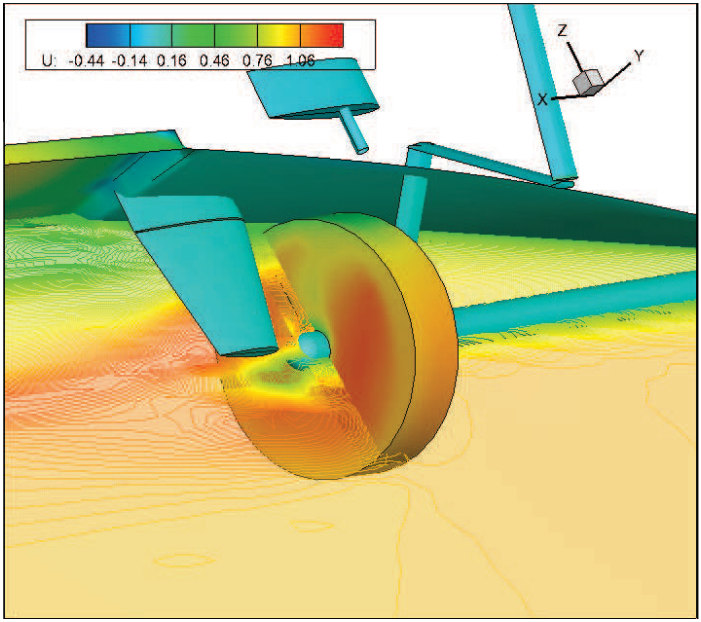

Fig. 83 Axial velocity distribution on the aft part of the hull at Fn = 0.28 with appendages and no propeller - longitudinal slice at propeller plane - Less contours

There is an increase in the size of the shapes of axial velocity acting on the rudder from the propeller disk. This velocity increase develops further down the water stream and can be seen on Figure 84.

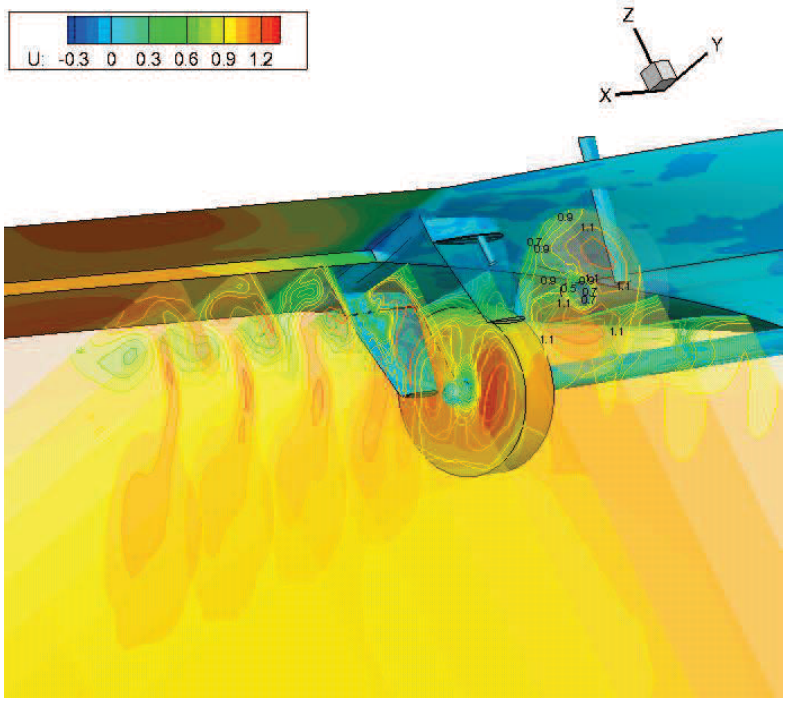

Fig. 84 Axial velocity distribution on the aft part of the hull at Fn = 0.28 with appendages and no propeller - longitudinal slice at propeller plane - More contours

Compare of axial velocities on the propeller plane

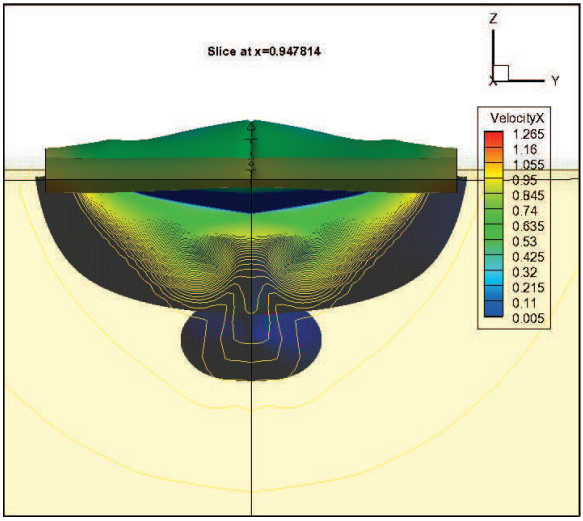

Fig. 85 Axial velocity at the propeller slice x=0.947814 at Fn=0.28 – bare hull

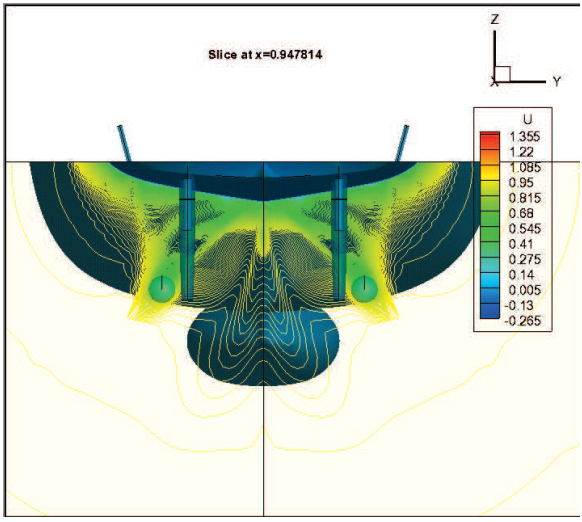

Fig. 86 Axial velocity at the propeller slice x=0.947814 at Fn=0.28 - hull with appendages

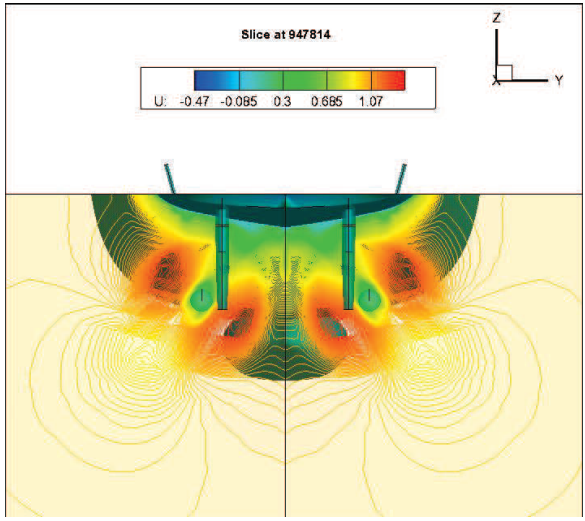

Fig. 87 Axial velocity at the propeller slice x=0.947814 Fn=0.28 - hull with appendages and propeller

On Figures 85 through 87 is seen how axial velocity develops in the propeller cross section at x=0.947814. The strong contra rotating vortexes created from the sonar dome traveling through the ship's hull interfere with appendages and the addition of the propeller actuator disks further complicates the axial velocity distribution. On Figure 87 can be seen how velocity is further increased from the propeller discs and their pressure there is low, which is perquisite for cavitation. On the hull surface there are two low velocity zones, creating high pressure from the propellers, which may induce vibrations, and must be investigated.

6.2. Conclusions of Viscous Flow Computation

Comparing with refinement in the sonar zone proved better results for capturing the second-high pressure point in the aft of the sonar. As it seems RANS solution using EASM approximated turbulence model proved to be better than K-omega SST for describing the turbulent structures with better performance for tested cases –information is taken from article [34].

Comparing between axial velocity and pressure distribution for Froude numbers 0.28 and 0.41 showed that pressure acting on the leading side of the rudder is increased from lower to higher Froude as well as when propeller is put. Axial velocity acting on the bottom part of the rudder is increased from lower to higher Froude as well as when propeller is put. There is a negative axial velocity region acting on the leading edge on the rudder. Longitudinal cross section at rudder can be seen on the rudder plane with the developing high in the bottom part of the leading edge with solid lines and low pressure distributions with dashed lines.

Comparing between pressure and axial velocity of appended solutions and appended with propeller with two different Fn around the propeller disk region showed that there is increase in the pressure acting on the hull of the connection between the rudder bracket and the hull. Axial velocity acting after the shaft is increased from lower to higher Froude as well as when propeller is put using Actuator disc theory. There is a positive axial velocity region coming from propeller and streaming bottom portion of the rudder.

An example code has been applied found in the Appendix 2.

7. CONCLUSIONS AND PRESPECTIVE

Numerical CFD analyses of the flow with resistance determination for fully appended DTMB 5415 combatant hull has been made. A lot of pilot computations have been performed by changing the size of the grid. Later the computation investigation was continued with good grid for potential flow solution. Further detailed investigation of different Froude numbers with or without appendages and propeller, using viscous flow solution has been made. The focus was in the regions with appendages and sonar dome, by utilizing hybrid method fitting potential flow free surface to the viscous computation. A solution of mesh resolution with around 2-3 million cells and 6000 iterations took five days with current computer systems year 2013 I5 processors. Improvements of the grid was realized where more detailed investigation of the flow was needed like additional overlapping grids for the appendages and mesh refinement in the sonar region.

For the computation a hybrid method is being used, in which free surface computation from potential flow was fitted in viscous flow solution, and the wave resistance has been computed. The potential flow solution with help of boundary layer theory determined wave resistance and frictional resistance. After more comprehensive viscous RANS solution was performed. It utilizes EASM approximated turbulence model. Actuator disk model was used for simulating the propeller.

Main simulated cases are for Froude numbers 0.28 and 0.41, and with the configurations: bare hull, hull with rudder, and hull with full appendages and propeller. They also prove good correlation with the theory.

Conclusion about the results:

SHIPFLOW software proved to be robust, user-friendly and fast for predicting the flow with accompaniment of post processing TECPLOT for visualization. Good correspondence between the accuracy of the solution compared with the experiments with differences between 1% and 15% for most of the Froude numbers for the potential flow solution. Potential flow theory determined the free surface elevation successfully, which give good quality and accuracy as a starting point for further investigation with viscous flow theory. It is recommended to use for free surface elevation computation the cases without transom for smaller Froude numbers, and cases with transom for bigger Froude numbers which gives less than 3% deviation from the experimental data except for the Froude number 0,35. Possible reasons for deviations with experimental results is not good meshing for the free surface or too much turbulence flow with eddies created by sonar part in front of the ship, which cannot be captured with boundary layer method as well as form factor definition, which is not defined in resistance computation of potential flow.

Boundary layer theory does not capture well the turbulence effects around the appendages, and for investigation of the local differences of the flow was used viscous flow computation.

The software validates its ability to capture the flow precisely enough for the purpose of investigating the DTMB 5415 hull with appendages. Results for this benchmark case were capturing reasonably well the free surface wave elevation with main Kelvin wake pattern developed by the hull.

Investigated configurations of bare hull and with different appendages and propeller made more comprehensive investigation of the flow in the stern region as well as in the sonar region, where more complex geometry curvature changes and appendages can be found. Compare of influences exerted by different configurations of the appendages on the wake structure in the propeller disk shown increase in drag from the appendages and propeller.

The results showed graphical and numerical differences in pressure, axial acceleration and wave surface elevation between the bare hull solutions and appended solutions, also between solutions with different Froude numbers and with or without propeller. These tests prove the hull shape to be complex, and used as a basis for further development of the flow around fully appended hull and it is good basis for different design cases depending on the Froude number.

Found bugs which break the solution at certain Froude numbers in the software and reported to the support team of SHIPFLOW version SHIPFLOW4.6.00-x86_64. A Workaround of the problematic Froude numbers was found with inserting dummy values after wanted Froude numbers were got from experimental results. This gives correct solution for potential flow with Xbound and later possibility of using the data for viscous computation. All good results and also bad are reported to support team of the software product.

Future development of the thesis:

For future developments of the thesis is recommended to compare between CD Adapco StarCCM+ software and SHIPFLOW for speed, accuracy of the results, what time takes to prepare geometry as well as executable time for the whole solution. The reason behind is in different method to treat free surface called Volume of fluid and webinar organized by CD-Adapco professor Milovan Peric in which reported 0.38 percent error from experimental data for the same hull shape DTMB 5415 for refined grid and for coarse grid around 2 percent error for specific Froude number using software StarCCM+ of CD-Adapco, Numeca Fine/Marine, Open Foam, VOF-FLOW of HydroOcean. In References the link of the webinar is given. Propeller can be used using bladed geometry with lifting line theory and not with actuator disk assumption for taking account local differences in pressure, as well as rotating and also simulating self-propulsion tests. Rudder and propeller positions and shapes can be checked with variations of hull form for optimization purposes using SHIPFLOW DESIGN or

Mode Frontier. Further refinements of the grid and mesh can be made, and more customisations incorporating new futures of SHIPFLOW software. Parametric models for the appendages to be used to compare resistance performances of the hull with different configurations.

Future trends:

Biggest advantage is in the number of possible different designs that can be tested in the virtual laboratory, simulated from computers, is enormous. Weakness is about that some assumptions on the Reynolds stresses using averaging models are made. Therefore, the solution cannot provide exact perfect match with the reality and make representation for the flow behaviour at each point. Solution gives general interpolated idea for small areas of particles, which is good enough to describe the behaviour of the fluid. So much detail for exact solution is not needed because the gain in design performance will be very little in a matter of less than half percent comparing to computational cost and also this could be loosed in the way if tried to technically produce.

Generally, the realization in lowering resistance of the design, comparing thousands of shapes cannot be captured only by analytical thinking that is the reason the computers can help to describe and compare the solutions, and the designer will choose the selective criteria for finding the optimum design for hull, appendage form and arrangement for better performance, economical benefit and efficiency. This can be achieved using multi-objective classical, evolutionary (genetic algorithms, multi objective genetic algorithm) or behaviour (particle swarm optimization, simulate annealing) optimization approaches to derive Pareto functions utilizing correct weighting function for specific requirements of the design.

With increasing of parallel computing, CUDA GPU technology, and cloud computing, these solutions for engineering problems becomes more and more feasible for industrial practices not only in research departments.

8. REVIEWER COMMENTS

Title of Thesis: Numerical investigation of flow around an appended ship hull

Student's name: Svetlozar Neykov

Period of study: 2011-2013.

University (where the thesis is performed): **UGAL**

Name of the reviewer: Lionel Gentaz

Affiliation of the reviewer: Ecole Centrale Nantes

General comments (scientific and technical aspects) - about 5-10 lines:

This work is a very interesting study on CFD capabilities for flows around ships with appendages. The report is globally well written with a lot of details and explanations; an effort has been made to comment each result and each figure. To my opinion it shows a great amount of work done by Svetlozar during creation of his book.

The Chapter 1 is a good introduction to capabilities of CFD in naval design.

Chapter 2 gives a general presentation of the solver and Chapter 3 a description of the potential flow module in the solver.

Results obtained with potential solver are presented in Chapter 4. Some remarks about this part:

p. 33 it seems strange to me that low speed case is on the left (figure 18); is there really a part of the free surface behind the transom stern which is not meshed in this case? More details should be useful.

p. 36 Is the ship fixed in calculations (and in experiments)? Why computations are done with or without trim? Is trim not defined for each case that has been tested?

p; 38 how Cf is calculated ? With a k form factor (and an empirical formula) or with a boundary layer numerical model?

p 39: my concern is : for a hull where experiments are not known how to choose transom option or no transom option in calculation ?

Chapter 5 is a fine presentation of RANS equations and viscous solver.

Chapter 6 presents results obtained with the viscous flow solver for a DTMB hull with appendages - propeller and rudder - which are quite promising and interesting; influence of propeller is well highlighted (figure p. 78).

It is a pity that there are no comparisons between numerical results and experimental data in this part (for global grad or velocity and pressure fields in planes located in the wake of the ship ...) but it does not alter the quality of the work.

Quality of the presentation - 2 lines:

Editorial Remarks and English quality:

Equation (9) p. 28: partial derivative symbols are not visible! - fixed

Equation (12) p. 28: ti is not an equality! - fixed

p. 29 "wave breaking" instead of “wave braking" - fixed

Except this mistakes, the report is well written and structured.

Recommended grade: My proposal is **15**

Not acceptable (7/20 or below)

Failed: 8 or 9/20

Weak (10 or 11/20)

Average (12/20)

Good (13 or 14/20)

Very good (15 or 16/20)

Outstanding (17 or 18/20)

Exceptional (on student each 10 years): 19 or 20/20

Date 2013/02/01 **Signature:** 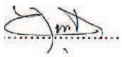

Responses to the review:

p. 33 it seems strange to me that low speed case is on the left (figure 18); is there really a part of the free surface behind the transom stern which is not meshed in this case? More details should be useful.

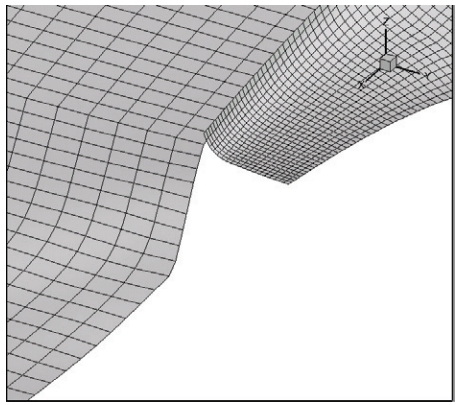

Fig. 88 Transom region views of Potential flow mesh

Svetlozar: In SHIPFLOW software for potential flow solution the grid of free surface is considered separated from hull and it is treated differently. With this treatment the body is assumed like is finishing smoothly and the free surface is closing after the hull so no grid is made in the stern region. There is not taking into account the hard changes of curvature behind the transom stern region, which in low speeds lead to the effects of "dead water zone" making not clean separation and incorporating viscous effects. These effects cannot be computed by potential flow theory due to their nature and are left for the viscous computations. The information how exactly free surface is calculated using linearized Dawson's method for boundary conditions, the body double model solution and iterative processes is mathematically extensive and can be found in SHIPFLOW presentations [36].

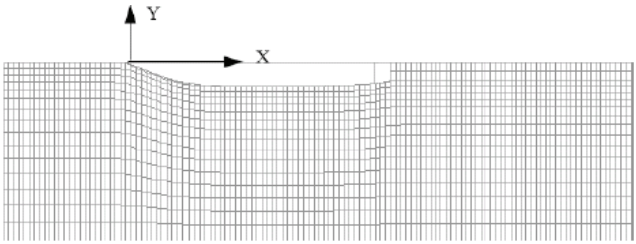

Fig. 89 SHIPFLOW User Manual example

As seen in the Figure 89, when the command transom is not used, free surface grid is made as if the body is extended.

Additional information taken from User Manual of SHIPFLOW

p. 36 Is the ship fixed in calculations (and in experiments)?

Svetlozar: The simulated cases are using options FREE and NONLINEAR for the calculations.

FREE - The ship is allowed to sink and trim during the computation.

NONLINEAR - The non-linear free surface boundary condition is used

Example part of output for command file for potential flow computation:

For experimental data, was not found information about how the experiment was performed.

Why computations are done with or without trim? Is trim not defined for each case that has been tested?

Svetlozar: Trim option is part of the command IPOSITION that sets initial position of the ship. The command makes possible to use same offset point coordinates for different roll and trim conditions. There is no information for the trim in experimental data, and because different internet resources give different information for sinkage and trim and almost no results to compare other than Rt, trim option has been tested as alternative for cases with and without transom just to compare the differences with the experiments. That is

why trim option is only hypothesis test case to see the variation of the results due to initial trim.

So initial position was using ipos(trim=0.41) just as test, after the initial trim initialization, the trim is left free during the simulation with utilizing option free in the control command. For the other experiments was initially no trim and later in the computation it was left free together with the sinkage as usual resistance computation in towing tank and other degrees of freedom locked from the carriage. One paper that I found with STARCCM+ used fixed sinkage and trim, but it was not relevant, because it did not have results shown, so was choosed option free in SHIPFLOW and obtained good correlation with experiments.

p; 38 how Cf is calculated ? With a k form factor (and an empirical formula) or with a boundary layer numerical model?

Svetlozar: Cf is calculated using integral momentum equations of boundary layer theory by numerical method in Xbound module described below. In tested cases formula Rt = 0.5*rho*U^2*WSA*Lpp^2*(Cw + Cftot) has been used SHIPFLOW output. Cftot is the friction resistance computed in XBOUND if executed. Information taken from User Manual of SHIPFLOW [20]. Theory behind Cftot computations using integral momentum equations of boundary layer theory by numerical method. Information taken from Ship flow user presentations [36].

p 39: my concern is: for a hull where experiments are not known how to choose transom option or no transom option in calculation?

Svetlozar: Transom option of potential flow module XMESH makes discretization of the flow near the stern. It is used for high speed vessels, sailing yachts, tunnel sterns and for flat overhang sterns usually works with higher Froude numbers. This is because the speed of flow is high enough to detach in

the aft part of the ship. If velocity is smaller, there will be so-called dead water and viscous effects, which cannot be captured with potential flow so they

exclude this region for the viscous computations, and just finish the body smoothly.

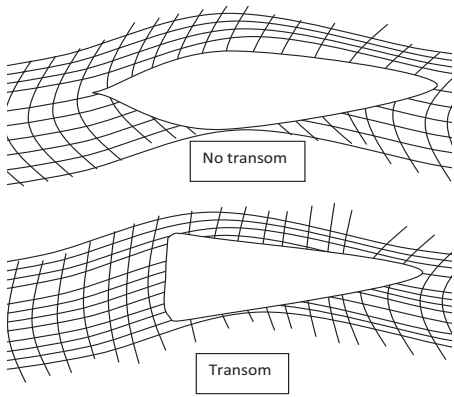

Fig. 90 With transom and no transom functions for XMESH module

Generally, transom option is used for high Froude numbers like yachts, this is written in the manual from SHIPFLOW [20].

It is a pity that there are no comparisons between numerical results and experimental data in this part (for global grad or velocity and pressure fields in planes located in the wake of the ship ...) but it does not alter the quality of the work.

Svetlozar: During the research there was not found results information which can be compared, if there is such available and provide to the author it will be subject to future work, which will be extension of this.

9. ACKNOWLEDGEMENTS

The author wishes to express his great thanks to Professor Adrian Lungu, to Professor Florin Pacuraru, and Professor Oana Marcu for their valuable help, critique, comments and observations trough creation of the book and during the experimental model without which the thesis could not be done.

Big appreciations are given also to the support team of FLOWTECH – Ship Flow in the face of Magnus Östberg (support@flowtech.se), who helped always in hard moments of computation, with priceless advices for completing the job.

Deep acknowledgements for the reviewer Professor Lionel Gentaz, Ecole Centrale de Nantes.

Enormous gratitude to Professor Philippe RIGO for always understanding and giving opportunities to the students, which are priceless such as EMSHIP project. Thanks to the great teachers and minds involved in this program from all over the world.

Thank you all for the help that you have given to me in my study journey!

This book was developed in the frame of the European Master Course in "Integrated Advanced Ship Design" named "EMSHIP" for "European Education in Advanced Ship Design", Ref.: 159652-1-2009-1-BE-ERA MUNDUS-EMMC.

10. REFERENCES

Journal article	1.Larsson L., Bertram V., Stern F., 2000, Proceedings of GOTHENBURG 2000, A Workshop on CFD in Ship Hydrodynamics, Gothenburg, Sweden, 2000
	2. Y. Toda, Y., Stern, F., J. Longo, J., 1992, "Mean-Flow Measurements in the Boundary Layer and Wake and Wave Field of a Series 60 CB = 0.6 Ship Model – Part 1: Froude Numbers 0.16 and 0.316", Journal of Ship Research Vol. 36, pp.360-77.
	4.Van, S.H., Kim, W.J., Yim, G.T., Kim, D.H., Lee, C.J., 1998, "Experimental Investigation on the Flow Characteristics around Practical Hull Forms", Proceedings of Osaka Conference.
	5.Tryggvason, G., Bunner, B., Esmaeeli, A., Juric, D., Al-Rawahi, D., Tauber, W., et al., 2001, "A Front-Tracking Method for Computations of Multiphase Flow", Journal of Computational Physics, Vol. 169, pp. 708–59.
	6. Hirt, C.W., Nichols, B.D., 1981, "Volume-of-Fluid (VOF) Method for Dynamics of Free Boundaries", Journal of Computational Physics, Vol. 39, pp. 201–210.
	7. Osher, S.J, Sethian, J.A., 1988, "Fronts Propagating with Curvature-Dependant Speed: Algorithms Based on Hamilton–Jacobi formulations", Journal of Computational Physics, Vol. 79, pp. 12–40.
	8. Sussman, M., Smekerda, P., Osher, S.J., 1994, "A Level Set Approach for Computing Solutions to Incompressible Two-Phase Flow", Journal of Computational Physics, Vol. 114, pp. 146–159.
	9. Hoekstra, M., 2006, "A RANS-based analysis tool for ducted propeller systems in open water condition", International Shipbuilding Progress, volume 53, pp.205 – 227.

	10. Xingrong,, S., Xuemei, F., Rongquan, C., Yuejin, C., 2009, “Study on Hydrodynamic Performance of Podded Propulsion in Viscous Flow”, First International Symposium on Marine Propulsors’09, Trondheim, Norway
	11.Funeno, I., 2009, “Hydrodynamic Optimal Design of Ducted Azimuth Thrusters”, First International Symposium on Marine Propulsors’09, Trondheim, Norway
	13. I. Senocak and G. Iaccarino, 2005, “Progress towards RANS simulation of free surface flow around modern ships” Center for Turbulence Research Annual Research Briefs
	14. Zhang, D.H., Broberg, L., Larsson, L., Dyne, G., 1992, “A Method for Computing Stern Flows with an Operating Propeller”, RINA Transactions, Vol.134.
	15.Zhou, L., Zhao, F., 1994, “An Integrated Method for Computing the Internal and External Viscous Flow Field around the Ducted Propulsor behind an Axisymmetric Body”, Proceedings of the 20th ONR Symposium, pp. 1011–1020.
	16. Steger, J.L., 1991, “The Chimera Method of Flow Simulation, Workshop on Applied CFD”, University of Tennessee Space Institute/
	17. Steger, J.L., Dougherty, F.C., Benek, J., 1983, “A Chimera Grid Scheme Advanced in Grid Generation”, ASME FED, Vol. 5,pp.59-69.
	18. Wang, Z., 1995, “A Fully Conservative Interface Algorithm for Overlapped Grids”, Journal of Computational Physics, Vol.122, pp. 96-106.
	19. Regnström, B., Broberg L., Larsson, L., 1999, “Overlapping Composite Grids for Ship Stern Flow Calculations, MARNETCFD First Workshop, Barcelona.
	20. *** ShipFlow User’s Manual, FlowTech International, 2003

	21. Olivieri, A., Pistani, F., Avanzini, A., Stern, F. & Penna, R., 2001, “Towing Tank Experiments of Resistance, Sinkage and Trim, Boundary Layer, and Free Surface Flow around a Naval Combatant INSEAN 2340 model”, IIHR Technical Report No. 421, The University of Iowa.
	23. A.M. Tocu, M. Amoraritei., 3 December 2008, “Numerical study of the flow field around a ship hull including propeller effects”,Journal of Maritime Reasearch, Vol. V. no.3.
	26.“ITTC – Recommended Procedures and Guidelines 7.5-03 01 – 01, Page 4 of 12 : CFD General Uncertainty Analysis in CFD Verification and Validation Methodology and Procedures with Effective Date 2002, Revision 01 , chapter 4: VERIFICATION PROCEDURES , 4.1
	27. F.R.Menter:ZonalTwoEquationk-!TurbulenceModelsforAerody-namicFlows,In24thFluidDynamicsConference,Orlando,July1993,AIAApaper-93-2906
	28. G.B.Deng,P.Queutey,M.Visonneau:Three-DimensionalFlowCom-putationwithReynoldsStressandAlgebraicStressModels
	29. STARCCM+ User manual
	33. Janson, C-E., (1997) Potential Flow Panel Methods for the Calculation of Free Surface Flows with Lift, Ph.D. Thesis, Chalmers University of Technology
	34. Free-surface flow around an appended hull - A Lungu and F Pacuraru Department of Ship Hydrodynamics, “Dunarea de Jos” (http://iopscience.iop.org/1755-1315/12/1/012079)
	35. Numerical Simulation of the Flow around an Steerable Propulsion Units, 25th IAHR Symposium on Hydraulic Machinery and Systems, September 20-24, 2010, Timisoara, Romania, Florin Pacuraru, Adrian Lungu, Costel Ungureanu and Oana Marcu Department of Ship Hydrodynamics, “Dunarea de Jos” University of Galati, Available from: URL [http://iopscience.iop.org/1755-1315/12/1/012032]

	36. Presentations for SHIPFLOW users- Personal web site of Tsung-Yueh Lin http://nas.tinyla.idv.tw/~F96525033/Instruction/Flowtech%20Shipflow/
	37. XchapTheoreticalManual34 by SHIPFLOW FLOWTECH
Internet document	12. International Towing Tank Conference 1996 [online]. Source. Available from: URL [http://ittc.sname.org/2002_recomm_proc/7.5-03-02-02.pdf].
	22. *** "Gothenburg 2010 A Workshop on CFD in Ship Hydrodynamics", [online]. Source. Available from: URL [http://www.iihr.uiowa.edu/gothenburg2000/5415]
	Geometry file for combatant DTMB in iges file format: [online]. Source. Available from: URLs [24, http://www.simman2008.dk/5415/combatant.html 25. http://www.nmri.go.jp/cfd/cfdws05/Detail/5415/combatant.html]
	30. Resistance prediction formulae of Maxsurf module HullSpeed[online]. Source. Available from: URLs [http://www.formsys.com/extras/FDS/webhelp/hullspeed/viewing_results.htm]
	31.NPTEL national programme of technology and enhanced learning [online]. Source. Available from: URLs [http://nptel.iitm.ac.in/]
	32. Webminar by prof. Prof Milovan Peric about resistance computation of DTMB 5415 using STARCCM+ [online]. Source. Available from: URLs[http://www.cd-adapco.com/downloads/webinar_recordings/streams/70140000000MRuRAAW.html]
Thesis	3. Longo, J., 1996, "Yaw Effects on Model-Scale Ship Flow", Ph.D. Thesis, The Department of Mechanical Engineering, The University of Iowa.

APPENDICES

Appendix A1: Resistance theory describing physics of the problem

Resistance of ship to forward motion is the force required to pull the towed ship by another ship at a constant speed.

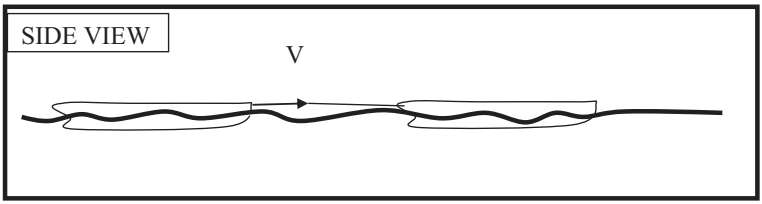

Fig. 91: Ship resistance representation

Resistance is equal to the towed rope pull. Normally in the seaway, they are many disturbances such as air, waves, and current. The towrope pull is determined in calm sea condition, and then the resistance to forward motion is approximated only due to the movement of water and some amount of air resistance. This resistance is called calm water resistance. The ship could be with or without appendages.

Appendage is structure or attachment of the ship outside the hull. If there is no appendages attached to the hull resistance is called naked hull or bare hull. If appendages are there when determining the resistance of the ship this is called appended hull resistance. When the ship speed is described, there must be indication of the condition in which the speed is measured. The speeds in which ship operates are: trial condition speed, which is called trial speed, or speed in actual service in which ship operates.

Resistance corresponding to the trail conditions is called trail resistance or resistance in trail condition, which is more than the calm water resistance. When the ship goes in service, there is addition to the trail resistance from the waves, current, corrosion and, fouling. This resistance is bigger than trail resistance and it is called service resistance or resistance in service condition. It

will be varying depending on hull and sea condition and it is estimated with adding allowance to the trail resistance. Service resistance is then used for powering purposes.

Used units are in Si system with reference of units used in ship operation. Resistance in ship is expressed in force unit kilo Newtons – kN.

Speed is expressed in meters per second – m/s [SI], knots [conventional ship operation]

1 knot = 1 nautical mile per hour = 1.852 km = 0.5144 meters / second

Effective power is the power required to overcome ship resistance without propulsion measured in Kilowatts. $P_E = R_T.V$

$$P_E = R_T.V$$

1 KW = 1 HP (metric)/ 0.735=1 HP (British) / 0.746

Components of resistance in ship in calm water.

If the body is not moving in the water the pressure that acts on the body will be hydrostatic pressure.

Hydrostatic pressure = $\rho.g.h$

ρ - density of the water kg/m^3

h – height of submergence of the body's centre of gravity to surface level – m

g – gravitational acceleration of object caused by gravity ≈ 9.82 m/s^2

If there is a flow (from the current) passing around the ship, the hydrostatic body pressure will change and will add new components to $\rho.g.h$, acting on the body called hydrodynamic components. The pressure will be called hydrodynamic pressure, because of the dynamics of water acting on the body.

The total pressure acting on the body will be hydrostatic pressure plus hydrodynamic pressure. Hydrostatic pressure is not considered, because

it gives buoyancy to the body. The buoyancy is an opposing up force to the weight of the immersed object.

Hydrostatic case

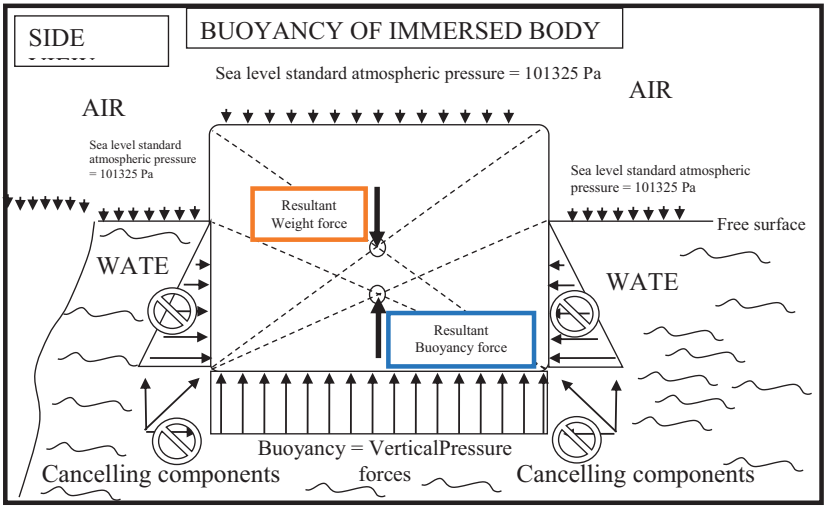

Fig. 92: Buoyancy of immersed body

Hydrostatic pressure is normal force and acts as shown in the Figure.92. Horizontal components will cancel acting on the sides and the diagonals of hydrostatic pressure will cancel too, because the symmetry of the body. The rest existing forces are vertical components of the diagonals, which will add to vertical pressure components on the bottom pushing the body outward. This resultant vertical push located at the centre of the underwater part of the body is called buoyancy.

The vertical pressure acting in completely rectangular body tries to push it above the water and it is ρ.g.h. The magnitude of this vertical push force will be equal to the mass of the water body displace or in other words the pressure acting on the underwater area of the body so ρ.g.h. area of the body. In this case will be ρ.h.B.L.g. = ρ.volume.g=mass.g=weight = force on object due to gravity trying to push the body up = Buoyancy

From the equilibrium of forces Buoyancy = Weight of the body + atmospheric pressure for body to float.

Principle of Archimedes says that - “The weight of the water displaced is equal to the weight of the body”.

B= breath of the body underwater part of the body

L= length of the body underwater part of the body

The weight force is acting on geometry centre of the body, which is found by perpendiculars in this case.

In case of fully submerged body:

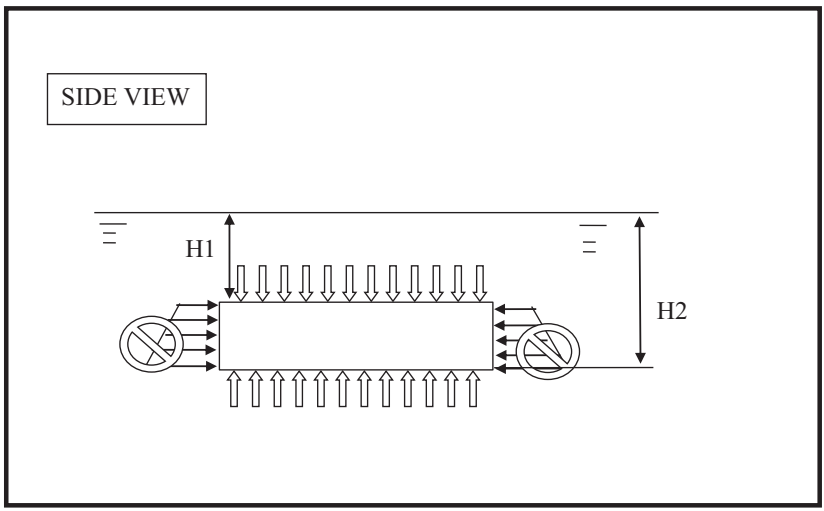

Fig. 93: Buoyancy of fully submerged body

Force acting on submerge body is upward force and it is equal to the mass of the total water displaced = ρg.(h2-h1).B.L

If the body is in equilibrium this upward force must be equal to the weight of the body, which is acting downwards and this is called neutral equilibrium of a submerged body. If the body is left in any place it will stay there, if the weight is more and the buoyant force is constant the body will go down until it rests on the ground. If the body is resting on the ground the

buoyancy force plus reaction of the ground equals the weight of the body. If the weight is less than the buoyancy, then the body will be pushed up. The body will come out of the surface until the buoyancy is equal to the weight. This all is hydrostatic force, but ship resistance problem is dealing with hydrodynamic force.

Hydrodynamic case with no viscosity. Submerged body case.

The body is completely submerged in the water with streamline shape (without any sharp curvature in each surface).

Such body is submerged completely like a submarine, and with the assumption that the body is non viscous, there is no viscosity on the fluid. Fluid is air, water or any liquid. The moving body at constant speed in calm water will experience the same motion as if the body is stationary and the water is moving at opposing direction.

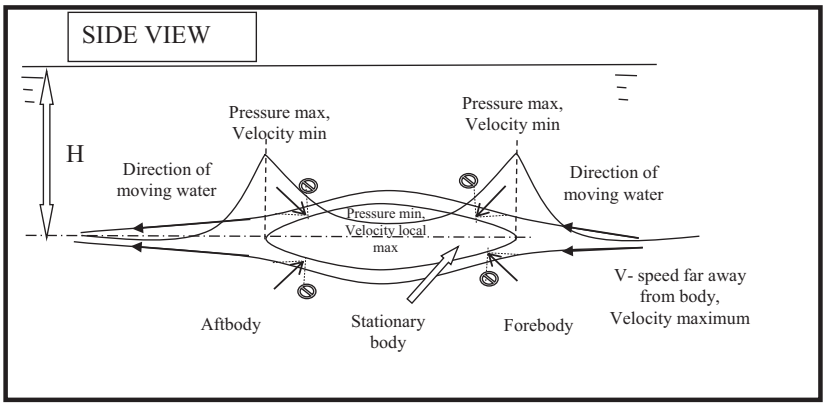

Fig. 94: Dynamic Pressure on fully submerged body

When there is a body submersed in the water and there is no viscosity of the fluid the water will flow around the body in the way shown in the figure.94

The pressure will be more in the ends and less in the middle. There will be two-pick pressure in front and the aft, because of the discontinuity of the flow from the body that is closing in. This is coming from the assumption of non-viscous fluid, no boundary layer, no free surface and no friction forces between

the layers of the fluid and on the body. This no friction hypothesis is made for the advantage of the theoretical investigation of the resistance. Due to Bernoulli equation which states that pressure and velocity are interrelated. If the pressure increases, velocity drops, because everywhere in the fluid the pressure and velocity combination is constant. This is valid only if hydrostatic pressure is ignored and considered only hydrodynamic pressure in the investigation.

As the pressure reduces velocity is maximum at the midship region, then the velocity has to come back to normal value so the pressure has to increase again and velocity is reducing. If the body is represented in mathematical form and used in potential flow calculation with assumption that the flow is non-viscous so there is no vorticity (no circulation the flow, the flow do not circulate) the high pressure of the two ends can be calculated.

Hydrodynamic case with viscosity

Fig. 95: Dynamic pressure on fully submerged symmetrical body with viscosity

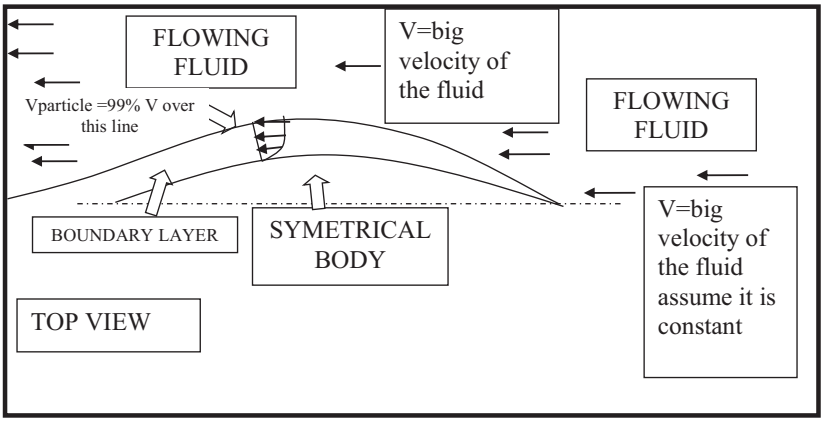

The water that was pushed out from the body needs to come back and fill the empty place in the aft part. This is the same principle as the airfoil. Vertical components of the pressure cancel each other and with all hypothesis plus no disturbance of the flow like separation and assuming that the interflow is streamlined, the horizontal forces will cancel each other. The forward horizontal

components oppose the motion and the horizontal components in the aft part support the motion of the body. Therefore, the resultant force in the longitudinal direction will be equal to zero. This means that if the fluid is no viscous and the body is moved there will be no resistance to this forward steady (constant) speed. This is a paradox of D'Alambert that in a no viscous fluid the resistance to forward motion is zero. But fluids are viscous water more than air. Viscosity is a frictional force between two layers like body or particle moving against another one (water) there occurrence of a force generated between this two parts called frictional force, which is the measure component of viscosity.

When the water is flowing past around the body. The body surface and the first layer of water will be in contact with each other. If there is any viscosity, the particle in contact with the body will move along with the body and will not move separately. This means that relative velocity of the particle to that of the ship will be equal to zero at the body surface. Opposite to the potential flow theory, and the submerged streamline body with no viscosity in which the particle moves freely on the surface on the body.

The fluid will not have any velocity at the point of contact to the body. The fluid is also getting friction between its particles, so the particle as it moves away from the surface of the body will not have velocity equalling velocity of the flow. Instead, as the fluid particle moves away from the body, the velocity will gradually increase. There will be some time and distance from the surface so the full velocity can develop and match the velocity of the flow.

The water is flowing in the forward end of the body has smaller thickness required to develop the full velocity because of the streamlined shape of the body. The distance from symmetry plane trough the most outward waterline shape fibre is bigger in the midship than in the bow, and stern region. As the distance increases friction force will build up and the thickness of this so called boundary layer will also increase. Once become bigger it will stay until end of the body shape, so that's is why in stern region thickness is not smaller

even tough geometry gets smaller (collapses at a point). Velocity profile as going away perpendicular to the body will increase as well.

In the forward end the fluid particle has stuck and the velocity will quickly develop full velocity of the flowing fluid around. If the particle around aft part of the body is taken, because of the history of the caught particles on the body it will require some distance to develop full velocity, which will be function of the length over which the fluid has flown. The reason is the friction between the body, the fluid surface, and the velocity of the surface on each particle of contact is equal to zero. If a velocity somewhere far away from the body is taken, the velocity will be the same, as being calculated with potential flow theory with non-viscous fluid, because viscosity effect is only near the body.

Prandtl theory of thin boundary layer over a long narrow body

Theory states that the boundary layer develops around the body, which is thin - meaning the thickness of the boundary layer is small compared with main dimension of the body (length in the ship). Assumption is made that beyond the boundary layer the flow is as if there is no friction and all the frictional effects are bounded in the boundary layer. Then the boundary layer that starts from the forward flowing part of the body slowly will start to develop enlarge itself and will lag after the body becoming the shape shown in the figure 96. The area between the body and the fluid and the line drown around the body is called boundary layer. The velocity of the particle in this borderline is equal to 99% of the velocity of the flow. The velocity profile going perpendicularly away from the body surface is shown in the figure 95 and it is including viscous effects of the velocity to the potential flow pressure composition diagram get from non-viscous flow case. The body is moving and it will be with varying pressure and velocity distribution near the body. Far away the velocity is supposed to be constant to this distribution if standing on the ship and looking the flow around the hull, with known constant speed. In the Figure 95, ship is still and the

velocity of the particles of the water will take ship speed value if there is current it should be incorporated summed with the ship speed velocity. In the boundary layer, the velocity is much less than this velocity of the particles far away. This means that one can assume that a lot of water has been taken away or said in other words pulled along with the ship. In flow of full-scale ship this pulling of water can be observed in a small region near the stern called wake and it is moving with the ship "is being dragged". Beyond this region the sea is behaving as before. Contrary in the boundary layer the pressure is very high and the hull construction must be made to resist this outside pressures.

When non-viscous potential flow theory and viscous boundary layer theory are combined pressure and viscosity will act together. The potential flow theory will behave after the boundary layer, which is controlled by viscous boundary layer theory. The pressure will act as if body I prolonged, and it acts on the boundary layer not on the body directly.

Fig. 96: Combined non-viscous and viscous theories

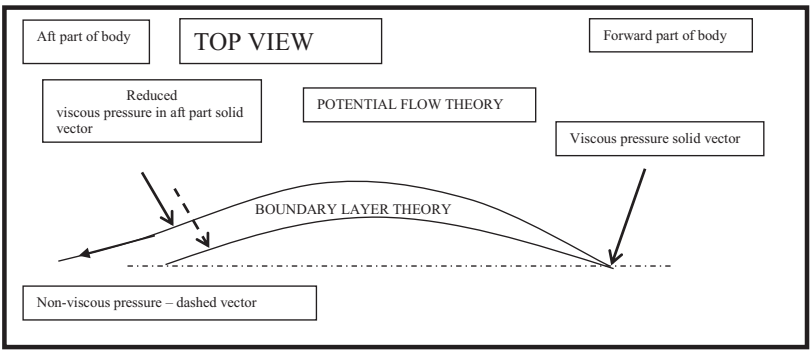

The figure shows that the boundary layer is small in the front body part and the pressure will act similarly as in the potential flow theory. Contrary in the aft body part, the viscosity is acting more prominent in the developed boundary layer, which plunges the flow, and the body acts as if it is smooth more and the pressure distribution changes. The pressure is acting directly on the boundary layer, and in the aft part, it will be reduced. This means that there the pressure is

not equal to the pressure acting on forward part of the ship as in separate potential flow theory; therefore, there is a resulting opposing force to the moving body called resistance. The components acting on the boundary layer are called viscous pressure resistance, which is a pressure resistance coming due to viscosity controversy to the potential theory where the pressure resistance is equal to zero.

When body is blunter than usual streamlined foil shape the effect is more prominent. The pressure drop is more substantial. Maybe there will be negative pressure at some point, which means that the flow will start separating from the body. Instead of flow, going past the body it will go further and then curl in, because there is big curvature in the body end, which will increase the pressure gradient, and this will develop big jump from high pressure to negative pressure. This makes velocity higher and the flow and cannot follow the surface curvature so quickly, so it will start curl behind the body, because there will be large separation and it will dissipate as eddies into the water.

Fig. 97: Symmetrical blunt submerged body

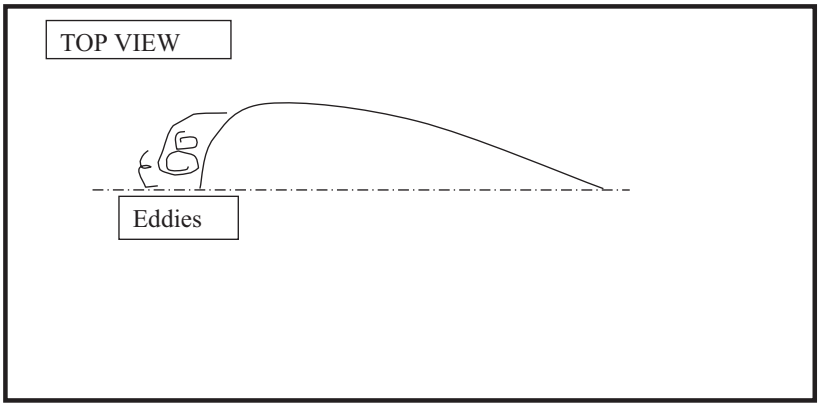

This effect can happen primary into viscous flow; it may happen also in no viscous flow. Primarily at the stern of the ship, it will occur due to viscous

flow. There is no non-viscos flow near aft portion of the body opposite to forward part of the body. This is phenomena in which the flow separates from the body and creates eddies. This is another component of resistance called separation or eddy drag and dissipates into the water loosing energy given for this process. If the flow was non viscous the flow will go around the body and circulation may appear but not separation and eddy drag behind the ship.

The energy that ship gives to the water comes from the tangential forces between the layers of the flow and creation of boundary layer, in which the mass of the water is following the hull, comes from the ship. The energy that comes out of the ship is called frictional resistance purely due to friction.

Primary in submerge body there is: viscous pressure resistance, frictional resistance, separation, and eddy drag. If the flow is at an angle maybe there will be perpendicular force to the direction of the flow called lift, which will be dynamic used in aircraft engineering, additional to the static lift called buoyancy mentioned earlier. Buoyancy is purely dependent to geometric of the body not on the flow. Lift is vertical force generated due to the flow. In conventional ships, there is no lift force unless particularly designed. In case of the ship, if there is a lift force it will lift the ship up. If there is an intention the lift to be generated, the body geometry must be designed using best profile giving maximum generated lift; airfoil shape is the best for lift generation. In a displacement, ship, which is based on the displacement phenomena, this states that buoyancy equals to weight there, will be no lift force.

Body floating on the surface of the water further complicates the physics, because the main difference is that body behaves in two fluid media: water and air. Between the media, there is a surface, which is free called: free surface. The geometry of that free surface will depend on the interaction from this two media and the pressure. If there is, a water wave on the sea surface the pressure on the top of the free surface is constant and equal to atmospheric pressure.

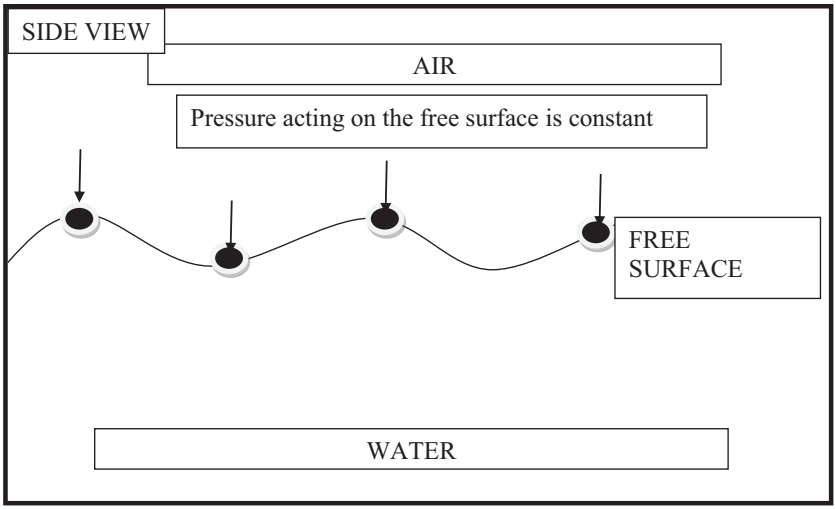

Fig. 98: Pressure acting on the free surface

This pressure will vary drastically as it going down and will increase with increase of depth. In addition, it will vary when it goes up from the free surface, because the air becomes less dense and weight's less so it will reduce the air pressure with the rise of the elevation, also there is the velocity of the air which will change the pressure gradient.

If a potential theory is combined with free surface the behaviour changes, as soon as there is a high-pressure force it will push the water up until such height that the pressure becomes constant atmospheric pressure and will generate a wave. In the forward part of the ship the effect of viscosity is

neglectable and no viscous theory will be dominant to predict generating a big wave. Similarly, there will be big wave generated in the aft part of the ship. There may exist small waves generated along the length of the ship, because of generation of high pressure. Wherever there is a high pressure point along the length of the ship a wave will be generated. There are two sets of waves:

a. Transverse waves
b. Divergent waves

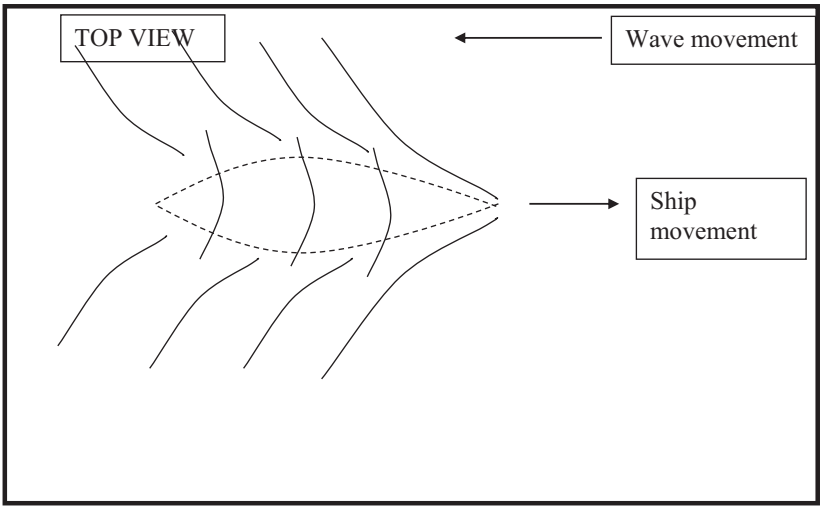

Fig. 99: Free surface waves

A set of transverse waves, the crest of which is at transverse direction to the longitudinal axis of the ship. Crest is highest point on the wave and trough is lowest point in the wave elevation. There are set of transverse waves perpendicular to the direction of the ship and a set of divergent waves diagonal to the direction of the ship, which will go far away in transverse direction as they diverge. The crest will be near the ship hull and far away from it as it will dissipate – spread in different directions and absorb in the water.

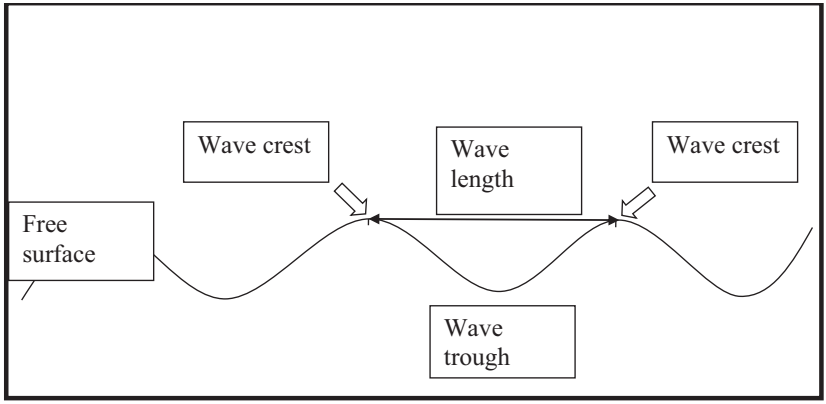

Fig. 100: Wave parameters

$\lambda = \frac{\upsilon}{f}$ - Wavelength is equal to velocity over frequency

These waves carry big amounts of energy; to sustain this wave making continuously the ship spends energy, which is called wave-making resistance. This resistance was not there when the body was submerged in the water and it is not zero when is at the surface. Waves are gravitational phenomenon and are not affected by friction forces and viscosity. Contrary to the D'Alambert paradox with the assumption of no viscous fluid of submerge body that there is no pressure force resistance to forward motion, if the body is up on the free surface there is resistance to forward motion from generations of waves due to pressure phenomena.

The viscosity is there with frictional resistance, and the boundary layer develops and becomes wider as we go towards the back of the ship. The same thin boundary layer is coming on the free surface. Viscous pressure resistance damps the stern wave. The effect of the stern wave will be the same it will try to support the motion but this depends on the location on the stern wave.

If the stern wave is generated aft of the stern due to odd shape of the body underwater then the support of the ship will be loosed.

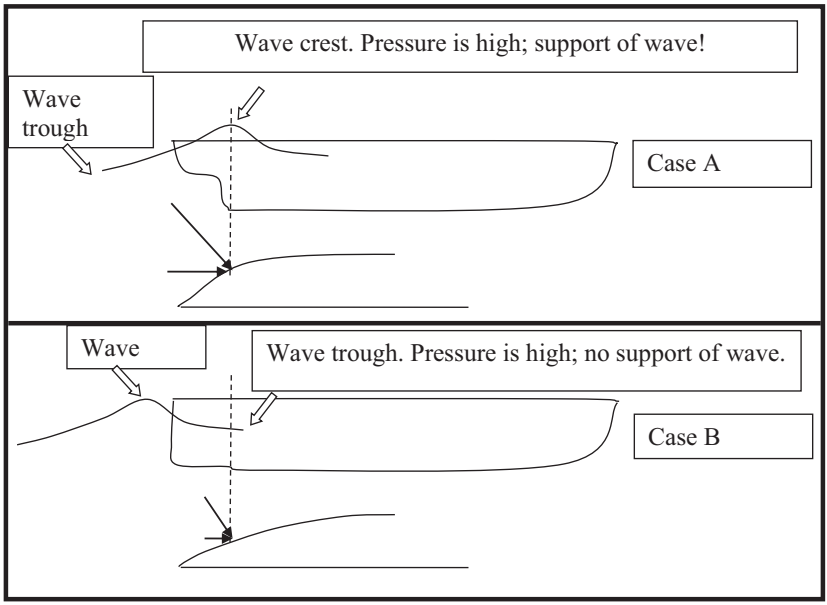

Fig. 101: Two cases of position of waves crests generated on the stern depending on geometry of the stern without viscosity.

In case A, the pressure is high in the crest located in the stern part and there is big horizontal pressure component supporting the forward motion.

In case B, the pressure is high behind the stern part there is trough so the horizontal component of the pressure is smaller, and the support to forward motion form the wave is smaller, which increases the drag.

Where the wave is generated in, the stern has an effect of the total resistance of the ship, because it is not only effected by the wave height but from the slop of the body at that point. Wave making is very complicated phenomenon, especially in the stern because from the boundary layer.

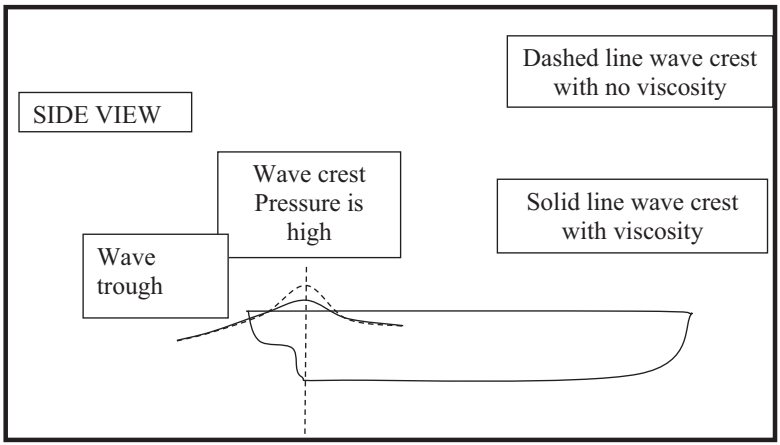

Fig. 102: Reduces of the wave crest in viscosity case

Wave crest reduces in viscosity case compared with non-viscous so as the supporting pressure to the forward motion of the hull and the total resistance is decreasing. There is blunting and decreasing of the wave making resistance (which is helping the ship in this case) in the aft case due to presence of boundary layer decreases the supporting force of the ship. So wave making part is primary due to contribution of the fore body of the ship, aft body also has small role for the wave making resistance.

Blunt ship like tanker or bulk carrier, the fore body beam is very large, block coefficient is very high around Cb =underwater volume of ship/Lpp.B.T= 0.85 or higher. Lpp – length between perpendiculars, B – ship breadth, T ship draught (height from most bottom part of ship to the sea surface)

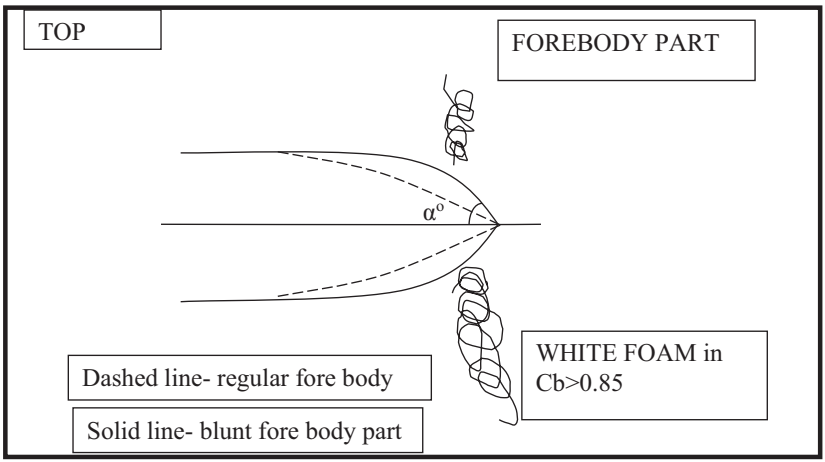

Fig. 103: Wave breaking on blunt hull types

The waterlines closing at the water level

Fore body part is very blunt – full body is with large half angle of entrance α so the discontinuity is very large. It will give very large wave slope on the surface, because wave will depend on the discontinuity of the body. That large generated wave cannot come along the length of the ship but the body will push it out. These waves that being created will have a large amplitude even at low speed and they will be pushed to the side. The wave slope will become high.

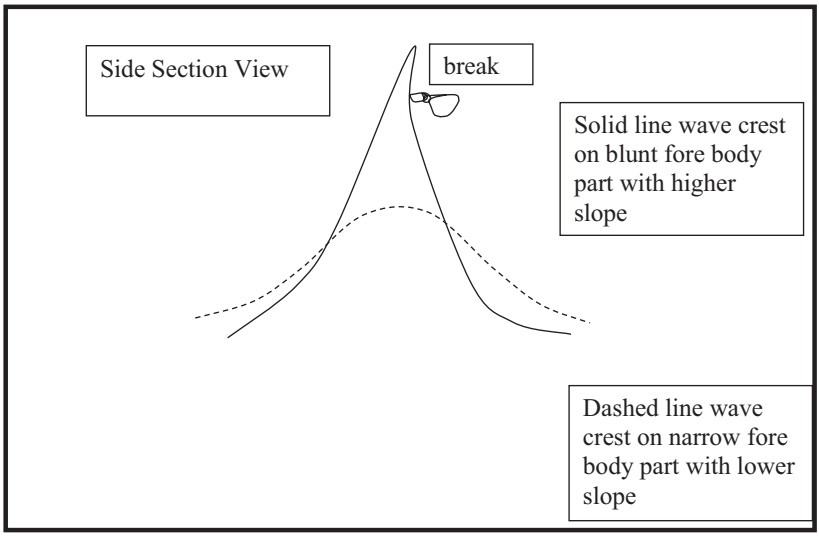

Fig. 104: Wave slope on blunt body

The gravity wave with very large slope cannot retain itself, and cannot maintain the shape anymore and it will break. This is usually represented visually in seacoast. Because of the reduction of depth as the wave comes to the coast, the wave height increases it cannot be maintain itself and it will break. The same situation is in forward body part a large wave slope will be generated, the waves will start climbing up, they cannot maintain itself so they will break. As soon as the wave breaks the energy transfers in form of sound and creation of eddies, that wave is absorbed by sound and the water particles, eddies are formed, there is foam creation in form of white mass.

Similarly, in forward body part the wave will not propagate as wave anymore once it breaks there will be the white mass. In large ships like tankers or bulk carriers, there is white mass diverging on the forward body, which means that the wave is broken, there is no large waves far beyond like in fine smooth ships. There is a big difference between these two phenomenons. In the case of smooth fine forward body the waves are carrying over the energy as wave making resistance, but in blunt fore body shapes the waves are generated

due to potential flow effect and loose energy butt the bigger effect of lost energy is in form of breaking waves. In slow full form ship, wave making is very small compared with wave breaking resistance. Similarly, in the forward bottom end there maybe eddies and separations exactly for the same reason in the aft body part, because of the sharpness of the curvature as phenomenon in full form ships. In fine form ships like frigates or naval vessels or container ships or passenger ships, this may not be there. In full form ships this behaviour can effect drag resistance, some formation of eddies and vortices can be prominent, and going away from the bilges in the forward end his vortices can take away energy.

On the surface ship there is wave making resistance and depending on the fore body shape maybe there will be wave breaking resistance if the fore body has big difference in curvatures like sonar part of the DTMB 5415, frictional resistance, separation drag or eddy drag and viscous pressure drag, which may be substantial.

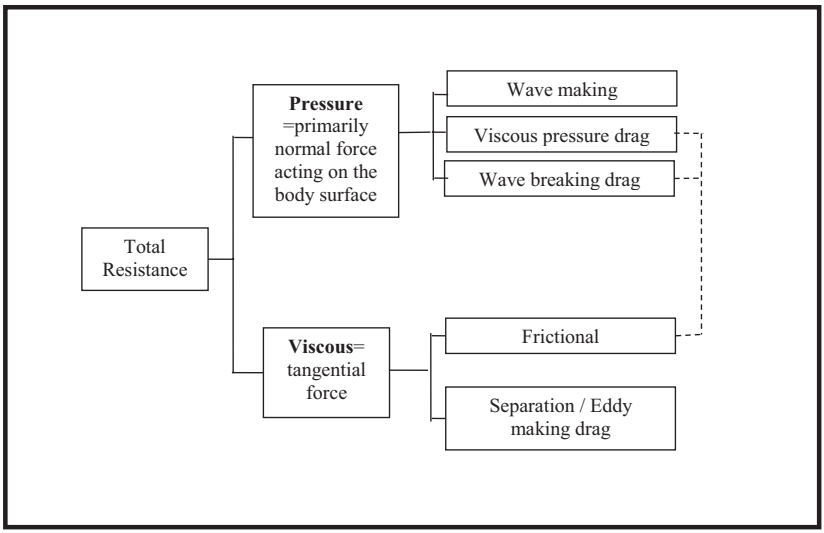

Fig. 105: Total resistance components

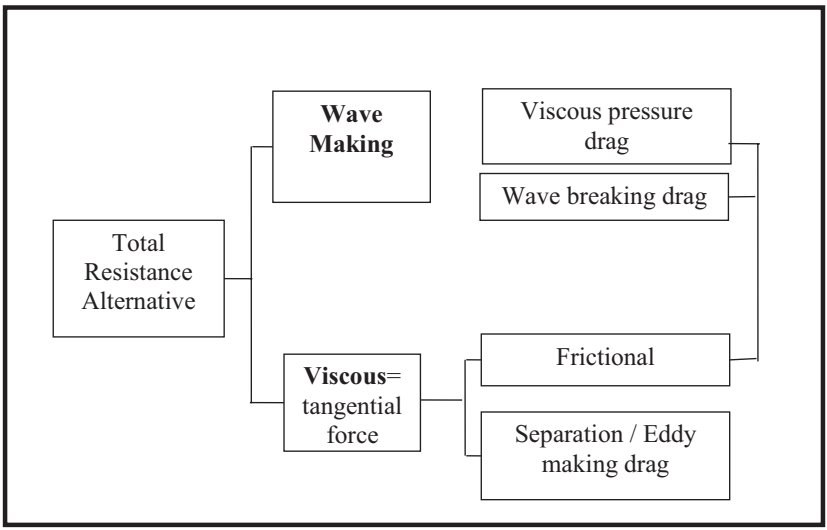

Fig. 106: Total resistance alternative

Total resistance is separated between two main phenomena: pressure and viscous resistance. Pressure resistance is normal pressure acting on the body surface, normal force. The components on the axial direction give resistance and the components in transverse direction cancel each other. The viscous resistance is primarily tangential force perpendicular to the pressure. Boundary viscous layer effect makes adjustments to pressure vectors to act on the edge of the boundary layer not on the surface body directly and transforms the normal direction of the pressure forces.

Viscous pressure drag and wave breaking drag are due to viscosity effects and sometimes are incorporated as viscous resistance. Their origin is pressure to maintain streamlined shape of the body in non-viscous fluid and to make the wave in fore body part but the biggest effect of losing energy they have is in viscous pressure drag.

The frictional resistance is not the same as if the body was completely two-dimensional in nature as in three-dimensional case. This is if there is flat plate, which is moved in water it will have one frictional resistance. If there is nice streamlined body, which is with very large ratio of depth compared to

length it will have different frictional resistance. The body could be considered as two-dimensional and it will have two-dimensional friction resistance. All the flow will be horizontal.

In three-dimensional body like ship, there are changes. There is a waterline with some shape, in sectional plane there is a bilge at the junction of the board and the bottom, which curves in the fore body and aft body end and in the middle plane, bilge is less curvy.

The flow around free surface there is a crest in the front and trough drop in the middle and crest in the aft body part. Far away, there are divergent and transversal waves. If there is traced particle just below the free surface, the particle will go in different manner than described before in the free surface, and it will normally go very fast downward sharply, expanding as it goes. Suddenly under the bilges, the particle goes flat horizontally and the flow is highly complex, so the viscous resistance will depend on this complex flow going around the body, which is no more two dimensional behaviour of the flow. In two-dimensional flow the fluid will go around two dimensions in one plane past trough body, but in three dimensional flow the particle behaves different and the travelled distance is more plus addition of eddy making and separations, because of the curvature will increase.

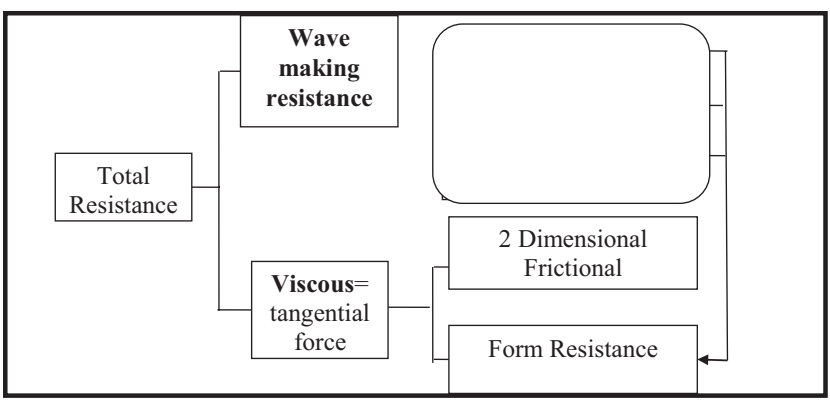

Fig. 107: Total resistance diagram - final

Therefore, the frictional resistance in the flat plate and the frictional resistance in the body having the same wetted surface but three dimensional shape will be different and this is called “form effect”. Viscous pressure drag, wave breaking drag, and separation/eddy making drag, three components together are called “friction form effect”.

Form resistance is taken as a percentage of Two Dimensional Frictional Resistance which is estimated by different formulations.

It is extremely difficult to calculate all components of resistance theoretically to an accurate level, which can be used by engineering practices. That is why there is a use of focused model experiments and rules how to get the resistance experiments extrapolated to full scale using Froude (for investigating waves (hull resistance prediction)) or Reynolds (for viscous effects ex. Propellers tests) numbers are kept the same as similarity of the models.

This components of resistance are all in calm water. Other components of resistance that affect moving of the ship is air resistance, which is very small compared to water resistance. Air resistance is estimated by statistical data run from various wind tunnel experiments of the portion of the ship which is above water level and it is extrapolated statistically to the needed ship and superstructure.

This is trial resistance and in a ship there is resistance from the appendages typically in the merchant ship there are bilge keels, rudder, A frames, bossings, shaftlines, rolling stabilizers attached outside the hull. Propeller geometry is not considered as resistance, because if it is free to rotate there is very low resistance, but if it is locked the resistance is very high. Normally the propeller is left free when the ship is towed. Rudder, appendages and shaft bossing’s and shaft brackets, bulbous bow, sonar domes in naval vessels like combatant DTMB 5415 affect resistance. Bow or stern thrusters add to the resistance.

All appendages have to be added and the trail resistance at zero speed condition can be calculated. Bilge keel is a flat surface and affects mainly frictional resistance. If the bilge keels are aligned in streamline that will flow past the ship then the resistance into bilge keel it will only be due to two dimensional frictional resistance. Contrary if they are not aligned in the streamline the bilge keel will disturb the flow creating separation and eddies. Therefore, before finalizing the bilge keel it is essentially to make paint flow test on the model so the direction of the flow can be visible, and based on that the bilge keel is aligned.

Whenever there is a flow disturbance it is not only about the drag but it will cause also sounds, coming from vibration. If that vibration is sufficiently large it can affect the ship, which is case in many small vessels. For large vessels, vibratory force is very low compare to the length of the ship except on passenger ships which has requirements for the comfort. In small vessels with large number of appendages like twin rudders, they have problems with flow, which influences living and operation conditions on the ship.

The trail speed has to be obtained in the wind speed up to Belfort scale three. Mainly the wind resistance is augmented due to the large speed. Because below Belfort scale three the sea ripples, and there is an assumption that there is no added resistance due to waves with this assumption this behaviour is simulated as if there is calm water with regard to sea condition. Wind resistance increases because Belfort three means 20 knot wind speed will be added to the speed of the ship. When the ship is going with 15 knots the wind is going in opposite direction with fast with speed 15 knots, if Belfort three is used another 20 knots will be added and the wind speed will become 35 knots. That wind resistance part increases which has to be taken into account in trail condition.

In service condition it is very difficult to estimate what will be the added resistance due to waves, because wave condition itself it is varying. That is the reason to assume standard sea state in a particular seaway in a Pacific or North

Atlantic and add some value due to such sea condition, which maybe supported with model experiments. This is rarely used instead for particular sea condition it is added percentage of total resistance 10-15 % depending on the sea called service allowance.

As the ship goes into service its paint peals of, the ship corrodes and fouling grows around the hull which gives large increase in frictional resistance. This has to be added to resistance for good estimation of service speed. There is existence of two layers of boundary layer: laminar and turbulent. The turbulent is taking care of small variations or weld marks on the surface of the hull but they add to roughness of the ship. Due to roughness there is an increase in turbulence, which has to be taken into account.

Before years the ships were constructed lap jointed and riveted which gives large portion to frictional resistance. After the welding start being used in the ship industry the discontinuity due to weld mark is not so prominent.

Scaled models tested in towing tanks are usually with very smooth surface, waxed or in fibreglass. In actual ship the surface is rough and it cannot reach to that smoothness of scaled models that is the reason to add so called correlation allowance, which is small increase in the total resistance.

As results being extrapolated to full scale, they take into account the initial roughness of the ship, which includes weld marks and any small discontinuities on the hull surface. If the discontinuities are large they will create separation, which must be investigated deeply and included into total resistance not using correlation allowance formula.

Dimensional analysis is the technique used to understand the phenomenon, when the exact solution of the problem is not known. If there is only partial knowledge of the problem dimensional analysis make investigation in empirical manner, about what could be the nature of the problem in the mathematical sense.

Resistance of the ship is complex phenomena and depends on certain variables but the functionality of the resistance cannot be found exactly. It is possible to find out an approximate relationship between the variables and the quantity resistance trough dimensional analysis procedure. The resistance is expressed in terms functionality between variables, and with this is trying to achieve dimensional homogeneity. The dimensions on the left hand side on the quantity must be equal to the dimension on the right hand side of the quantity.

Generally, in case of mechanics of fluids and solids, they are three basic dimensions on which all quantities - variables can be defined.

Dimensions are:

Length denoted with L [m]

Mass denoted with M [kg]

Time denoted with T [s]

Speed denoted V is with dimension a distance travelled over the period of time.

$$V=L/T \text{ [m/s]}$$

Acceleration denoted with a rate of change of velocity per unit time.

$$A=L/T^2 \text{ [m/s}^2\text{]}$$

Force denote F is mass multiplied with acceleration.

$$F=M.L/T^2 \text{ [N=kg.(m/s}^2\text{)]}$$

Linear dimension L [m], Area dimension L^2 [m^2],

Volume dimension is L^3.[m^3]

Variables that influence resistance of ships are:

Average Speed V = L/T distance travelled/ duration of travelled time [m/s]

Size of the body (expressed as a linear dimension): L [m]

Mass density (density of the fluid in which the ship is moving):

$$\rho \text{ [Mass per unit volume] } =M/ L^3 \text{ [kg/m}^3\text{]}$$

Acceleration due to gravity

$$g=L/T^2=9.81 \text{ m/s}^2$$

Pressure is force exerted on certain area

$P = M/LT^2$ [$Pa = N/m^2 = kg/(m.s^2)$]

The sheering force between two layers of fluid or solid and fluid will depend on

$$F = \mu A.\frac{dy}{dx}$$

Viscous force between two layers of fluid will depend on coefficient of viscosity multiplied by area and by the rate of change of velocity in transversal direction.

$\frac{du}{dy}$ - Rate of change in velocity into transversal direction which represents the difference between the velocities from one layer of fluid moving over another layer of fluid.

$$\frac{ML}{T^2} = \mu .L^2 \frac{L}{T}.\frac{1}{L} = \mu.\frac{L^2}{T}$$

$$\mu = \frac{ML}{T^2} .\frac{T}{L^2} = \frac{M}{L.T}$$

Dynamic viscosity of the fluid: μ [(Pa·s) equivalent to $(N.s)/m^2$, or kg/(m·s)]

Kinematic viscosity υ derived then by relationship between dynamic viscosity and mass density, it is measured in [m^2/s]:

$$\upsilon = \frac{\mu}{\rho}[\frac{M}{L.T}.\frac{L^3}{M} = \frac{L^2}{T}]$$

SI: m – meter, s – second, Pa – Pascal, kg – kilogram, N – Newton

General equation form of the Resistance using variables which may affect it.

R ≈constant of proportionality. $\rho^a V^b L^c \mu^d g^e p^f$

Better relationship can be found by equating the dimensions on the left hand side with those on the right hand side.

$$\frac{ML}{T^2} = \left(\frac{M}{L^3}\right)^a \left(\frac{L}{T}\right)^b (L)^c \left(\frac{M}{LT}\right)^d .\left(\frac{L}{T^2}\right)^e (\frac{M}{LT^2})^f$$

If there is separately equating of the coefficients M,L,T between left and right hand side:

$$M: 1 = a + d + f$$
$$L: 1 = -3a + b + c - d + e - f$$
$$T: -2 = -b - d - 2e - 2f$$
$$a = 1 - d - f$$
$$b = 2 - d - 2e - 2f$$
$$c = 2 - d + e$$

R ≈constant of proportionality. $\rho^{1-d-f} V^{2-d-2e-2f} L^{2-d-e} \mu^d g^e p^f =$

$$R = V^2 L^2 [\left(\frac{\mu}{VL}\right)^d \left(\frac{gL}{V^2}\right)^e (\frac{P}{V^2})^f$$

This dimensional analyses shows that resistance is a function of three quantities, and will depend on the shape of the body. Therefore, if there are two bodies, which are geometrically similar – the shape is the same, only the linear dimensions of one body is exactly proportional to the linear dimension of another body, then these quantities will become constant so the functions d, e and f, will be the same.

L^2 is an area, which can be rewritten as surface area (S) of the ship which is wetted by the water.

Resistance formula is in general form and it is rewritten as:

$$\frac{R}{\frac{1}{2}V^2 S} = fn\left(\frac{VL}{\upsilon}\right), \left(\frac{V}{\sqrt{gL}}\right), (\frac{P}{V^2})$$

$$Ct = \frac{R}{\frac{1}{2}V^2 S} - general\ drag\ coefficient\ of\ the\ body\ in\ water$$

Ct is a function of Reynolds and Froude numbers also is described as coefficient of total resistance.

Resistance problem is defined by Reynolds and Froude numbers.

$$Rn = \frac{VL}{\upsilon} - Reynolds\ number$$

$$Fn = \frac{V}{\sqrt{gL}} - Froude\ number$$

$$Cp = \frac{p}{V^2} - pressure\,coefficient$$

Where ρ and μ are the density and viscosity of the fluid respectively, V is the ship speed, L is the length between perpendiculars of the ship and g is the acceleration due to gravity. The viscosity of water varies with temperature so that model scale tests carried out in water at 10 - 15 C° are different to the full scale viscosity of deep sea-water at 15 C°.

$$\frac{V}{\sqrt{L}} = \frac{knots}{feet} - dimentional\,term\,used\,in\,ships\,practices$$

$$Fn = 0.298\frac{Vk}{\sqrt{Lft}}; \frac{Vk}{\sqrt{Lft}} = 3.355$$

Two are the major components of resistance: wave making resistance and frictional resistance or pressure resistance and viscous resistance. Major component of viscous resistance is frictional resistance.

William Froude in 1868 divide's the resistance of the ship in two parts: frictional resistance and all other resistance, which he called residual resistance.

$$Rt = Rf + Rr$$

Rf – frictional resistance

Rr – residual resistance

Rf = Two dimensional frictional resistance and three dimensional frictional resistance.

Rr = Wave making and eddy making resistance, and all other components of viscous resistance.

"The residual resistance of geometrically similar ships is in the ratio of the cube of their linear dimensions if their speeds are in the ratio of square root of their linear dimensions" – Law of comparison by Wiliam Froude.

This law states that if there are two geometrically similar ships for their linear dimensions designated with suffix 1 for the full scale ship and suffix 2 for the model scale and if L is length of the ship is true that:

$$\frac{L1}{L1} = \lambda - scale\,ratio$$

The two ships are moving with corresponding speeds - V1 and V2 in such manner that:

$$\frac{V1}{V2} = \sqrt{\lambda} - Speeds\,ratio$$

Residual resistance between the two geometrical ships will be:

$$\frac{Rr1}{Rr2} = \lambda^3 - residual\,resistance\,ratio$$

If two ships are geometrically similar and if their length measurement is constant the arias will be in ratio λ^2, volume and displacement will be in the ratio λ^3.

Froude numbers formulation gives opportunity of using scaled model of the real ship for tests in small water basins called towing tanks instead of making duplicate copy of the big ship. By this means the residual resistance can be found for the small ship and extrapolated using this formulation for the big ship.

Corresponding speed means that the ships have same Froude number:

$$\frac{V1}{\sqrt{L1}} = \frac{V2}{\sqrt{L2}} = constant\,or\,Fn1 = Fn2$$

If two ships are geometrically similar and they are moving with the same Froude number, then the residually resistance coefficients are constant.

$$Cr1 = \frac{Rr_1}{\frac{1}{2}\rho S_1 V_1^2} = \frac{\frac{Rr_2}{\lambda^3}}{\frac{1}{2}\rho \frac{S_2}{\lambda^2}\frac{V_2}{\lambda}} = \frac{Rr_2}{\frac{1}{2}\rho S_2 V_2^2} = Cr2$$

If fluid is non viscous then the dependence on Reynolds number will vanish and resistance will dependent only by Froude number and Pressure coefficient. And Ct – total resistance coefficient will become equal to Cr coefficient of residual resistance, because Cf – coefficient of frictional resistance won't be there anymore.

For non-viscous fluid:

$$Ct = Cr = Fx[Fn, \frac{P}{\rho Vp^2}]$$

P=atmospheric pressure p_o + static water head + dynamic water head

Between full scale ship and model scale ship similarity of $\frac{P}{\rho Vp^2}$ is very hard to be achieved, because the atmospheric pressure is constant, and in towing tank the pressure must be scaled down which is difficult to do. But this atmospheric pressure affects slightly the total resistance in normal circumstances so it is neglected and the rest is only the static water head and the dynamic water pressure, which are proportional to the length of the ship. If there is h1 and h2 distance from the water to the investigated point on the body, this would be in the ratio of ships length L of the full scale ship if ignoring the atmospheric pressure. Water density ρ remains the same for model scale ship and ships speed V is proportional to $\sqrt{\lambda}$. Therefore, is assumed that:

$$\frac{P}{\rho Vp^2} = Froude\,number$$

So this dependence vanishes if atmospheric pressure doesn't act and resistance became dependent only on Froude number. Atmospheric pressure is important when the pressure falls to very low values up to atmospheric pressure or less than that, this is the case that occurs in cavitation. If there is any cavitating flow than this assumption cannot be made. In normal merchant ships cavitation is not considered for resistance purposes.

As a result, if the ships and model are moving in non-viscous fluid, the total resistance measured in the model can be multiplied by λ^3 to get the total resistance of the full scale ship. But water is viscous so different approach is done.

If the body is submerged into the water, then wave making resistance will vanish, because there will be no wave making on the free surface so dependence on gravity will disappear and Cr will become zero for submerged body. And Ct=Cf[Rn]

Generally, if the body is immersed and viscous the formula can be separated on two effects depending on Reynolds number and Froude number.

$$Ct = Cf + Cr = fx\left(Rn, Fn\right) = fx_1\left(Rn\right) + fx_2(Fn)$$

This is fundamental relationship of surface ship resistance obtained by dimensional analyses, which justifies the Froude law of comparisons between two geometrically similar ships. If Cf coefficient is obtained and the scaled model is moved with corresponding speeds, then Cr can be obtained of the model, and by the law of similarity extrapolated for full scale so the total resistance can be found. This all works with the assumption that no atmospheric pressure is acting.

If Froude number and the residual resistance is the same. Frictional coefficient for geometrically similar ships can be found by law of compare.

Reynolds similarity states:

$$Rn_1 = Rn_2$$

$$\frac{V_1 L_1}{\upsilon} = \frac{V_2 L_2}{\upsilon}$$

$$V_1 L_1 = V_2 L_2$$

$$V_1 = V_2 . \frac{L_2}{L_1}$$

$$V_2 = V_1 . \frac{L_1}{L_2} = V_1 . \lambda$$

To have Reynolds similarity the model must be moved at a speed of the ship multiplied by the factor λ.

But for Froude number similarity $Fn_1 = Fn_2$ states:

$$V_2 = V_1 . \frac{1}{\sqrt{\lambda}}$$

Suppose there is a ship with length between perpendiculars Lpp_1=125 m, and model Lpp_2=5 m with 1:25 scale so λ=25. If this model is moved 5 meters at particular speed V_2=10 m/s (≈20 knots) to predict the resistance.

$$V_2 = V_1 . \frac{1}{\sqrt{\lambda}} = 10 \frac{1}{5} = 2 \frac{m}{s} \; for\ Fn\ similarity$$

For Reynolds similarity V_2=V_1. λ=10.25=250 m/s in water, which speed cannot be obtained in the testing facility like towing tank. So alternative is to have fluid of different viscosity, and then maybe the speed will come down, or the other is to adjust the speed. Different viscosity to increase the speed of the ship means to test in air – wind tunnel test. But the test in air is different with test in water, because the air is compressible, and water is assumed to be incompressible so the characteristics will change, therefore this test in air cannot be simply extrapolated to test in water, to get Cf, because air is fluid but has different characteristic than water and kinematic similarity cannot be obtained and air water interface cannot be generated for example.

Reynolds similarity cannot be achieved and only the Froude similarity is preserved. That's why normally there are tests of frictional resistance coefficient for a large number of two dimensional bodies or tri-dimensional bodies at smaller length and size than the ship which are then extrapolated to the ships length and suppose that this is how the ship resistance will look. This is the basis on which the present model tests are conducted. Model experiments and extrapolation to full scale ship steps given from Froude:

a. Model is geometrically similar to the full scale and runs at corresponding speed.
b. Measure the speed and the total resistance Rt and calculate Ct
c. Calculate Cf_2 (or Rf_2) from formulation based on Reynolds Number of model
d. Rr_2=Rt_2-Rf_2
e. Rr_1=$Rr_2.\lambda^3$
f. Calculate Rf_1 using previous formulation based on Reynolds Number of the ship
g. Rt_1=Rr_{1+} Rf_1

FRICTIONAL RESISTANCE

Frictional resistance is developed on the basis of experiments for planks conducted in 1860s by William Froude and later by his son Robert Edmund Froude. William Froude give formulation of frictional resistance based on plank experiments. Planks at particular length and height ware submerged in water and towed measuring the resistance. Based on this experiments he gave frictional formulation:

$R=f.S.V^n$ (Fictional resistance measured in Pounds force)

S – Area measured in feet square

V – Speed is measured in feet per second

f – Constant dependent on surface finish, the roughness of the surface and increases if the surface is rougher

n – Constant dependent on length of the body

Reynolds number was not explicitly used in this formulation and n factor varied. The length was up to limit in the towing tank in Torquay where the experiments were taken. The surfaces ware make rough with sand paper put sand particles on the surface to make the surface rougher, and measured from very smooth to very rough surfaces. This results were used until around 1950s as a method of estimating the frictional drag of planks, two dimensional bodies and even ships. Later Osborne Reynolds made a lot of experiments of fluid flowing through glass pipes. On the surface Reynolds injected dyes (collared dust substance that colours the water) so the flow pattern can be observed and it can be visualised. He realised that there must be friction between the surface of the solid pipe as fluid flowing through it so injected dye on the surface and followed the movement of it. When the dye started leaving the surface for some length the it flew in straight line form. There was a pattern between the flow and the die.

The die separated from the surface but it went parallel to the surface slowly separating. As the length of the die injection point move away from the fluid particle (so the fluid flew over long distance), the fluid got disturbed and

mixed with the water leaving no pattern. It can be found that the length the distance over which the die maintained the pattern.

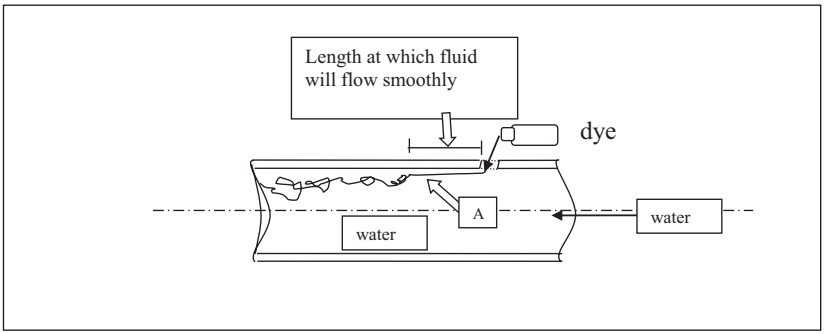

Fig. 108: Reynolds experiment

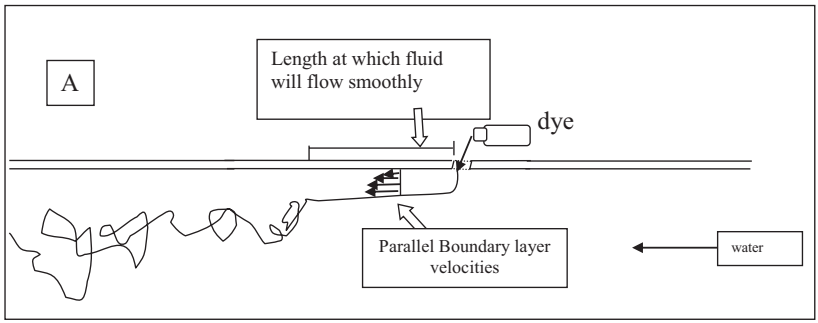

Fig. 109 Reynolds experiment zoom in

There is a length at which the flow pattern is smooth and it reduces if the speed of water increases. So this length depends on speed. The critical speed by repeated experiments Reynolds found as formulation.

$$Vc = \frac{2000\upsilon}{D}$$

$$\text{Or } \frac{VcD}{\upsilon} = 2000$$

Vc – critical speed for the fluid to mix with water.

Speed at which the die is mixed with water is called critical speed. Before 2000 the fluid did not mix with the water. This lead to Reynolds number for the flow in the pipe.

$$Reynolds\,number = Re = \frac{VD}{\upsilon} = \frac{inertial\,effects}{viscosity\,effects}$$

It must be checked if Reynolds number is bigger than 2000 when the flow becomes turbulent. If it is lower than the flow is laminar.

The boundary layer will develop transversally next to a solid boundary in a velocity gradient until reach the speed of the water. It will be zero at the beginning of the injection and going away from injection point it will slowly increase its thickness up to a certain length that the fluid inside will have velocity, which is predominantly parallel to the axis of the pipe. Beyond this point the fluid velocity will become random, overlaying flow will stay but there will be perturbation velocity, which is small and determines particle direction at any point will be randomly distributed in different directions.

For a certain range of Reynolds numbers, the perturbation velocity of each particle inside the boundary layer will be parallel to the axes of the pipe, but beyond the certain Reynolds number that perturbation velocity will be randomly distributed in different directions. This shows how the fluid gets mixed up. This critical speed divides the boundary layer in two types: laminar boundary layer and turbulent boundary layer.

Laminar boundary layer is when velocities inside the boundary layer will be predominantly parallel to the axis or surface if it is a three-dimensional surface.

Turbulent boundary layer is when the velocities of the particles act random inside the boundary layer.

In case of ships frictional resistance Rf can be represented as formula:

$$Rf \rightarrow Cf = \frac{Rf}{\frac{1}{2}\rho S V^2}$$

To estimate Cf there is no much information from experiment of the pipe.

Theoretical explanation of flow around planks is given by Blasius.

$$Cf = 1.327\left(\frac{VL}{\upsilon}\right)^{-\frac{1}{2}} - Blasius\,equation\ for\ resistnace\ of\ laminar\ flow\ on\ plank$$

Flow around ships is basically turbulent. A critical Reynolds number for a pipe for transitioning from laminar to turbulent zone is 2000 but in case of ships it will change, because there is no diameter, and the flow phenomenon will be different. In ships the turbulent flow will primarily depend on the length factor. There is also critical Reynolds number in case of ships where flow will change from laminar to turbulent. If the ship is long thin body and water is flowing past it, initially at the beginning of the flow, when length is small just like in pipes, there will be a portion where the flow will be laminar. As the length increases and Reynolds number increases flow will become turbulent. There will be a zone where the flow is laminar and turbulent called transition zone, and it is very difficult to be defined where that zone will be. The ship will also have surface which is not strictly smooth nor is very rough if it is new ship. Similarly, ship is not a plank but three dimensional surface. This phenomenon is seen in models of full scale ships where it is slightly reduced the effect of laminar flow, because the ship surface generally has enough roughness to induce turbulence. So the flow around the ship is considered to be mostly turbulent.

Prandtl and von Karman in 1921 gave theoretical formulation for Cf in boundary turbulent layer. This is for planks in two dimensional flow without any edge effect and as if the flow was only in two dimensions without having any curvature.

$$Cf = 0.072\left(\frac{VL}{\upsilon}\right)^{-\frac{1}{5}} - \text{Cf in boundary turbulent layer for planks in two dimensional flow}$$

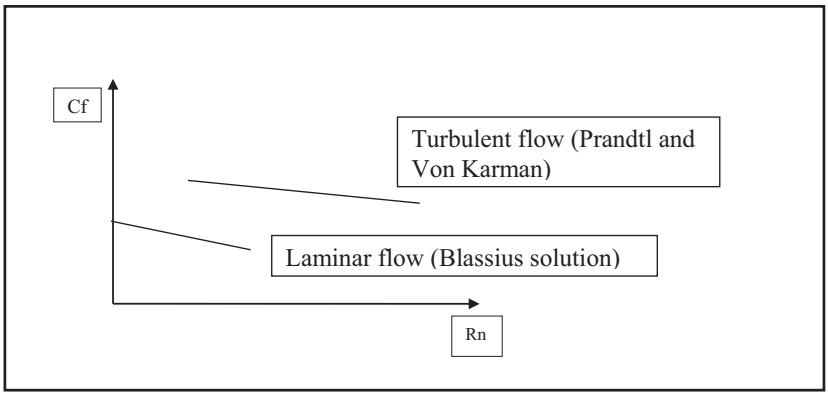

Fig. 110: Cf as function of Reynolds number

So if using Laminar flow formulation there will be underestimation of the resistance. In 1940 and early 50's Schoenherr, collected a lot of data on plank experiments, he had taken all resistance data available and theoretical formulation from the Prandtl and Von Karman, and tried to fit all the resistance data in a statistical manner to curve. He arrived to a friction line for two-dimensional flow, which was better than Prandtl and Von Karman formulation and was accepted by ATTC – American Towing Tank Conference and was called ATTC line.

$$\frac{0.242}{\sqrt{Cf}} = Log_{10}\left(Rn.Cf\right) - Schoenherr's friction\, line - ATTC\, line$$

The background of the formula is smooth planks towed in water. Around same time Huges made a lot of experiments of pontoons in towing tank in United Kingdom.

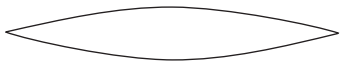

Figure 1: Pontoon cross-section top view

$$Cf_o = \frac{0.066}{\left[log_{10}Rn - 2.03\right]^2} - Huges\ formulation\ for\ two\ dimentional\ friction\ coefficient$$

Suffix "o" on Cf, Cf_o means that the flow is two dimensional.

Formulation Huges friction line varies little bit from Schoenherr line, having differences in lower Reynolds numbers but in higher Reynolds numbers becoming more or less equal. In 1957 ITTC – International Towing Tank Conference chooses simplified modification of Huges formulation for two dimensional friction line.

$$Cf_o = \frac{0.075}{\left[log_{10}Rn - 2\right]^2} - ITTC\ '57\ ship\ model\ correlation\ line$$

ITTC friction line is slightly higher than Huges friction line. The resistance tests in full scale trials did not match very well with this three formulations, because of unknown three dimensional behaviour of the flow, and of edge effects due to end of the body. This is the reason why ITTC called this line two dimensional frictional resistance by ship model correlation line. This ITTC line is used to correlate the ship model resistance to full scale ship resistance calculating two dimensional frictional resistance coefficient Cf_o from it for both the model and scale. Model is normally made of wax, wood or fibreglass or other composite material with finishing coat is very smooth. And ship is rougher, ship roughness measured on full scale ship is around 125 microns. Micron is 10^9, and for the roughness of the model is 25 microns. The roughness in ship is much more than the model, which have to be added into account for extrapolation from model scale resistance data. To incorporate this effect there is addition to ITTC correlation line called correlation allowance C_A=0.4x10^{-3} for extrapolating to full scale the results from model. If suffix "m" is model, and "s" is full scale ship.

$$Ctm = Cfom + Crm$$

$$Crs = Crm$$

$$Cts = Cfos + Crs + Ca$$

Ship body is three dimensional that's why the formulation for Cf is extended.

$$Cf = (1+k)Cfo$$

k - Form factor. A factor with which ship resistance increases for three dimensional body over two dimensional body.

Cfo is taken from ITTC two dimensional friction line so called ship model correlation line.

$$Ct = (1+k)Cfo + Cr \; Extended \; Total \; Resistance$$

$$(1+k)Cfo - Depends \; on \; Reynolds \; Number$$

$$Cr - Depends \; on \; Froude \; Number$$

Cf is found by using empirical formula, Cr is found by measurements. Component k.Cfo is separated from residual resistance. If the ship is towed the total resistance can be measured but if the ship is moving at very low speed around 2 knots, there will be almost no wave making resistance, because of the dependence of speed. If the ship is moving at very low speed the total resistance is only frictional in nature. At low Fn, Cr=0 so Ct(Rn)=(1+k)Cf_o.

$$1+k = \frac{Ct}{Cf_o} \; at \; low \; Fn$$

With this formulation k can be calculated for model scale and used for the full scale ship with the assumption that k is independent by the speed and will be constant – the same over entire speed range.

At low speed the resistance is very low and in experimental procedures there is small error. And if this small error is made over a small quantity it will make very big error and form factor can be very wrong at low speeds. Still this method is accepted by ITTC and if the experiment can be achieved at low speeds for measuring the resistance, this will give good value of the form factor. Recommendation states that the measurement should be done at Fn = 0.1.

Another method for estimation of k value is:

$$Ct = (1+k)Cfo + Cr = (1+k)Cfo + c.Fn^m \; with \; m = 4-6$$

Cr is dependent on Froude number and it is assumed to be between 4-6.

c- Constant

$$\frac{Ct}{Cf_o} = (1+k) + c.\frac{Fn^n}{Cf_o}$$

If n and c values are known, then 1+k can be calculated. This two values can be found using mathematical fitting of curve to the equation of the resistance curve to find out the value of n and c for the residual resistance and calculate the value of k. This is other method, which is recommended by ITTC. Since the errors are not constant neither are always positive over the entire speed range this regression equation treatment can also give errors. So the value of factor k must be always be used with cautious.

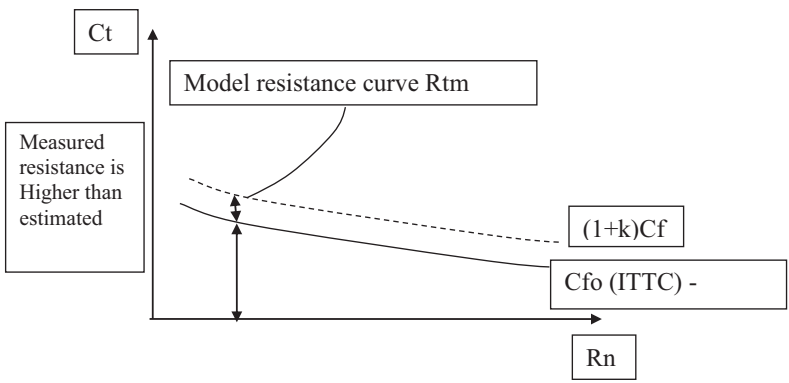

Fig. 111: Total resistance coefficient in function of Reynolds number

If there is a plot of total resistance coefficient for different Reynolds numbers on the abscissa. ITTC prediction for friction coefficient and model resistance curve Rtm will look like in the figure 111. At low speed there is no wave resistance and the entire resistance is dependent on friction resistance,

which is estimated by Cfo(ITTC) curve. But the actual resistance is higher than Cfo(ITTC) friction line, and if is multiplied by (1+k) the line will be higher receiving good results for low speeds, which proves it the estimation is correctly done.

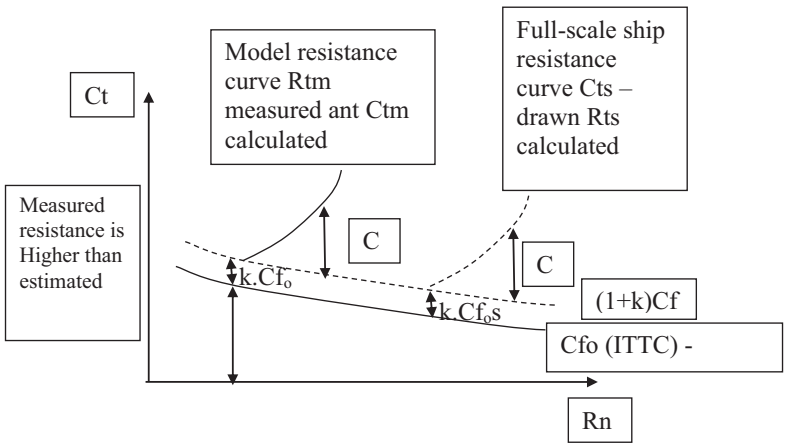

Fig. 112: Total resistance coefficient in function of Reynolds number 2

For higher speeds Froude number starts acting for wave making and the rest of the curve is coefficient of residual resistance Cr. So the Ship curve can be found by extrapolation of model scale curve.

This principle can be used for determine the k, which and it is called geosymetrical or geosym tests. Two ships models are made geometrically similar to the full scale ship and are tested in towing tank so two curves are obtained of Ct. For constant Froude numbers Cr remains the same and the remaining part is (1+k)Cfo. If two lines of same Froude numbers for different curves are joined they are parallel to each because Cf remains, the same. Advantage is that both data is available and it is easier to calculate the k by drawing a constant Froude lines slightly to the end. And if there is an error the

curves can be faired so they are parallel to each other because Cr is constant. For a better estimate of k value.

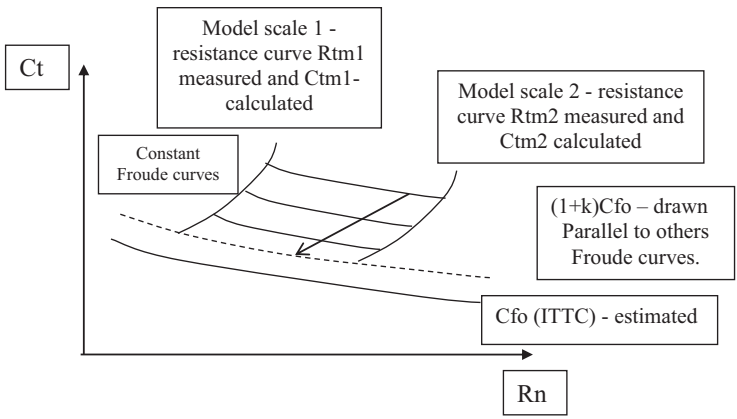

Fig. 113: Total resistance coefficient in function of Reynolds number 3

$$Ct1 = (1+k)Cfo1 + Cr$$

$$Ct2 = (1+k)Cfo2 + Cr$$

$$Ct1 - Ct2 = (Cf1 - Cf2)(1+k)$$

$$1+k = \frac{Cf1 - Cf2}{Ct1 - Ct2}$$

This is done for number of different speeds to get 1+k values, which will be the same, but because of experimental inaccuracies the values will be close but different. So the average is taken to get good assumption for exact k value. From geosyim tests it is possible to estimate the values exactly but it is expensive and it is done rarely.

The estimate of the resistance must satisfy trial condition requirements and service condition requirement. Service condition requirement is not very well known and margin on trail resistance requirement is done. More accurate geosym tests are done only if it is economically feasible.

If (1+k) is not used, ship resistance coefficient Cts is overestimating and it is higher than reality because Cf, which is reducing with the speed is small value, 3d form effect has not taken into account Cr and more percentage of resistance are taken in to residuary part. With correct form factor the accuracy is increasing and power prediction is reducing which is economically beneficial. If k is not estimated properly better to not being use and the formula (57) is taken into consideration.

$$Cts = Cfs\left(ITTC\right) + Crm$$

ITTC states that the phenomenon of three dimensional frictional effects is not very well known, so both equations can be used.

WAVE MAKING RESISTANCE.

$$Rt = Rf\left(ITTC57\right) + Rr$$

Pressure resistance is equal to the wave making resistance, but there could be some interference between pressure resistance and frictional resistance, which is giving viscous pressure drag. All those components are included in Residual resistance the main component remains the pressure resistance or wave making resistance.

Whenever body moves in fluid there is a pressure force which develops around the body and it is normal to the body surface. If the body is submerged in non-viscous fluid then the axial components of pressure in the forward part of the ship are equal and opposite to the axial components of pressure in the aft part of the ship. They will cancel each other so the body will experience no resistance to forward motion. But as the body comes up to the surface the pressure developed around the body generates waves. The wave generations is a phenomenon due to existence of free surface between the air and water and the effect of gravity. All water waves are gravity based phenomenon and are created, because a constant gravity pressure has to be maintained on the water surface by physical law.

When the ship moves, because of the physical forces around the body waves are generated on the free see surface. This will also happen if the body was submerged just below the free surface. Whenever the dynamic pressure on the water surface is not equal to the atmospheric pressure on the flat surface. Waves will be created to make the top layer of dynamic pressure on the free surface atmospheric. The shape of the free surface will change and the wave will be generated. For submarines going just below the water surface there will be visible generation of waves on the free surface but less that if it was moving on the surface of the water. As the submarine goes down the waves on the surface vanish. The drag due to submarine just below the free surface will be more than drag of the submarine deeply submersed.

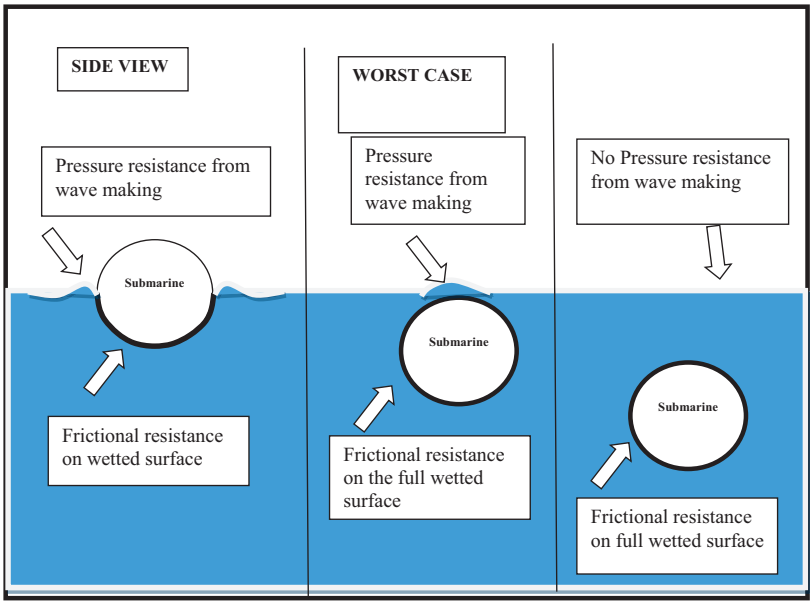

Fig. 114: Worst case of summation of surface frictional and winemaking pressure resistance in submarines

In 1887 Lord Kelvin showed by theoretical analysis that if there is pressure point on the flat free surface, and that pressure point move with particular velocity or water flow past the pressure point in the opposite direction there will be rise for set of waves look like in the figure 115 . There will be set of divergent waves, which will be created by passing of the pressure point. As the point moves forward the divergent waves will keep being generated and they will start moving aft. Other set will be of transverse waves represented only by crests in the figure 115, there will be troughs in between. They are not straight but slightly curved and expand by wave width as they move away from the pressure point and reduces in height. Wave height is difference between elevation of crest neighbouring trough and it is twice the amplitude of the wave. The divergent waves diverge more and more as they go away from the pressure point. The entire wave system is contained within two straight lines emitting from the pressure point making a constant angle on the either side with the axis of movement. This Kelvin angle is 19°28″

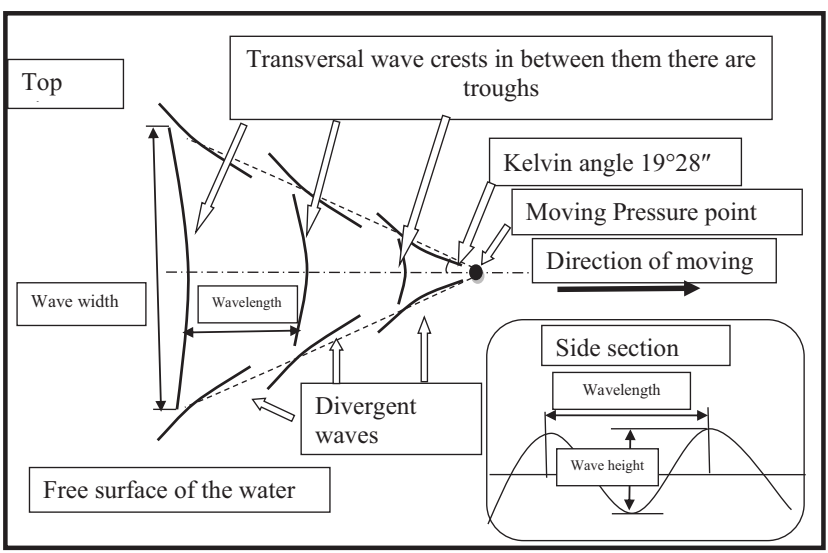

Fig. 115: Moving High pressure point forward in fluid

Far away from the pressure point the transversal wave height will reduce and the waves will be not visible on the free surface. Divergent waves in long thin ships will be visible standing on the bow of the ship and look at the behind stern. The minor transverse waves can be seen at wave surface elevation near forward part of the ship.

High pressure point on forward part will give wave system like figure.116

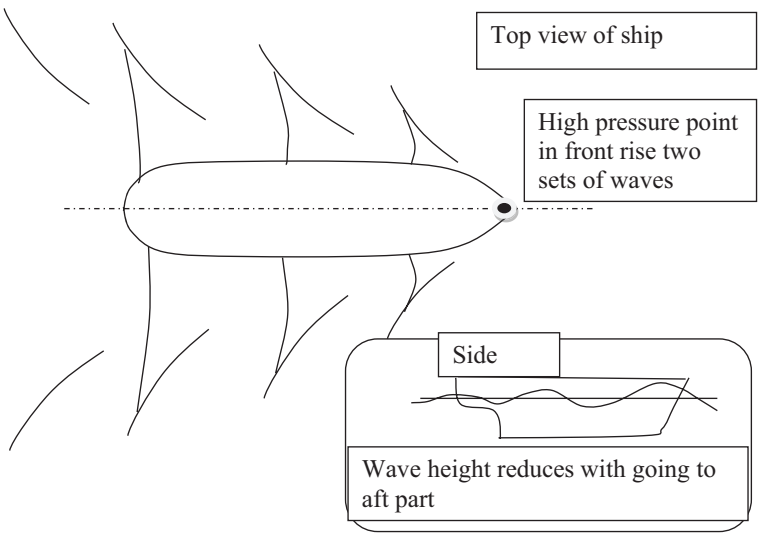

Fig. 116: Free surface waves on conventional merchant ship

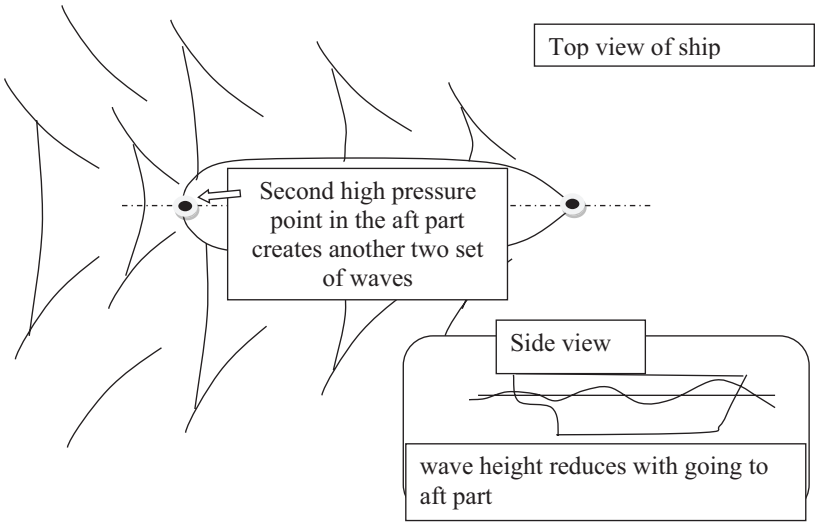

Fig. 117: Free surface waves on conventional merchant ship 2

The high pressure points are created from the large slopes at both ends in the waterline section of the hull.

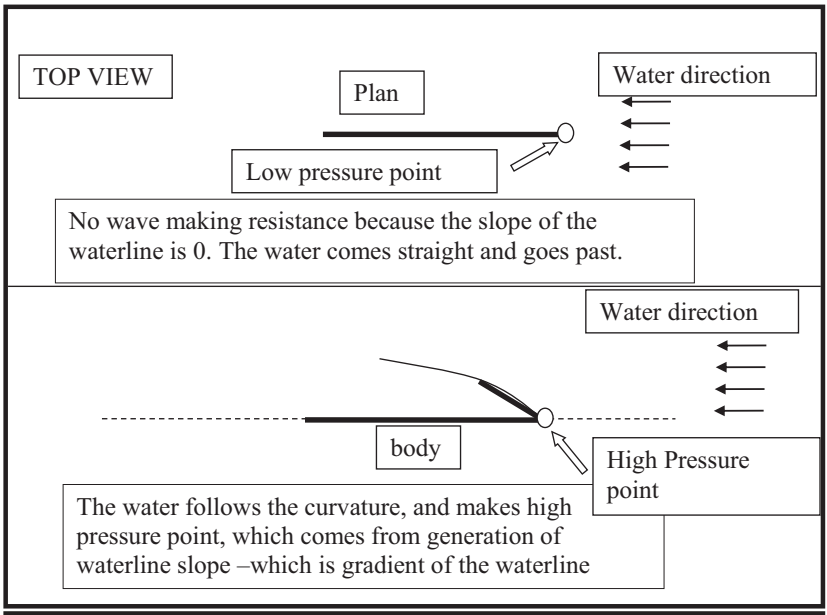
TOP VIEW
Plan
Water direction
Low pressure point
No wave making resistance because the slope of the waterline is 0. The water comes straight and goes past.
Water direction
body
High Pressure point
The water follows the curvature, and makes high pressure point, which comes from generation of waterline slope –which is gradient of the waterline

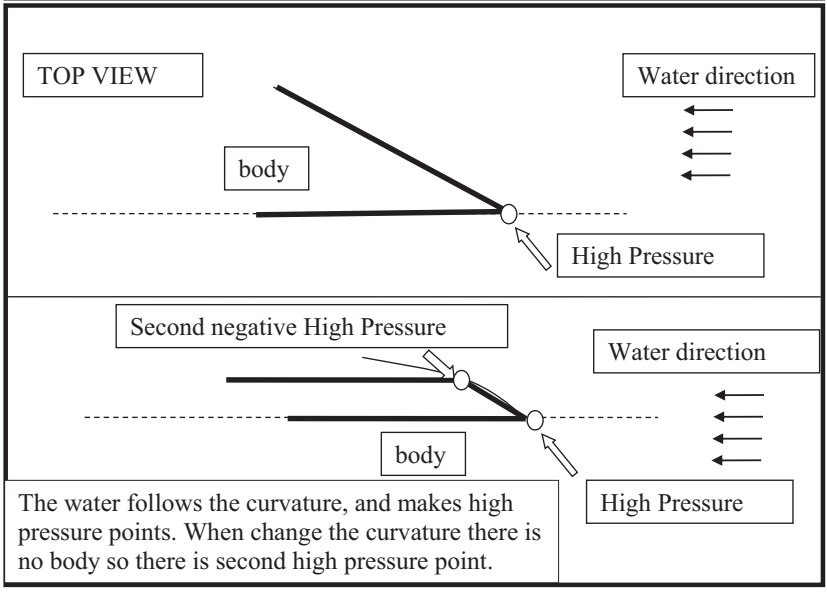
TOP VIEW
Water direction
body
High Pressure
Second negative High Pressure
Water direction
body
High Pressure
The water follows the curvature, and makes high pressure points. When change the curvature there is no body so there is second high pressure point.

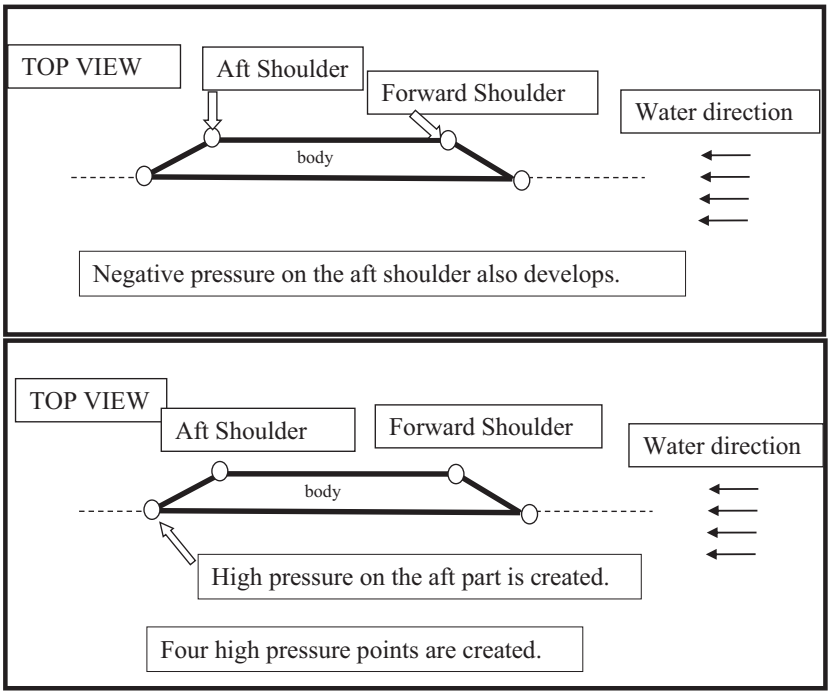

Fig. 118: Pressure resistance on point on symmetry. Wigley hull

In 1931 C. Wigley made a lot of experiments for the flow around wedge shaped body which are proven experimentally to be correct. Wedge body that he used was with symmetrical shape investigated on the figure 119. Mr Wigley stated that there are five wave systems of the ship. From the four pressure points there are four waves generated. Fifth one wave is generated by the ship, which doesn't move and it doesn't take any energy. Basic pressure then develops because the shape of the body. The wave that is generated due to forward end will have dominant wave crest, generated due to forward discontinuity. The most prominent wave systems with crests are in the forward end and in the stern end. In case of sharp corners, the shoulder waves are very prominent and they are visible, because the shoulder is very well defined. In case of the ship the shoulders are smooth, and these waves are less prominent. If there is observation

of the sea standing on the side of the ship there is combination of this system of waves. Mathematical solution exists for combining all these waves, called linear superposition of waves and resultant wave elevation will be from linear addition of all the waves together.

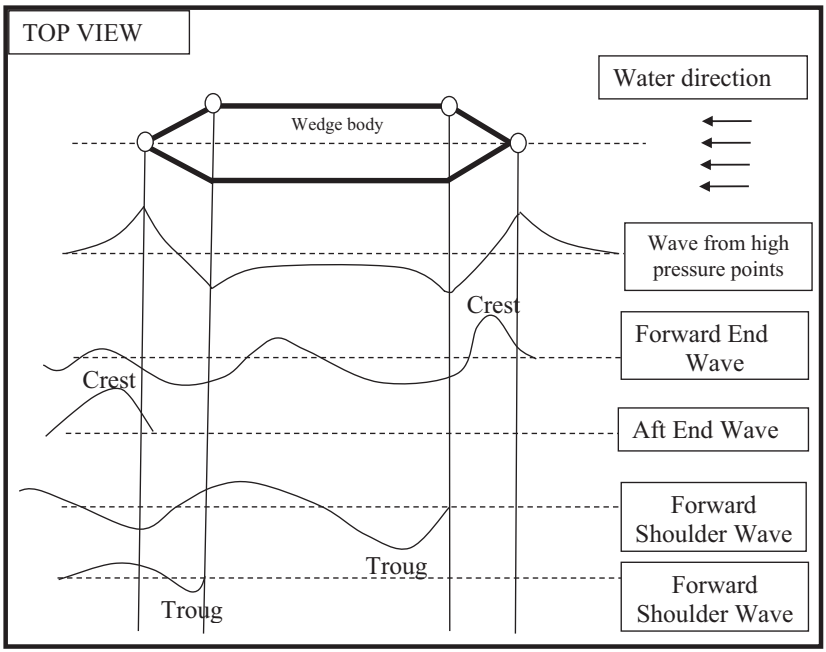

Fig. 119: Wigley free surface wave distribution

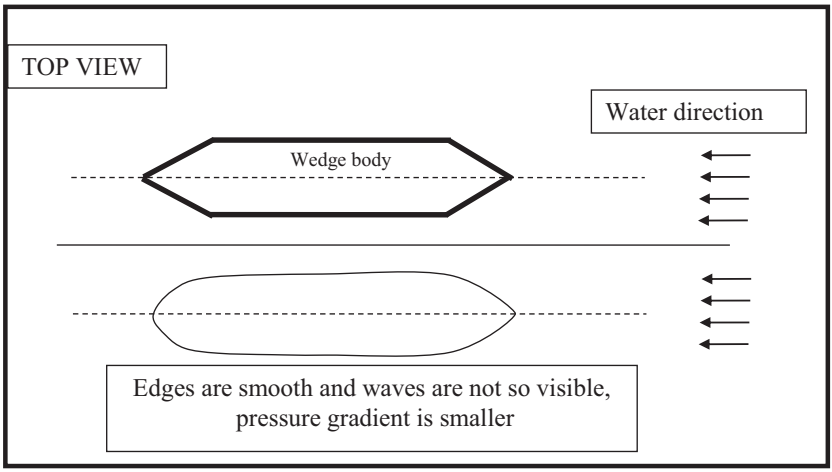

Fig. 120: Difference between Wigley hull and conventional merchant ship

The resultant wave may look different from any of these, but the crest on the forward part of the ship, which is most prominent stays as it the Wigley solution and it is not disturbed by the other waves.

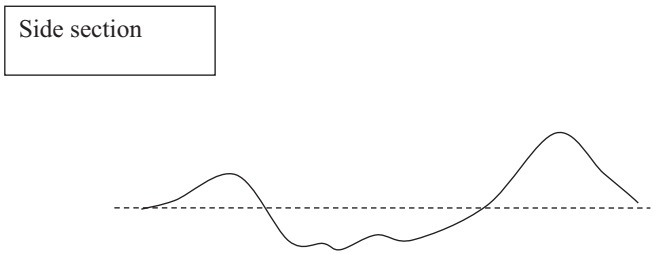

Fig. 121: Resultant wave visualization in side view

What is seen from the ship looking at behind the stern part back, mainly due to divergent forward wave system. The other wave systems, coming after the forward part system get affected by it, because the water is already disturbed, and the smoothness by the shoulders also contributes to difficult

distinction of the waves. As boundary layer develops towards the stern the pressure changes and, the waves in the aft region are not so well defined.

The generation of waves will require energy and since they are completely travelling they are caring the energy with them, and this energy have to be supplied by the ship in form of force that generates energy called wave making resistance. If the pressure is calculated around the ship hull the longitudinal components integrated over the length of the ship it will be found certain resistance called “pressure resistance”. Making wave cut will take the total energy content on the free surface measuring the wave profile and seeing the rate at which the wave is traveling, and its elevation is changing. There will be a force required for generating this energy, it can be found experimentally and it is called wave making resistance.

People have done number of experiments ignoring the boundary layer, and found that the wave making resistance and the pressure measurement on the body of surface gives nearly same results. So an assumption is made that the wave making resistance and pressure resistance, due to generation of normal pressures on the body of the surface are the same.

If crest on the bow wave and crest on the stern wave (which are more prominent than other two wave systems) match, then there will be a bigger crest at that point. This effect is that the pressure at those points will increase therefore the axial component of the force supporting motion will increase and the resistance will reduce. But if aft wave is trough and forward is crest on the same point the resultant wave will be flatten reducing the wave support and therefore increasing the total resistance.

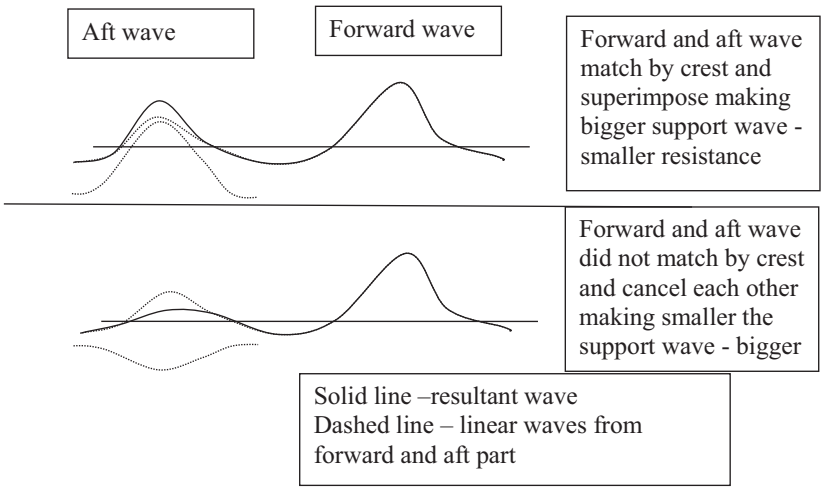

Fig. 122: Wave interference with the hull

The interference – interaction between the waves may increase, reduce the resistance or make no change for the resistance and will depend on the speed of the ship. When the wave is moving forward the ship is moving forward, since is generating the waves as it moves forward. The transverse waves will have the velocity equal to the velocity of the ship, therefore the transverse wavelength is given by formula:

$$Lw = 2\pi \frac{V^2}{g} - thransverse\, wavelenght$$

V- Speed of the ship

$$Lw = 2.\pi.\frac{V_2}{g} cos^2\theta$$

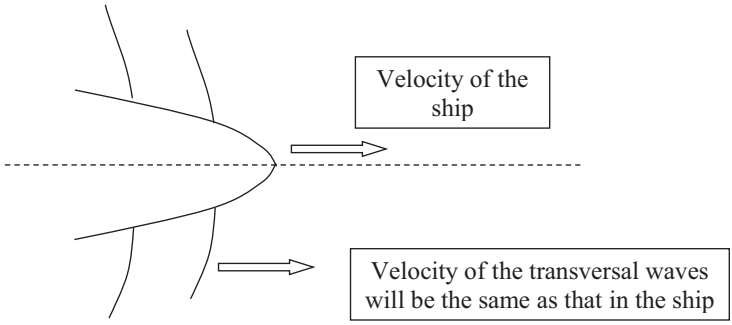

Fig. 123: Transversal wave velocity

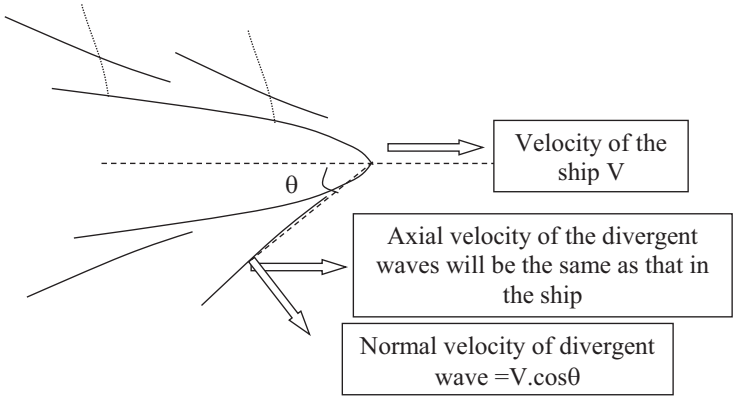

Fig. 124: Velocity of transversal and divergent wave systems

θ - enclose, envelop angle.

From these formulations can be calculated how the interference of wave systems will be using some statistical norms as example.

Cw will be maximum at Fn = 0.173 0.205 0.269 0.476

and will be minimum at Fn = 0.187 0.231……0.345

Pressure resistance depend on the Froude number, wave length is a function of speed so the interference will depend on how long the wavelength is from crest to crest.

$Rw=V^6$[constant + 4 oscillating terms] – wave resistance

$Cw=V^4$[constant + 4 oscillating terms] – coefficient of wave resistance

This 4 oscillating terms may coincide to give local hump in the coefficient of wave resistance curve or a hollow in wave resistance curve. Hump means there is a rise in the curve represented by Froude numbers of Cw maximum. And hollow means there is a drop in the curve, which is represented by Froude numbers of Cw minimum.

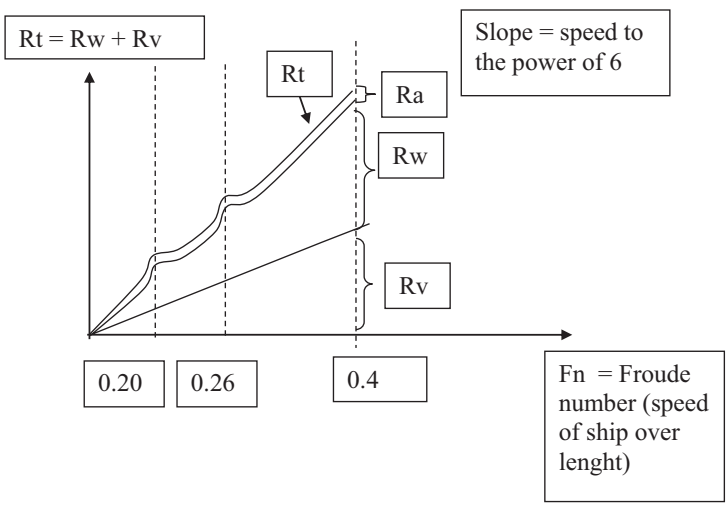

Fig. 125:Rt vs Fn

Rt - Total resistance, Ra - Air resistance, Rw - Wave making resistance, Rv - Viscous resistance

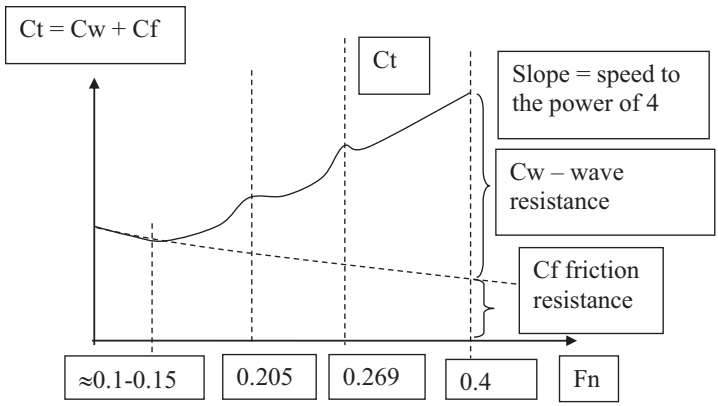

Fig. 126: Ct vs Fn

Estimation of wave resistance is done by experimental method which follows Froude numbers hypothesis and the other way to find it is trough theoretical methodology.

In 1898 Mitchell suggested theoretical estimation of the ship wave resistance called thin ship theory, which is followed by slender ship theory. Both theories have similar assumptions and the only change was in the body shape: the fluid is non-viscous and irrotational (The fluid particles do not have rotational component of velocity like vortexes. Vortex or circulation can happen in the flow with no need to be placed in boundary layer and also in non-viscous fluid, so then the flow is rotational.). All velocities are linear and there can be assumed with a function called "velocity potential" ϕ.

Hull assumption in thin ship theory is that any breath dimension is times smaller to length of the ship or slender in which both breath and draught are small compare to length.

The wave height of the generated waves is small compared to its wavelength. This means that if wave height is squared or cubed it will become smaller and it can be neglected.

No sinkage and trim condition is used.

Radiation condition is imposed, which means that the waves exist only in one half of the horizontal plane, which is aft to the ship and they can travel to infinity in that direction but there will be no wave in the forward side. With these assumptions a pressure point can be represented by a source. A source is a point, which gives out fluid continuously it doesn't accept anything, and it is not practical but imaginary point. A sink is opposite of the source and accepts fluid from everywhere to itself.

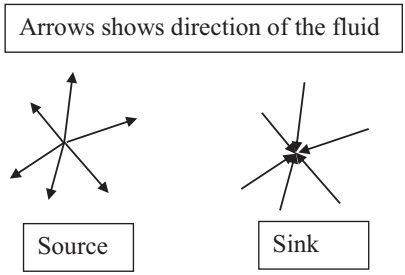

Fig. 127: Source and sink

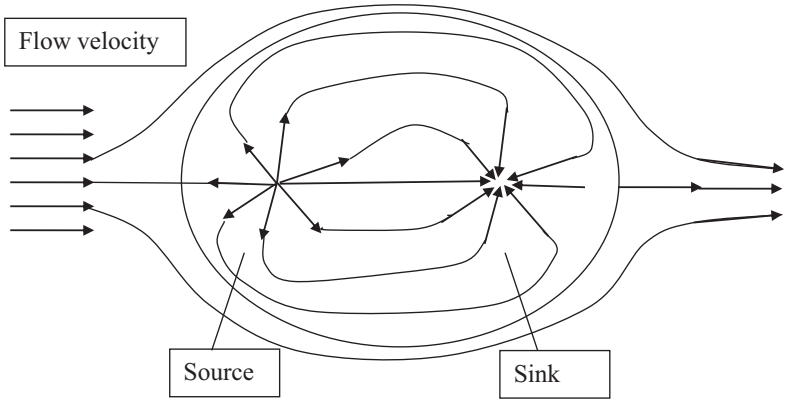

Fig. 128: Source plus sink dipole represent discontinuity in uniform flow

If source and a sink is taken nearby, an effect of dipole will happen and if they are in a uniform flow they will form a body that isolates the stream, the fluid cannot enter the body. Since the ship is a closed body it can be represented by a number of sources and sinks. The strength of the source is the slope of the waterline, this means that there must be large strength sources in the forward end and in the aft end of the ship. Middle sources and sinks with lesser strength are used to represent ship hull.

The strength of sinks and sources distribution should be such as they represent a body. Where the slope is highest there must be source with large strength. Supposing the forward wave crest is a phenomenon of the strength of the source on the forward end, and there is need of reducing of wave making resistance one of the ways to do it is to reduce the source strength on the forward end or reduce the slope at the forward end because forward wave crest is the prime component of the total wave making resistance.

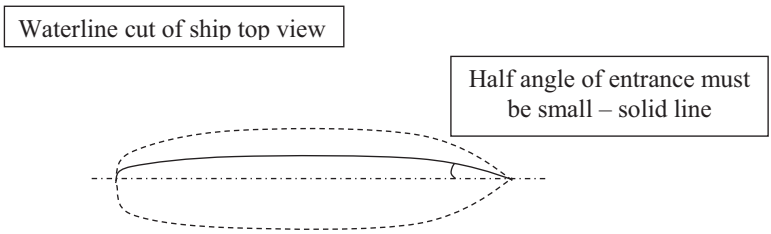

Fig. 129: Angle of entrance importance in ship wave making resistance

Better wave resistance will have the ship with smaller slope or half angle of entrance in the water surface. As going down the water, the effect of entrance angle is decreasing on the wave making resistance. If the beam of the ship is reduced but the length is increased to keep the displacement the same so L/B ratio is increasing then the wave making resistance is going down, which is better economically. Other way of reducing resistance is to use the body that

creates wave trough where bow wave crest exists this is the effect utilized in the bulbous bow concept.

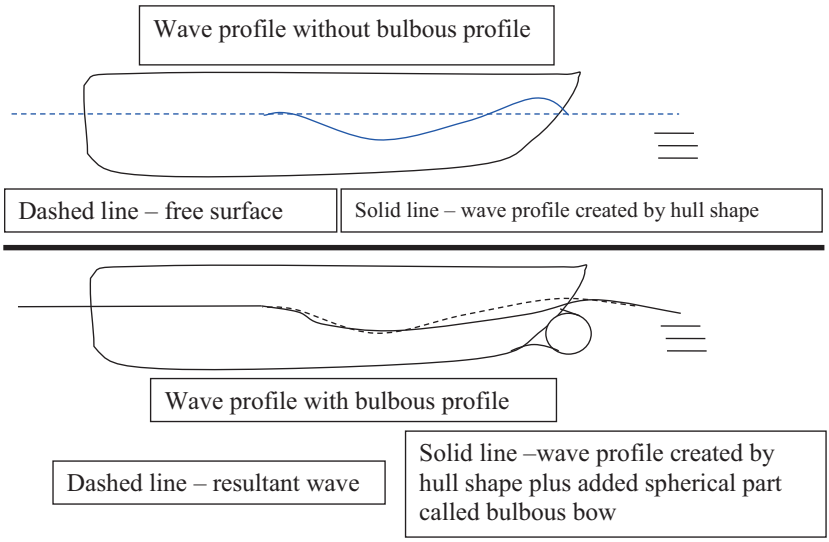

Fig. 130: Interference of waves in front part of the ship with and without bulbous profile

The shape of bulbous was found by moving a soup in the water, and the form was created by eroding the soup in this manner. For ships that have large component of resistance as wave making resistance is recommended to have forward bulb which saves around 25 % of wave making resistance, because it reduces the prime component of wave making resistance – wave crest created on the forward bow. Bulbous bow is used to create wave, which opposes to the wave on the forward part of the ship. If the wave is crest, bulbous bow is designed to create trough, if the wave created by hull form is trough, bulbous bow is designed to create crest, and superimpose the wave system. Bulbous bow must be carefully designed, because it can also increase ship resistance. Other effect of bulbous bow is that it changes the volume distribution and the area of the free surface decreases with respect to that.

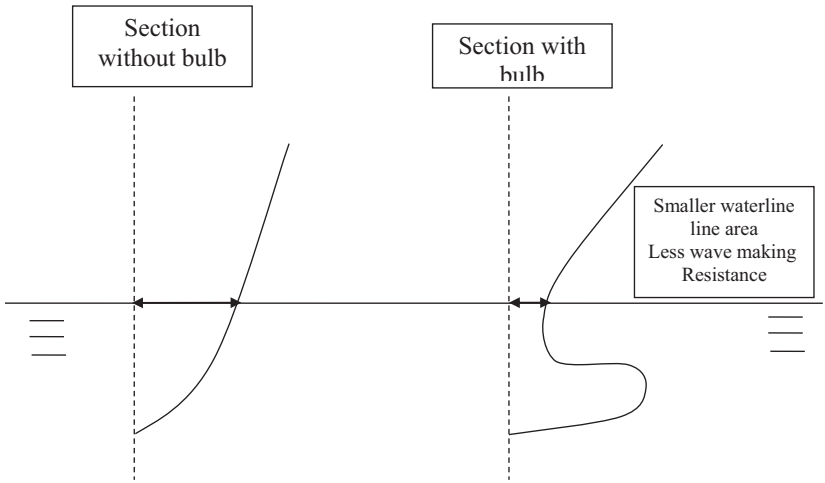

Fig. 131: Cross section view of normal ship and ship with bulbous form

By putting, the bulb half angle of entrance is reduced considerably, and the shoulder can be smoothed more. A part from the interference effect the waterline is more beneficially shaped. With the bulbous bow the oscillating terms can be drastically reduced.

Ct=Cfo(ITTC friction resistance coefficient)+Cr(residual resistance coefficients)

Ship shape is three-dimensional and two effects are recognized by that compared to a flat plate the water on the waterline has to travel a longer distance because the ship is curved.

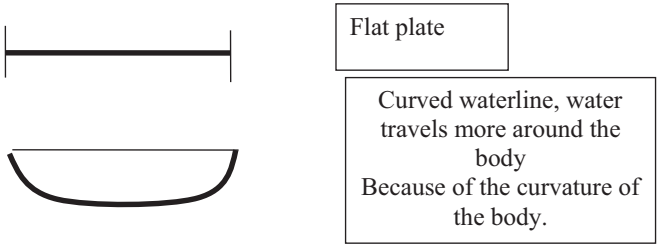

Fig. 132: Waterline of flat plate and curved plate, with same Reynolds number

Waterline of flat plate and curved plate, with same length and Reynolds number, which depending on the ship length, the water will travel more in the curved shape. There will be additional to frictional resistance in 2d dimensions extension.

In three dimensions, there is a vertical component also, and the length of traveling of the particles will be even more. Because of the existence of boundary layer, the pressure distribution will change, as going to the aft of the ship, and this will change the velocity magnitude. Generally, there is higher velocity in the midship and lower velocity in the aft region, if boundary layer is added there will be another change of the frictional resistance called friction form effect. Effect is primarily three dimensional:

$$Cf=(1+k)Cfo()$$

k – form factor with assumption that is independent of speed.

Pressure also changes

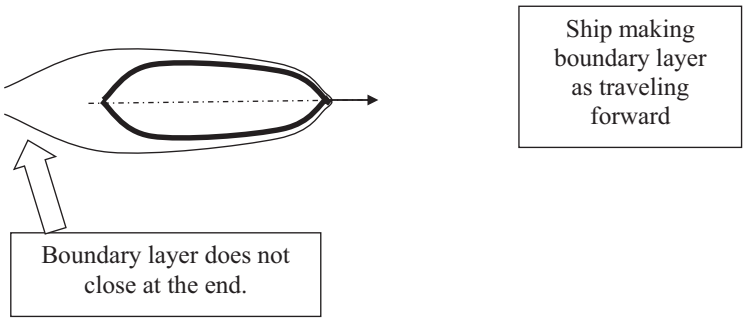

Fig. 133: Boundary layer on the moving ship

Boundary layer does not close at the end because there is water inside the boundary layer. This water is dragged along with the ship, because the water has less speed than the ship. With the assumption that the flow beyond the boundary layer is with potential nature.

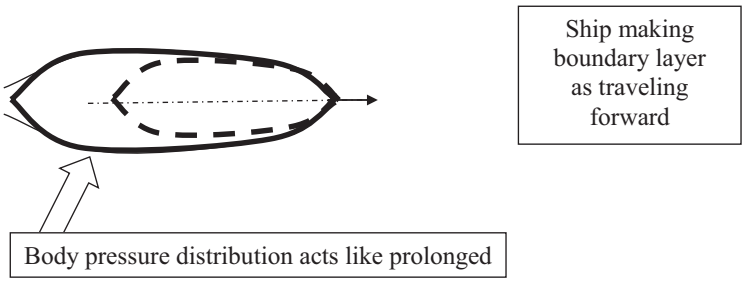

Fig. 134: Prolonged imaginary body due to effect of boundary layer

The body acts like it is prolonged the slopes are much less than original body and the pressure distribution changes compared than if there is no viscosity. The contributing of aft body for reducing the resistance is smaller.

Higher pressure in the aft part is being damped, it becomes slightly less pressure there, and the created helping wave from pressure at the stern now is smaller because is damped. This changed pressure due to resistance of boundary layer is called viscous pressure resistance.

Because of the shape and the boundary layer, there is effect of eddy or separation drag. The slope of the body is important parameter in determining what will be the pressure of the body. In the forward part pressure increases if the slope is more, in the mid part of the ship pressure may reduce. In the aft part, there is a peak of pressure and velocity drops because of the closing curvature but just forward of this pressure peak there is a drop of pressure, at that place if there is a large curvature the pressure will drop further, and the velocity increase. This will create big pressure gradient and just after the pressure peak, the velocity may become zero. If the pressure increases father the velocity may reverse itself because will be negative value.

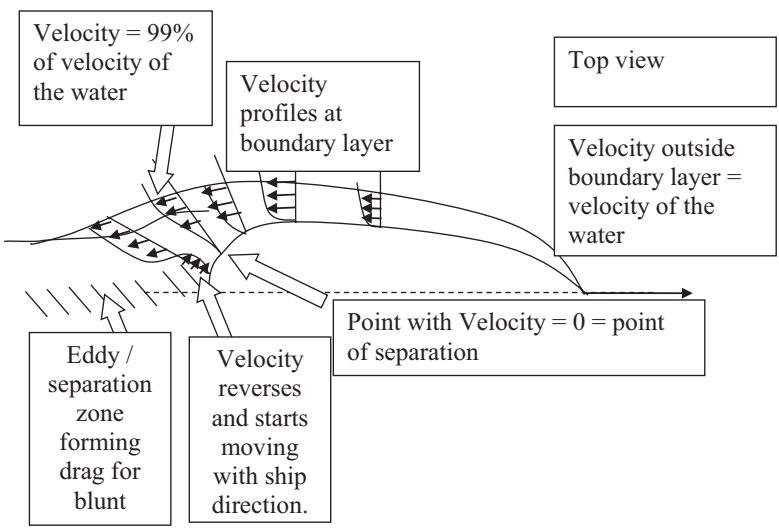

Fig. 135: Velocity distribution around the boundary layer

Boundary layer developing around the body creates different velocity profiles. If velocity profile is taken at the middle part, the velocity direction is behind the ship. As soon as the curvature starts changing, there is an increase of pressure and the velocity decreases, to such point that the velocity is zero. This point is called point of separation, and if the curvature continues to change, the velocity starts altering its direction and a layer starting from point of separation is formed inside the boundary layer. This separated flow will affect wave making, separation, and potential flow and small vortexes will be made inside the separation zone which will take energy for blunt bodies. The same effects will happen in the forward end, if there is big curvature and it will separate.

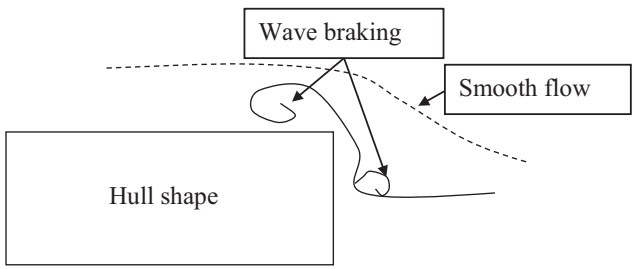

Fig. 136: Extreme blunt case in forward end

If extreme case is taken in, the forward part the water cannot pass smoothly and two-separation point will be created due to curvature.

Wave breaking resistance is the breaking of the waves due to steepness of the waves because the wave slope cannot maintain itself. This happens when generated wave has shorten length and larger height, in full form ships, having very large angles of entrance like bulk carriers and tankers. Wave breaking can occur at the bow of full ships; near the forward, aft bildges and stern so the waves can also break and make eddies.

Wave breaking will affect the viscous resistance, and if the pressure distribution is reduced around a blunt form, it is possible to reduce the viscous

resistance. If the wave slope can be reduced by reducing the height of the wave generated, then the wave does not break and will reduce this component of resistance. If there is taken container ship with Fn of around 0.3 or passenger ship, wave making resistance will be of around 70% of the total resistance so the bulb is put. But if there is tanker or super carrier, which has Fn of around 0.1-0.2, moving at low speed compared to its length around 200 m moving at 16 knots wave making resistance will be low. Wave making resistance in tankers is only 10-20 % and most of the total resistance is viscous, but there are ships with bulbous profile there also, this is because it reduces the steepness of wave making on the forward end. By doing this the component of resistance wave breaking also reduces. Bulbous bows are used today for low speed as well as high-speed form with different design considerations for reducing wave making or wave breaking.

Coefficient of form resistance Cform takes into account three-dimensional friction resistance, viscous pressure resistance and wave breaking resistance.

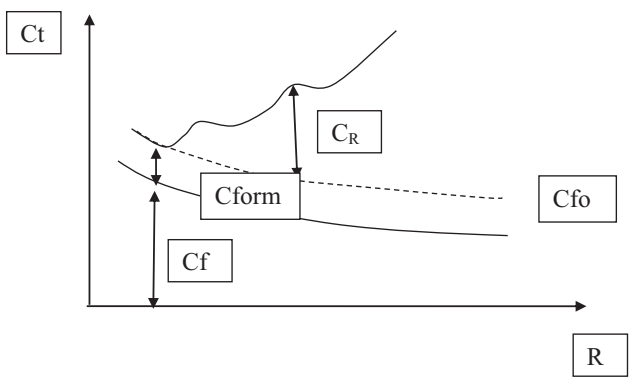

Fig. 137: Ct vs Rn

As a result, Cr (residual resistance coefficient (for high speed), separation drag, viscos pressure drag) cannot be said to be equal to Cw (wave resistance coefficient) because of the additional resistance effects included in Cr mentioned above. Cform (three dimensional form effect) is the form component that takes into account the major portion but not all of the bigger part of viscous resistance that incorporates two-dimensional form factor of total viscous resistance, because separation is relating with velocity and pressure that will change with increasing the speed and will be incorporated more and more in Cr.

Theoretical investigation of ship from resistance is still impossible, because the errors are too large, therefore there must be experimental method, by which the resistance of the ship can be estimated from model and extrapolated to full scale.

As the ship becomes fuller and fuller the component of Cform starts having more important role. Therefore, there is inaccurate zone, which is higher as it goes to fuller and fuller ship. If there is barge or higher curvature, where there is large separation on the front the mentioned method for calculating the resistance may not be accurate.

Foudes method of extrapolation works very well for normal ship forms, where the components of the resistance are well defined, and wave breaking drag is small compared to total resistance.

Other component of resistance is correlation allowance, which takes into account the roughness of the surface is put as correlation allowance:

$$Ca=0.4x10^{-3}.$$

ITTC 1978 updates to take into consideration length of the ship, because roughness takes more roll in shorten hull forms.

For ship trail there is another component of resistance called air resistance. Which is mainly considered that the wind is coming from the front, and the wave generated by it are neglected in the calculation. Suppose there is no wind the water is calm and when the ship travels it will have air resistance. It

will be assumed like in the water hypothesis that the ship is still and the air is moving and air velocities in still air is equal to ship velocity. But If there is a wind blowing head on, then this will be added into ship velocity. If the wind comes into direction of the ship hull.

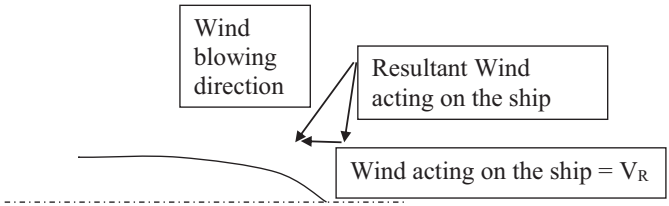

Fig. 138: Wind blowing at the angle through the ship

The most interest is put on the drag on forward motion, so wind coming from front. The wind area facing from the wind is tested in the wind tunnels.

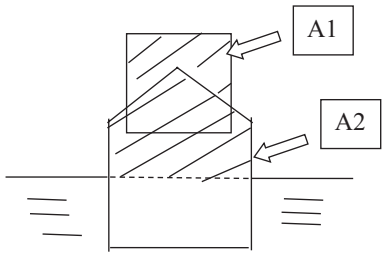

Fig. 139: Transversal projected area to the wind. Front view

Transversal area A1 and A2.

A_T=0.3A2+A1 – total transversal area used for calculation of wind resistance

There is formula because superstructure is not flat and when summing with above water part of the hull it gives mainly eddy resistance, which can be estimated only with experiments. Statistically from wind test resistance experiments has been shown that. $Raa=k\rho air A_T V_R^2$

V_R – Relative air (wind) velocity in the direction of axis.

ρair= 1.223 kg/m3 – air density

k=0.6 constant for drag coefficient

$Raa=0.734AtVrA_T V_R^2$

It the ship is very tall then there is a problem, because the wind velocity changes from in height. On the water surface there will be friction between water and air, theoretically wind velocity will be equal to zero, and very quickly will develop to wind speed.

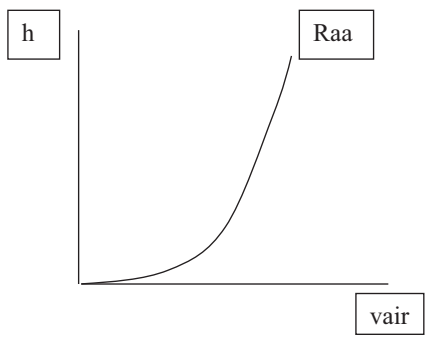

Fig. 140: Velocity of air changes in height above the water

If there is a long narrow body and fluid is, flowing around then there is a generation of perpendicular force, which is equivalent to lift force. The same effect happens in ships, if there is wind flowing in the small angle, the axial component of velocity will increase until 30 degrees and then will continue to increase slowly as well as the resistance until beam condition than the drag will be maximum.

Normally trail condition is specified with zero Beaufort or three. If it is Beaufort, zero means there is no wind speed so relative velocity of the wind is equal to ship velocity. Moreover, if it is Beaufort three wind speed must be added to ship speed to get the calculations for the total resistance. It is assumed that at Beaufort three the sea condition does not change. If the sea condition changes or at see whether there is wind or not but there is wave, maybe swell maybe wavy condition created by wind, which is blowned away, then there is augmented resistance, called resistance in waves Rwave ~ 15% (So Rt= Rw + Rv + Rwave) – because the see has waves added to the ship waves. This resistance at waves is required in service conditions, there is no way of knowing the resistance of the ship in the wavy condition, and most of these cases are experimental. Such experiments are performed on Series 60 and data is available for average increase in waves in sea conditions. The sea conditions vary depending on the sea and on the time of the year, in North Atlantic is rougher than in Passific. To get this additional resistance 15 % or service allowance are added to already calculated resistance.

Appendages are attachments on the ship of the outside of the hull which make drag. Typical attachments that merchant ships have are bilge keel, rudder, A – frames - shaft brackets, shaft bossings, sonar dome, bow thruster tunnel. These bodies are small and add to the frictional resistance. With known Reynolds number and assumed turbulent flow, wetted surface is calculated based on it Cf is derived, and multiplying them, it will give frictional resistance.

Appendix A2 Sample of used codes in SHIPFLOW

Used offset file was given for hull DTMB 5415 named “off_iihr.file”.

Example codes of command file (only first four letters are important for SHIPFLOW):

Potential flow code:

```
xflo
 titl(titl="DTMB")
 prog(xmes,xpan,xbou)
 hull(mono, fine, h1gr="hull",fbgr="bulb",tran,fsfl)
 offs(file="off_iihr",xaxd=1,ysig=1,xori=0,zori=0.248,lpp=5.7)
 opti(full)
 vshi(fn=[0.20],rn=[8.524656e6])
end
xmes
 body(grno=1,stat=103,poin=25,str2=5,df2=0.0025,dl2=0.0075)
 body(grno=2,stat=8,poin=17)
 free(grno=3,xdow=3,y4si=-1,xups=-
0.7,poin=25,str1=1,df1=0.02,stau=15,stam=25,stad=50)
 tran(grno=4,poin=4,stad=50)
end
xpan
 cont(free,nonl)
 para( nthr = 4 )
 iter(maxi=30)
 twcu(on)
end
```

Code 1: Sample config file for DTMB 5415 for potential simulation run

Viscous flow code:

```
xflow
 title ( title="DTMB" )
 program ( xgrid, xchap )
 hulltype ( mono, h1gr="hull",fbgr="bulb",transom, vfsflow, wsing )
 offsetfile( file="off_iihr", xaxdir=1.0, ysign=1.0,
 xori=0., zori=0.248, lpp=5.7 )
/ ipos ( trim = 0.41 )

 vship ( fn=[0.28], rn=[8.31E+06] )
/ propeller ( id="prop",
/ xsh=5.406091, ysh=0.16576, zsh=0.040097, zdir=-0.049399036,
/        dprop=0.248, dhub=0.044196, cts=0.5, cmo=0.5 )
 prtopt ( strlres )
 rudder( id="rudder",span=0.1647,
s=[0,0.5,1],c=[0.1829,0.1398,0.09669],dimension=[51,51,48],
         xle=[0.05476,0.03198,0.00919], orig=[5.5640,0.1248,0.1849],
angle=0,tp1f,tp2f,
 section=["p1",
 "p2",
 "p3"])
        shaft ( id="shaft", length=1.24966, origin=[4.236824,
0.166274,0.098055],dimension=[51,51,48],
         dir=[1,0,-0.049399036], r=0.022098)
 rudder( id="radder_bracket", span=0.061, s=[0,1],
c=[0.1829,0.1829], xle=[0.05476,0.05476],
         orig=[5.5640,0.1248,0.24793],angle=0,tp2f,tp1f,
dimension=[51,51,48],
 section=["p1"])
/ brack ( id="ax_carma", s=[0,1], c=[0.01488,0.01488],
dimension=[51,51,48],
/        from=[5.5640,0.1248,0.134163], to=[5.5640,0.1248,0.22],
rmax=1.6,
/ section="ax")
/ brack ( id="cav1", s=[0,1], c=[0.04064,0.04064],
xle=[0,0],dimension=[51,51,48],
/        from=[5.298136,0.167896,0.053014],
to=[5.298136,0.236144,0.307403], rmax=1.6,
/ section="cav")
/ brack ( id="cav2", s=[0,1], c=[0.04064,0.04064],
xle=[0,0],dimension=[51,51,48],
```

```
/       from=[5.298136,0.159757,0.050086], to=[5.298136,-
0.0018040,0.199264], rmax=1.6,
/ section="cav")
end
/xgrid
/singul( bow, xyzfwd=[0.0000,0.0000,-0.0577])
/       control(offtest, rawoffset)
/ size ( etamax=80, zetamax=80)
/ xdistr ( xstart=-0.5, xend=2.0, nu=40, nf=80, nm=70, na=60, nw=60,
/ xapu=0.83,xfpu=-0.1, xfpd=0.2, xapd=1.03 )
/end

xgrid
 size(global, medium)
end

xchap
 / actu(id="prop",on)
 parallel(nthread=4)
 control ( restart, maxit=3000, scheme="Fromm", easm, ROTCORR,
dump=3, verbose=3)
 refi ( level=[0.42,0.42,0.42], low=[0,-1,0.13], high=[0.65,1,0.35], eno)
        wake (on)
end
```

Code 2: Sample config file for DTMB 5415 for viscous simulation run

More Books!

yes I want morebooks!

Buy your books fast and straightforward online - at one of the world's fastest growing online book stores! Environmentally sound due to Print-on-Demand technologies.

Buy your books online at

www.get-morebooks.com

Kaufen Sie Ihre Bücher schnell und unkompliziert online – auf einer der am schnellsten wachsenden Buchhandelsplattformen weltweit!
Dank Print-On-Demand umwelt- und ressourcenschonend produziert.

Bücher schneller online kaufen

www.morebooks.de

OmniScriptum Marketing DEU GmbH
Heinrich-Böcking-Str. 6-8
D - 66121 Saarbrücken
Telefax: +49 681 93 81 567-9

info@omniscriptum.com
www.omniscriptum.com

OMNIScriptum